OPERATIONS REPORT

Issue 2/2021 rev. 2

Reporting period: July – December 2021

Authors	
Prepared by	
NAME	**INSTITUTE**
Jari Hovila	FMI
Contributions	
NAME	**INSTITUTE**
Jari Hovila, Jukka Kujanpää, Kaisa Lakkala	FMI
Axel Schmidt, Sander Slijkhuis, Pieter Valks	DLR
Olaf Tuinder, Robert van Versendaal	KNMI
Helge Jønch-Sørensen	DMI
Katerina Garane, MariLiza Koukouli	AUTH
Jeroen van Gent, José Granville, François Hendrick, Jean-Christopher Lambert, Bavo Langerock, Gaia Pinardi, Tijl Verhoelst	BIRA-IASB
Andy Delcloo	KMI
Peggy Tesche-Achtert	DWD
Anne Boynard, Cathy Clerbaux, Maya George, Camille Viatte	LATMOS
Rosa Astoreca, Pierre-François Coheur, Daniel Hurtmans, Catherine Wespes	ULB
Carlos Vicente	EUMETSAT
Approved by	

AC SAF Technical Manager	Jari Hovila / FMI	07/12/2022	*Signature*

Document change log		
Revision	Date	Description of change
1	07/04/2022	Initial revision
2	07/12/2022	List of abbreviations: updated
		Sections 3.1.1, 3.1.2, 4.1.1 and 4.1.2: Note to explain the absence of Metop-A data in December added
		Section 7.6.1: Statement of product accuracy remaining stable during the reporting period added
		Tables 3.2 and 3.5: Product IDs corrected
		Table 3.5: The word "successful" removed from the title of EOWEB order statistics
		Table 3.7: Reason for large number of error values explained
		Table 7.14: Review mode track changes accepted
		Table 7.28: Review mode track changes accepted

List of abbreviations

AC SAF	Satellite Application Facility on Atmospheric Composition Monitoring
ARP	Absorbing Aerosol Index from PMDs data product
ARP-A	Absorbing Aerosol Index from PMDs data product from Metop-A
ARP-B	Absorbing Aerosol Index from PMDs data product from Metop-B
ARP-C	Absorbing Aerosol Index from PMDs data product from Metop-C
ARS	Absorbing Aerosol Height data product
ARS-A	Absorbing Aerosol Height data product from Metop-A
ARS-B	Absorbing Aerosol Height data product from Metop-B
ARS-C	Absorbing Aerosol Height data product from Metop-C
ATMOS	Atmospheric Parameters Measured by in-Orbit Spectroscopy (DLR data service)
ATO	Assimilated Total Ozone
AUTH	Aristotle University of Thessaloniki
BIRA-IASB	Belgian Institute for Space Aeronomy
BrO	Bromine Oxide
CDOP	Continuous Development and Operations phase
CO	Carbon Monoxide
DLR	German Aerospace Center
DMI	Danish Meteorological Institute
DWD	German Weather Service
ECMWF	European Centre for Medium-Range Weather Forecasts
EDC	EUMETSAT Data Centre
EDD	Erythemal Daily Dose
EOWEB	Earth Observation on the WEB
EPS	European Polar System
EUMETCast	EUMETSAT's primary dissemination mechanism for the near real-time delivery of satellite data and products
EUMETSAT	European Organisation for the Exploitation of Meteorological Satellites
FMI	Finnish Meteorological Institute
GOME	Global Ozone Monitoring Experiment
H2O	Water Vapour
HCHO	Formaldehyde
HR	High resolution
KMI	Royal Meteorological Institute of Belgium
KNMI	Royal Netherlands Meteorological Institute
L1b	Level 1b data product
L1c	Level 1c data product
L2	Level 2 data product
L3	Level 3 data product

LATMOS	Laboratoire Atmosphères, Milieux, Observations Spatiales
LER	Lambertian-equivalent reflectivity data record
NHP	Near Real-time High-resolution Ozone Profile data product
NO2	Nitrogen Dioxide
NRT	Near Real-time
NTO	Near Real-time Total Column data product
NUV	Near Real-time UV index data product
O3	Ozone
O3M SAF	Satellite Application Facility on Ozone and Atmospheric Chemistry Monitoring
OHP	Offline High-resolution Ozone Profile data product
OHP-A	Offline High-resolution Ozone Profile data product from Metop-A
OHP-B	Offline High-resolution Ozone Profile data product from Metop-B
OHP-C	Offline High-resolution Ozone Profile data product from Metop-C
OEM	Optimal Estimation Method
OPERA	Ozone Profile Retrieval Algorithm
OTO	Offline Total Column data product
OUV	Offline Surface UV data product
OUV-A	Offline Surface UV data product from Metop-A
OUV-AB	Offline Surface UV data product from Metop-A and Metop-B
OUV-B	Offline Surface UV data product from Metop-B
OUV-BC	Offline Surface UV data product from Metop-B and Metop-C
PDU	Product Dissemination Unit
PGE	Product Generation Element
PMD	Polarisation Measurement Device
RD	Reference Document
RMS	Root Mean Square
RMSE	Root Mean Square Error
SO2	Sulphur Dioxide
TOC	Total Ozone Column data product
TrOC	Global Tropospheric Ozone Column data product
TTrOC	Tropical Tropospheric Ozone Column data product
ULB	Université libre de Bruxelles
UTC	Coordinated Universal Time

TABLE OF CONTENTS

1. Introduction

1.1. Scope

The scope of this document is to summarise the operational activities concerning the products in operation and the associated services during the reporting period to see that the general requirements applicable to these services and products of the AC SAF [RD1, RD2, RD3] are fulfilled. Intended readers of this document are the members of AC SAF project team, Review Board of the annual Operations Review, AC SAF Steering Group and EUMETSAT OPS/WG as well as the users of the AC SAF products.

Operations Reports include information about product availability/timeliness, quality assurance, website usage, and delivery statistics. Main events, major anomalies and software/hardware updates are reported also. AC SAF Operations Report is published twice a year.

1.2. Reporting period

This Operations Report covers the period July – December 2021.

1.3. Reference documents

Table 1.1. Operations Report reference documents

Reference	Title	Issued	Reporting period
RD1	Product Requirements Document (SAF/AC/FMI/RQ/PRD/001)	29/10/2021	N/A
RD2	Service Specification (SAF/AC/FMI/RQ/SESP/001)	22/09/2020	N/A
RD3	EUMETSAT Operational Services Specification (EUM/OPS/SPE/09/0810)	14/08/2015	N/A
RD4	EPS End User Requirements Document (EPS/MIS/REQ/93001)		N/A
RD5	O3M SAF Validation Report for NRT, offline and reprocessed total ozone columns	11/12/2015	January 2007 – December 2014
RD6	AC SAF Validation Report for NRT, offline, reprocessed and level 3 total/tropospheric NO2 columns	10/11/2017	Metop-A: January 2007 – July 2015 Metop-B: January 2013 – July 2015
RD7	O3M SAF Validation Report for Metop-A NRT and offline coarse/high-resolution ozone profiles	20/02/2012	January 2007 – May 2011
RD8	O3M SAF Validation Report for Metop-B NRT and offline coarse/high-resolution ozone profiles	30/06/2013	December 2012 – April 2013

Reference	Title	Issued	Reporting period
RD9	O3M SAF Validation Report for Metop-B NRT UV indexes	27/05/2013	May 2013
RD10	O3M SAF Validation Report for NRT, offline and reprocessed total SO2 columns	09/12/2015	January 2007 – December 2014
RD11	O3M SAF Validation Report for offline and reprocessed total BrO columns	09/12/2015	January 2007 – December 2014
RD12	O3M SAF Validation Report for NRT, offline and reprocessed total HCHO columns	30/10/2015	January 2007 – July 2015
RD13	O3M SAF Validation Report for offline and reprocessed total H2O columns	30/10/2015	January 2007 – August 2015
RD14	O3M SAF Validation Report for NRT and offline aerosol products	25/06/2013	January 2007 – May 2013
RD15	O3M SAF Validation Report for Metop-B offline UV products	03/02/2015	June 2012 – May 2013
RD16	O3M SAF Validation Report for Metop-A reprocessed total ozone columns	19/02/2010	January 2007 – June 2009
RD17	AC SAF Validation Report for GOME-2 surface LER product	27/03/2019	MSC: February 2007 – June 2018 PMD: April 2008 – June 2018
RD18	O3M SAF Validation Report for offline tropospheric ozone columns (cloud slicing)	03/07/2015	January 2007 – December 2014
RD19	O3M SAF Validation Report for NRT and offline tropospheric ozone columns (ozone profiles)	09/09/2015	January 2007 – December 2014
RD20	O3M SAF Validation Report for NRT IASI CO	17/11/2015	September 2015 – November 2015
RD21	AC SAF Validation Report for OClO data record	29/05/2017	January 2007 – September 2016
RD22	AC SAF Validation Report for NRT IASI SO2	17/11/2017	Metop-A: January 2007 – December 2013 June 2017 – October 2017 Metop-B: June 2017 – December 2017

Reference	Title	Issued	Reporting period
RD23	AC SAF Validation Report for level-3 total H2O data record	06/11/2017	Metop-A: January 2007 – December 2014 Metop-B: January 2013 – December 2014
RD24	AC SAF Validation Report for Metop-C offline tropical tropospheric ozone columns	05/06/2020	February – December 2019
RD25	AC SAF Validation Report for Metop-C NRT and offline global tropospheric ozone columns	05/06/2020	February – December 2019
RD26	AC SAF Validation Report for Metop-C NRT and offline high-resolution ozone profiles	05/06/2020	February – December 2019
RD27	AC SAF Validation Report for Metop-C NRT and offline total ozone columns	25/05/2020	February – July 2019
RD28	AC SAF Validation Report for Metop-C NRT and offline total/tropospheric nitrogen dioxide columns	25/11/2019	February – July 2019
RD29	AC SAF Validation Report for Metop-C NRT and offline total formaldehyde columns	19/05/2020	February – July 2019
RD30	AC SAF Validation Report for Metop-C offline total bromine monoxide columns	19/05/2020	February – July 2019
RD31	AC SAF Validation Report for Metop-C offline total water vapour columns	30/03/2020	February – July 2019
RD32	AC SAF Validation Report for NRT, offline and reprocessed absorbing aerosol height products	03/07/2020	2007-2019
RD33	AC SAF Validation Report for Metop-C NRT and offline absorbing aerosol index from PMDs products	09/10/2019	January – October 2019
RD34	AC SAF Validation Report for Metop-C NRT and offline total sulphur dioxide products	21/01/2021	February – July 2019

Online documents:

Service Specification, Validation Reports

1.4. Definition of terms

Availability is based on the definition in the EUMETSAT Operational Services Specification [RD3].

Product-specific clarifications:

- For NRT products, the monthly availability limit is 97.5 %. The availability is calculated as a "worst case scenario":

$$\frac{\text{in time processed and disseminated L2 PDUs}}{\text{received L1b PDUs } + \text{ missed L1b PDUs marked as "reception confirmed" in the EUMETCast sendlist}}$$

- For offline products, the monthly availability limit is 95.5 %. The availability is defined by the ratio of the number of in time processed, archived and quality-approved L2 products to the number of orbits for which L1b PDUs have been received per month.

- NUV and OUV are daily L3 products, and availability is defined as the fraction of days in a month with products fulfilling the timeliness requirements.

Timeliness defines whether the product is near real time (NRT) product which is disseminated or ready for download in three hours from sensing at the latest or offline product which is available for download in two weeks after sensing at the latest, during system availability. System unavailability will in most cases not lead to loss of data but to delays with respect to the specified timeliness. In practice, timeliness of a product is determined by calculating the time from sensing to EUMETCast or archive upload. In the Operations Reports, the timeliness is presented as monthly average, minimum and maximum values.

Accuracy is defined as in the EPS End User Requirements Document [RD4]: the values of accuracy "represent RMS values" taking as reference the 'true value' measured by ground based instruments.

1.5. Accuracy requirements of AC SAF products

The following table lists all operational AC SAF products and their accuracy requirements as defined in [RD2].

Table 1.2. Accuracy requirements of AC SAF products

Product identifier	Product name	Product acronym	Threshold accuracy	Target accuracy	Means of quality assurance
O3M-01.1	NRT total O3	MAG-N-O3	20 %	4 % (SZA < 80°) 6 % (SZA > 80°)	Validation report
O3M-41.1		MBG-N-O3			
O3M-300		MCG-N-O3			
O3M-02.1	NRT total NO2	MAG-N-NO2	20 % of annual mean	8-15 % of annual mean	Online monitoring Validation report
O3M-50.1		MBG-N-NO2			
O3M-338		MCG-N-NO2			
O3M-36.1	NRT tropospheric NO2	MAG-N-NO2TR	50 %	30 %	Online monitoring Validation report
O3M-52.1		MBG-N-NO2TR			
O3M-341		MCG-N-NO2TR			

Product identifier	Product name	Product acronym	Threshold accuracy	Target accuracy	Means of quality assurance
O3M-54.1	NRT total SO2	MAG-N-SO2	100 %	50 % (SZA < 70°)	Online monitoring Validation report
O3M-55.1		MBG-N-SO2			
O3M-374		MCG-N-SO2			
O3M-176	NRT total HCHO	MAG-N-HCHO	100 %	50 % (polluted)	Online monitoring Validation report
O3M-177		MBG-N-HCHO			
O3M-344		MCG-N-HCHO			
O3M-38.1	NRT high-resolution ozone profile	MAG-N-O3HRPR	30 % in stratosphere 70 % in troposphere	15 % in stratosphere 30 % in troposphere	Online monitoring Validation report
O3M-47.1		MBG-N-O3HRPR			
O3M-311		MCG-N-O3HRPR			
O3M-68	NRT absorbing aerorol height	MAG-N-AAH	3 km (layer height < 10 km) 4 km (layer height > 10 km)	1 km (layer height < 10 km) 2 km (layer height > 10 km)	Online monitoring Validation report
O3M-78		MBG-N-AAH			
O3M-364		MCG-N-AAH			
O3M-62.1	NRT absorbing aerosol index from PMDs	MAG-N-AAIPMD	1.0 index points	0.5 index points	Online monitoring Validation report
O3M-72.1		MBG-N-AAIPMD			
O3M-362		MCG-N-AAIPMD			
O3M-409	NRT UV index, clear-sky	MCG-NUV_CLEAR	20 %	10 %	Online monitoring Validation report
O3M-410	NRT UV index, cloud-corrected	MCG-NUV_CLOUD	20 %	10 %	Online monitoring Validation report
O3M-181	NRT IASI CO	MAI-N-CO	25 % (normal conditions) 50 % (high pollution or low signal)	12 % (normal conditions) 20 % (high pollution or low signal)	Validation report
O3M-80		MBI-N-CO			
O3M-352		MCI-N-CO			
O3M-57	NRT IASI SO2	MxI-N-SO2	200 % (below 10 km) 100 % (above 10 km)	100 % (below 10 km) 35 % (above 10 km)	Validation report
O3M-377					
O3M-81	NRT IASI HNO3	MxI-N-HNO3	50 %	35 %	Validation report
O3M-336					
O3M-49	NRT IASI ozone profile	MxI-N-O3PR	30 % in stratosphere 50 % in troposphere	15 % in stratosphere 30 % in troposphere	Validation report
O3M-315					
O3M-06.1	Offline total O3	MAG-O-O3	20 %	4 % (SZA < 80°) 6 % (SZA > 80°)	Validation report
O3M-42.1		MBG-O-O3			
O3M-301		MCG-O-O3			
O3M-07.1	Offline total NO2	MAG-O-NO2	20 % of annual mean	8-15 % of annual mean	Online monitoring Validation report
O3M-51.1		MBG-O-NO2			
O3M-339		MCG-O-NO2			

Product identifier	Product name	Product acronym	Threshold accuracy	Target accuracy	Means of quality assurance
O3M-37.1	Offline tropospheric NO2	MAG-O-NO2TR	50 %	30 %	Online monitoring Validation report
O3M-53.1		MBG-O-NO2TR			
O3M-342		MCG-O-NO2TR			
O3M-09.1	Offline total SO2	MAG-O-SO2	100 %	50 % (SZA < 70°)	Online monitoring Validation report
O3M-56.1		MBG-O-SO2			
O3M-375		MCG-O-SO2			
O3M-08.1	Offline total BrO	MAG-O-BrO	50 %	30 %	Online monitoring Validation report
O3M-82.1		MBG-O-BrO			
O3M-317		MCG-O-BrO			
O3M-10.1	Offline total HCHO	MAG-O-HCHO	100 %	50 % (polluted)	Online monitoring Validation report
O3M-58.1		MBG-O-HCHO			
O3M-345		MCG-O-HCHO			
O3M-12.1	Offline total H2O	MAG-O-H2O	25 %	10 %	Validation report
O3M-86.1		MBG-O-H2O			
O3M-386		MCG-O-H2O			
O3M-35	Offline tropical tropospheric ozone	MAG-O-O3TR	50 %	25 %	Validation report
O3M-43		MBG-O-O3TR			
O3M-302		MCG-O-O3TR			
O3M-39.1	Offline high-resolution ozone profile	MAG-O-O3HRPR	30 % in stratosphere 70 % in troposphere	15 % in stratosphere 30 % in troposphere	Online monitoring Validation report
O3M-48.1		MBG-O-O3HRPR			
O3M-312		MCG-O-O3HRPR			
O3M-172	NRT global tropospheric ozone	MAG-N-O3TROC	50 %	20 %	Validation report
O3M-174		MBG-N-O3TROC			
O3M-304		MCG-N-O3TROC			
O3M-173	Offline global tropospheric ozone	MAG-O-O3TROC	50 %	20 %	Validation report
O3M-175		MBG-O-O3TROC			
O3M-305		MCG-O-O3TROC			
O3M-69	Offline absorbing aerosol height	MAG-O-AAH	3 km (layer height < 10 km) 4 km (layer height > 10 km)	1 km (layer height < 10 km) 2 km (layer height > 10 km)	Online monitoring Validation report
O3M-79		MBG-O-AAH			
O3M-365		MCG-O-AAH			
O3M-63.1	Offline absorbing aerosol index from PMDs	MAG-O-AAIPMD	1.0 index points	0.5 index points	Online monitoring Validation report
O3M-73.1		MBG-O-AAIPMD			
O3M-363		MCG-O-AAIPMD			
O3M-450 – O3M-464	Offline surface UV	MM-O-UV_*	50 %	20 %	Online monitoring Validation report

Latest validation reports for all pre-operational and operational AC SAF products are listed in Section 1.3.

Online monitoring, when applicable, can be used to replace the regular validation reporting. Online monitoring results are found from dedicated sections "Online quality monitoring", if the processing centre in question has such functionality.

2. Processing centre: FMI

2.1. Offline surface UV

Offline surface UV (OUV) product is a multi-mission (Metop-B+C) product consisting of 15 sub-products which are listed in Table 2.1. Since they are all archived in the same file, single entries in the tables in the following sections represent them all.

Table 2.1. OUV sub-products

Product Identifier	Product Name	Product Acronym
O3M-450	Offline UV daily dose, erythemal (CIE) weighting	MM-O-UV_DD_CIE
O3M-451	Offline UV daily dose, plant response weighting	MM-O- UV_DD_PLANT
O3M-452	Offline UV daily dose, DNA damage weighting	MM-O-UV_DD_DNA
O3M-453	Offline UV daily dose, UVA range (315-400 nm)	MM-O-UV_DD_UVA
O3M-454	Offline UV daily dose, UVB range (280-315 nm)	MM-O-UV_DD_UVB
O3M-455	Offline UV daily maximum dose rate, erythemal (CIE) weighting	MM-O-UV_MDSR_CIE
O3M-456	Offline UV daily maximum dose rate, plant response weighting	MM-O-UV_MDSR_PLANT
O3M-457	Offline UV daily maximum dose rate, DNA damage weighting	MM-O-UV_MDSR_DNA
O3M-458	Offline UV daily maximum dose rate, UVA range (315-400 nm)	MM-O-UV_MDSR_UVA
O3M-459	Offline UV daily maximum dose rate, UVB range (280-315 nm)	MM-O-UV_MDSR_UVB
O3M-460	Offline UV solar noon UV index	MM-O-UV_NOON_UVI
O3M-461	Offline UV daily maximum ozone photolysis rate	MM-O-UV_MPHR_O3
O3M-462	Offline daily maximum nitrogen dioxide photolysis rate	M-O-UV_MPHR_NO2
O3M-463	Offline UV daily dose, vitamin D weighting	MM-O-UV_DD_VITD
O3M-464	Offline UV daily maximum dose rate, vitamin D weighting	MM-O-UV_MDSR_VITD

2.1.1. Availability

Availability requirement for OUV has been defined in Section 1.4. The availability statistics of FMI products are presented in Table 2.2. If the availability requirement has been violated, those values are marked with red colour, identified by numbers and reported in Table 2.7.

Table 2.2. Availability of OUV product during the reporting period

7/2021	8/2021	9/2021	10/2021	11/2021	12/2021
100 %	100 %	100 %	100 %	100 %	100 %

2.1.2. Timeliness

Timeliness indicates the elapsed time between sensing and product dissemination. Timeliness requirement is 15 days for offline products. If the requirement has been violated, those values are

marked with red colour. In addition, the violations are identified by numbers and reported in Table 2.7 if they have caused the availability values to drop below the allowed limits.

Note: timeliness violations are not listed as anomalies if the availability is above the limit.

The values in Table 2.3 indicate the elapsed times (days, hours and minutes in the format [ddT]hh:mm) from sensing to archive upload. In each cell, the values from top to bottom represent observed monthly average, minimum and maximum times.

Table 2.3. Timeliness of OUV product during the reporting period

7/2021	8/2021	9/2021	10/2021	11/2021	12/2021
avg: 03T01:43 min: 03T01:31 max: 03T01:51	avg: 03T01:42 min: 03T01:26 max: 03T01:46	avg: 03T01:53 min: 03T01:31 max: 03T07:36	avg: 03T01:47 min: 03T01:31 max: 03T02:01	avg: 03T01:59 min: 03T01:31 max: 03T09:00	avg: 03T01:36 min: 03T00:16 max: 03T01:46

2.2. Services, main events and anomalies

Table 2.4. FMI service statistics related to product archiving, ordering and AC SAF Helpdesk

Description of service / event	7/2021	8/2021	9/2021	10/2021	11/2021	12/2021
Product ordering [1]						
Number of users (cumulative)	497	500	506	511	518	530
Number of orders	22	50	35	9	14	6
Number of ordered products	OHP: 15 ARS: 13948 ARP: 480 OUV subset: 7	OHP: 1714 ARS: 3296 ARP: 422 OUV time-series: 61490	ARS: 42 ARP: 14 OUV time-series: 59007	OOP: 4198 OHP: 62 ARS: 596 ARP: 171 OUV time-series: 1513	OHP: 1758 ARS: 1360 ARP: 78 OUV subset: 10230 OUV time-series: 1418	OHP: 1341 ARP: 29
Ordered data volume	OHP: 3.51 GB ARS: 14.0 GB ARP: 3.30 GB OUV subset: 98.3 MB	OHP: 425 GB ARS: 3.37 GB ARP: 2.90 GB OUV time-series: 3.90 MB	ARS: 42.1 MB ARP: 94.2 MB OUV time-series: 4.28 MB	OOP: 206 GB OHP: 15.2 GB ARS: 612 MB ARP: 1.18 GB OUV time-series: 153 kB	OHP: 370 GB ARS: 1.40 GB ARP: 539 MB OUV subset: 242 MB OUV time-series: 103 kB	OHP: 331 GB ARP: 202 MB
Number of bulk orders	0	0	0	0	0	0
Number of failed orders [2]	0	0	0	0	0	0
Archive statistics [3]						
Number of archived products (Metop-A)	OHP: 439 ARS: 439 ARP: 439	OHP: 440 ARS: 440 ARP: 440	OHP: 425 ARS: 425 ARP: 425	OHP: 437 ARS: 437 ARP: 437	OHP: 205 ARS: 205 ARP: 205	
Size of archived products (Metop-A)	OHP: 102 GB ARS: 452 MB ARP: 2.90 GB	OHP: 105 GB ARS: 449 MB ARP: 2.93 GB	OHP: 103 GB ARS: 380 MB ARP: 2.84 GB	OHP: 105 GB ARS: 368 MB ARP: 2.92 GB	OHP: 49.1 GB ARS: 172 MB ARP: 1.36 GB	
Number of archived products (Metop-B)	OHP: 439 ARS: 439 ARP: 439	OHP: 440 ARS: 440 ARP: 440	OHP: 425 ARS: 425 ARP: 425	OHP: 438 ARS: 438 ARP: 438	OHP: 426 ARS: 426 ARP: 426	OHP: 439 ARS: 439 ARP: 439

Size of archived products (Metop-B)	OHP: 110 GB ARS: 453 MB ARP: 3.01 GB	OHP: 110 GB ARS: 453 MB ARP: 3.02 GB	OHP: 107 GB ARS: 435 MB ARP: 2.93 GB	OHP: 110 GB ARS: 447 MB ARP: 3.01 GB	OHP: 107 GB ARS: 436 MB ARP: 2.93 GB	OHP: 100 GB ARS: 450 MB ARP: 3.02 GB
Number of archived products (Metop-C)	OHP: 440 ARS: 440 ARP: 440	OHP: 439 ARS: 439 ARP: 439	OHP: 423 ARS: 423 ARP: 423	OHP: 440 ARS: 440 ARP: 440	OHP: 425 ARS: 425 ARP: 425	OHP: 435 ARS: 435 ARP: 435
Size of archived products (Metop-C)	OHP: 110 GB ARS: 454 MB ARP: 3.01 GB	OHP: 110 GB ARS: 452 MB ARP: 3.01 GB	OHP: 106 GB ARS: 433 MB ARP: 2.90 GB	OHP: 110 GB ARS: 449 MB ARP: 3.03 GB	OHP: 106 GB ARS: 435 MB ARP: 2.92 GB	OHP: 109 GB ARS: 445 MB ARP: 3.00 GB
Number of archived multi-mission products	OUV: 31	OUV: 31	OUV: 30	OUV: 31	OUV: 30	OUV: 31
Size of archived multi-mission products	OUV: 503 MB	OUV: 540 MB	OUV: 549 MB	OUV: 594 MB	OUV: 560 MB	OUV: 555 MB
GOME-2 L1b PDU rolling archive statistics [4]						
PDUs archived / PDUs "reception confirmed" (Metop-A)	14079/14878 94.6 %	13943/14874 93.7 %	13021/14397 90.4 %	13190/14777 89.3 %	5971/6890 86.7 %	
PDUs archived / PDUs "reception confirmed" (Metop-B)	14779/14875 99.4 %	14796/14880 99.4 %	14350/14400 99.7 %	14764/14849 99.4 %	14147/14399 98.2 %	14667/14878 98.6 %
PDUs archived / PDUs "reception confirmed" (Metop-C)	14790/14879 99.4 %	14621/14880 98.3 %	14233/14400 98.8 %	14573/14858 98.1 %	13893/14400 96.5 %	14467/14804 97.7 %
Helpdesk statistics						
Number of emails	1	1	0	5	0	7
Number of email threads	1	1	0	2	0	4
Average response time ([ddT]hh:mm)	02T17:42	15:07	-	01T06:43	-	16:39

[1] More detailed information about the orders is available in Appendix 1
[2] Failed orders are detailed in Appendix 2
[3] Based on sensing start time
[4] For Level 1b products, the availability is defined as the number of archived L1b PDUs divided by the number of L1b PDUs with status "reception confirmed" in the EUMETCast sendlist

Data archive statistics since 2008 are illustrated in Figure 2.1.
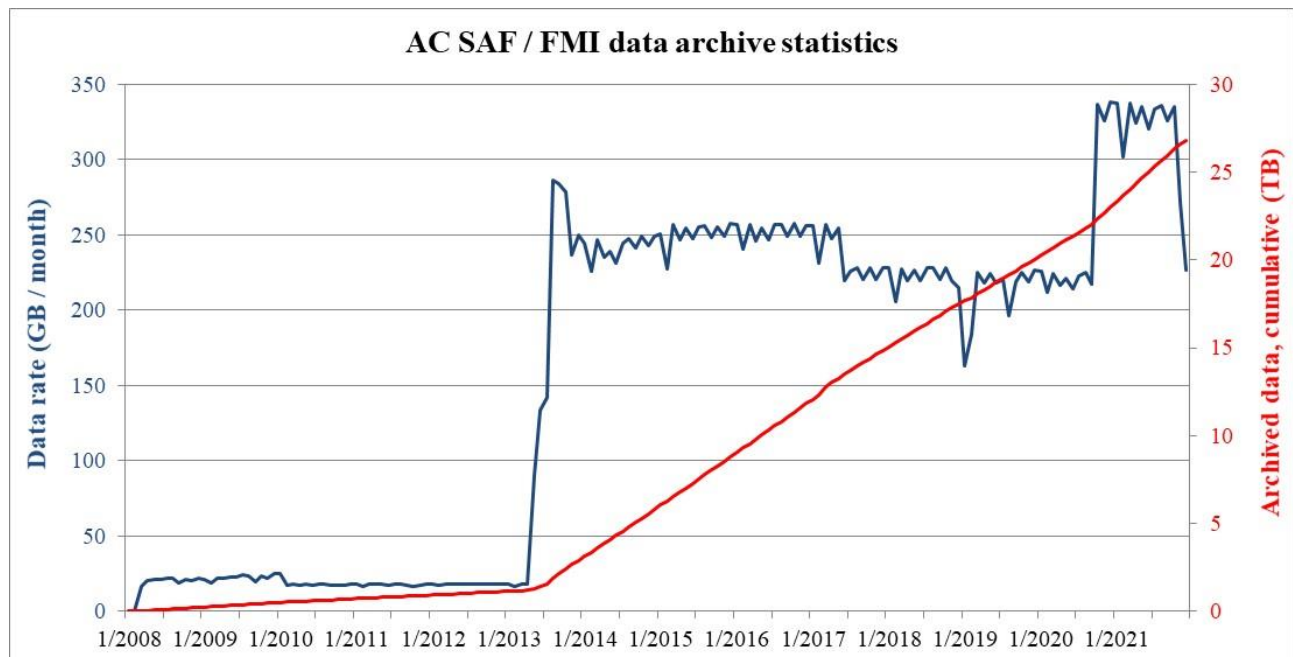
Figure 2.1. FMI data archive statistics: data rate and cumulative amount of data

Decrease of the data rate in December 2018 – February 2019 is due to invalid OHP data having smaller file size than normally.

Events affecting the data rate are presented in Table 2.5.

Table 2.5. Events affecting the FMI archive data rate

Date	Event	Data rate (GB/month)
03/2008	Archiving of OOP-A started	19.1 – 22.2
06/2009	Archiving of OUV-A started	19.2 – 23.8
11/2009	Archiving of ARS-A started	25.3
02/2010	Compression of OOP-A started	16.2 – 18.3
05/2013	Archiving of OHP-A started	133 – 142
08/2013	Archiving of OOP-B, OHP-B and ARS-B started	279 – 284
11/2013	Archiving of ARP-A and ARP-B started. KNMI implements shuffling algorithm in the hdf5 compression	226 – 250
03/2014	Archiving of OUV-A discontinued, archiving of OUV-B started	227 – 250
02/2015	OPERA algorithm update, tropospheric integrated profiles added	247-257
06/2017	Archiving of OOP-A and OOP-B discontinued	206-229
10/2020	Archiving of ARS-C, ARP-C and OHP-C started	302-338
11/2021	Archiving of OHP-A, ARS-A and ARP-A discontinued	227 - 271

Table 2.6 lists the main events (product/service/hardware/software updates etc.) at FMI during the reporting period.

Table 2.6. Main events at FMI during the reporting period

Date	Description
15 November	Due to the end of the Metop-A mission, archiving of new Metop-A products is discontinued

Table 2.7 lists the main local and external anomalies during the reporting period. Corrective and preventive actions should be provided also when applicable.

Table 2.7. Main local and external anomalies affecting FMI systems and performance during the reporting period

ID	Time period	Description
		Nothing to report.

3. Processing centre: DLR

3.1. NRT and offline total/tropospheric trace gas columns, tropical tropospheric ozone

This section reports availability and timeliness of the operational NRT and offline L2 products processed for GOME-2 on Metop-A, Metop-B and Metop-C.

3.1.1. Availability

For Level 1b products, the availability is defined as the number of L1b PDUs with status "reception confirmed", i.e. EUMETSAT received these L1b PDUs through its EUMETCast reference receiving station, divided by the total number of L1b PDUs listed in the EUMETCast sendlist.

Availability for offline L2 products has been defined in Section 1.4. The availability statistics of DLR products are presented in Table 3.1 and Table 3.2. If the availability requirements have been violated, those values are marked with red colour, identified by numbers and reported in Table 3.9.

Note: Statistics for December 2021 are missing due to Metop-A de-commissioning.

Table 3.1. Availability of Metop-A total and tropospheric trace gas column products during the reporting period

Product Identifier	Product Name	7/2021	8/2021	9/2021	10/2021	11/2021	12/2021
L1b	PDUs received / PDUs "reception confirmed"	13731/14878 92.3 % (1)	14863/14874 99.9 %	14205/14397 98.7 %	14774/14777 99.9 %	6912/6720 102.9 % (3)	
O3M-01.1	NRT total O3						
O3M-02.1	NRT total NO2						
O3M-36.1	NRT tropospheric NO2	92.1 % (1)	99.9 %	95.3 % (2)	99.9 %	102.8 % (3)	
O3M-54.1	NRT total SO2						
O3M-176.0	NRT total HCHO						
O3M-06.1	Offline total O3						
O3M-07.1	Offline total NO2						
O3M-37.1	Offline tropospheric NO2						
O3M-09.1	Offline total SO2	100 %	100 %	100 %	100 %	100 %	
O3M-10.1	Offline total HCHO						
O3M-08.1	Offline total BrO						
O3M-12.1	Offline total H2O						
O3M-35	Offline tropical tropospheric ozone	100 %	100 %	100 %	100 %	100 %	

Table 3.2. Availability of Metop-B total and tropospheric trace gas column products during the reporting period

Product Identifier	Product Name	7/2021	8/2021	9/2021	10/2021	11/2021	12/2021
L1b	PDUs received / PDUs "reception confirmed"	14866/14875 99.9 %	14879/14880 99.9 %	14400/14400 100 %	14849/14849 100 %	14400/14400 100 %	14752/14804 99.6 %
O3M-41.1	NRT total O3						
O3M-50.1	NRT total NO2						
O3M-52.1	NRT tropospheric NO2	99.9 %	99.9 %	99.9 %	99.9 %	99.9 %	99.6 %
O3M-55.1	NRT total SO2						
O3M-177.0	NRT total HCHO						
O3M-42.1	Offline total O3						
O3M-51.1	Offline total NO2						
O3M-53.1	Offline tropospheric NO2						
O3M-56.1	Offline total SO2	100 %	100 %	100 %	100 %	100 %	100 %
O3M-58.1	Offline total HCHO						
O3M-82.1	Offline total BrO						
O3M-86.1	Offline total H2O						
O3M-43	Offline tropical tropospheric ozone	100 %	100 %	100 %	100 %	100 %	100 %

Table 3.3. Availability of Metop-C total and tropospheric trace gas column products during the reporting period

Product Identifier	Product Name	7/2021	8/2021	9/2021	10/2021	11/2021	12/2021
L1b	PDUs received / PDUs "reception confirmed"	8696/14879 58.4 % (1)	14875/14880 99.9 %	14399/14400 99.9 %	14858/14858 100 %	14400/14400 100 %	14752/14804 99.6 %
O3M-300	NRT total O3	58.4 % (1)	99.9 %	99.9 %	100 %	99.9 %	99.6 %
O3M-338	NRT total NO2						
O3M-341	NRT tropospheric NO2						
	NRT total SO2						
O3M-344	NRT total HCHO						
O3M-301	Offline total O3	100 %	100 %	100 %	100 %	100 %	100 %
O3M-339	Offline total NO2						
O3M-342	Offline tropospheric NO2						
	Offline total SO2						
O3M-345	Offline total HCHO						
O3M-317	Offline total BrO						
O3M-386	Offline total H2O						
O3M-302	Offline tropical tropospheric ozone	100 %	100 %	100 %	100 %	100 %	100 %

3.1.2. Timeliness

Timeliness indicates the elapsed time between sensing and product dissemination. Timeliness requirements are 3 hours for NRT products and 15 days for offline products. If the requirements have been violated, those values are marked with red colour. In addition, the violations are identified by numbers and reported in Table 3.9 if they have caused the availability values to drop below the allowed limits.

Note: timeliness violations are not listed as anomalies if the availability is above the limit.

The values for NRT products in Table 3.4 and Table 3.5 indicate the elapsed times (days, hours and minutes in the format [ddT]hh:mm) from sensing to EUMETCast (NRT) upload. In each cell, the values from top to bottom represent observed monthly average, minimum and maximum times for NRT products.

Offline products (excluding the tropospheric product) are monthly aggregates and the reported value is the absolute time of archive upload to the EOWEB catalogue.

Note: Statistics for December 2021 are missing due to Metop-A de-commissioning.

Table 3.4. Timeliness of Metop-A total and tropospheric trace gas column products during the reporting period

Product Identifier	Product Name	7/2021	8/2021	9/2021	10/2021	11/2021	12/2021
O3M-01.1	NRT total O3	avg: 01:28:36 min: 00:36:19 max: 02:53:45	avg: 01:28:24 min: 00:34:23 max: 02:07:28	avg: 01:31:17 min: 00:32:20 max: 02:59:39	avg: 01:32:52 min: 00:32:20 max: 02:09:06	avg: 01:30:07 min: 01:08:17 max: 01:51:14	
O3M-02.1	NRT total NO2						
O3M-36.1	NRT tropospheric NO2						
O3M-54.1	NRT total SO2						
O3M-176.0	NRT total HCHO						
O3M-06.1	Offline total O3	2021-08-14T08:52:15 (4)	2021-09-13T14:20:09	2021-10-19T16:36:22 (5)	2021-11-13T14:14:13	2021-12-13T13:42:10	
O3M-07.1	Offline total NO2						
O3M-37.1	Offline tropospheric NO2						
O3M-09.1	Offline total SO2						
O3M-10.1	Offline total HCHO						
O3M-08.1	Offline total BrO						
O3M-12.1	Offline total H2O						
O3M-35	Offline tropical tropospheric ozone	N/A	N/A	N/A	N/A	N/A	

Table 3.5. Timeliness of Metop-B total and tropospheric trace gas column products during the reporting period

Product Identifier	Product Name	7/2021	8/2021	9/2021	10/2021	11/2021	12/2021
O3M-41.1	NRT total O3	avg: 01:04:29 min: 00:31:17 max: 02:13:35	avg: 00:52:08 min: 00:29:21 max: 01:48:34	avg: 00:51:52 min: 00:26:42 max: 01:48:24	avg: 00:53:09 min: 00:30:20 max: 01:53:41	avg: 01:40:41 min: 02:07:28 max: 01:09:23	avg: 01:40:16 min: 02:58:27 max: 01:10:43
O3M-50.1	NRT total NO2						
O3M-52.1	NRT tropospheric NO2						
O3M-55.1	NRT total SO2						
O3M-177.0	NRT total HCHO						
O3M-42.1	Offline total O3	2022-01-31T18:33:18 (4)	2021-09-13T14:20:03	2021-10-19T16:02:06 (5)	2021-11-13T13:42:08	2021-12-13T13:31:19	2022-01-14T13:35:37 (6)
O3M-51.1	Offline total NO2						
O3M-53.1	Offline tropospheric NO2						
O3M-56.1	Offline total SO2						
O3M-58.1	Offline total HCHO						
O3M-82.1	Offline total BrO						
O3M-86.1	Offline total H2O						
O3M-43	Offline tropical tropospheric ozone	N/A	N/A	N/A	N/A	N/A	N/A

Table 3.6. Timeliness of Metop-C total and tropospheric trace gas column products during the reporting period

Product Identifier	Product Name	7/2021	8/2021	9/2021	10/2021	11/2021	12/2021
O3M-300	NRT total O3	avg: 01:43:45 min: 00:34:32 max: 02:55:55	avg: 01:45:53 min: 00:33:19 max: 02:32:32	avg: 01:43:00 min: 00:32:43 max: 02:10:35	avg: 01:45:36 min: 00:43:30 max: 02:35:29	avg: 01:40:41 min: 02:07:28 max: 01:09:23	avg: 01:40:16 min: 02:58:27 max: 01:10:43
O3M-338	NRT total NO2						
O3M-341	NRT tropospheric NO2						
	NRT total SO2						
O3M-344	NRT total HCHO						
O3M-301	Offline total O3	2022-01-31T18:33:18 (4)	2021-09-13T12:57:19	2021-10-19T15:25:38 (5)	2021-11-13T13:03:56	2021-12-13T12:56:05	2022-01-17T10:06:51 (6)
O3M-339	Offline total NO2						
O3M-342	Offline tropospheric NO2						
	Offline total SO2						
O3M-345	Offline total HCHO						
O3M-317	Offline total BrO						
O3M-386	Offline total H2O						
O3M-302	Offline tropical tropospheric ozone	N/A	N/A	N/A	N/A	N/A	N/A

3.2. Services, main events and anomalies

Table 3.7. DLR service statistics related to product archiving and ordering

Description of service / event	7/2021	8/2021	9/2021	10/2021	11/2021	12/2021
Archive statistics [2]						
Number of archived products (cumulative) – according to product insertion time	330863	333283	333295	334815	335797	336673
Size of archived products (TB, cumulative)	10.9	11.0	11.1	11.1	11.2	11.2
Number of missing orbit products – according to sensing time	3	0	45	3	0	1
Number of archived products with good/poor/error[3] quality assessed per month – according to product insertion time	727/25/50	1263/27/31	1194/14/24	1250/50/15	1055/9/135	867/0/359 [4]
Online Access [1]						
Number of searches in the GOME.TC collection	124	71	91	106	529	135
Number of FTP (ATMOS/VELA) subscribers	446	447	452	455	461	470
Number of FTP (ATMOS/VELA) downloads	233916	256596	128154	174648	100845	82055
Downloaded data volume (GB)	1159	2285	48	1052	354	288
Product ordering						
Number of EOWEB orders	0	0	4	6	235	2
Delivered data volume (GB)	6.03	6.28	5.73	6.12	313	6.07

[1] NTO product and OTO product is stored at the DLR for external search and download
[2] O3MOTO product (collection GOME.TC, Metop missions) is archived and available to non-NRT users
[3] good: max. 2 PDUs missing, poor/error: more than 2 PDUs missing
[4] Reason for large number of error values is the reprocessing of data from July, when there was a reception system outage. Explained in more detail in Table 3.9 (ID 1)

Table 3.8 lists the main events (product/service/hardware/software updates etc.) at DLR during the reporting period.

Table 3.8. Main events at DLR during the reporting period

Date	Event
10 November	Upgrade of L2 NRT PSM instances for DWD L2 NRT product dissemination via WMO GTS and change of naming convention for disseminated files as per request by DWD
15 November onwards	Shutdown of Metop-A L2 NRT and offline processing and dissemination services due to Metop-A decommissioning

Table 3.9 lists the main and external local anomalies at DLR during the reporting period. Corrective and preventive actions should be provided also when applicable.

Table 3.9. Main local and external anomalies affecting DLR systems and performance during the reporting period

ID	Time period	Description
1	13 – 28 July	Outage of reception system servers. First reception server was affected by a hardware failure and performed no processing at all. However, the server was reachable via ping and therefore the monitoring tool did not sent a notification. The second server was affected by an EKU failure at the same time and transferred less data after 12 July. The third reception server stopped sending GOME files on 26 July (until 29 July) due to a receiver failure of unknown source. As a consequence substantially less data was received during the given time frame. Corrective actions: The first reception server recovered without any external actions after some time. Replacement EKU was ordered and installed for the second reception server. The issues on the third reception server were resolved. In addition, two reception servers from the new reception system (EUMETCast reception system renewal later in 2021) were added in order to support nominal reception and operations. On top of that a PDU retrieval client was created, which retrieved Metop PDUs from the FMI rolling archive. Preventive action: During the occurrence of the reception system outage the EUMETCast reception system renewal was already ongoing to replace the legacy system and to ensure stable and reliable reception of GOME data. The switch to the new reception chain was performed for the offline processing system on 30 November and for the NRT processing system 17 January 2022.
2	26 – 30 September	The HCHO product in the NRT chain could not be completed successfully and the entire product generation came to a halt in the NRT processing system. The root cause behind the non-successful HCHO product generation is related to the fact that no or too few measurements passed the DOAS fitting RMS check for the background correction. This was related to the gradual degradation of the data from the GOME-2 instrument on Metop-A at the end of its lifetime. Corrective action: Adaption of the RMS parameter in order to be able to perform the background correction of the HCHO product Preventive action: Adaption of the HCHO algorithm/processor to the changing viewing geometry of GOME-2A near the end-of-life and the strong degradation of the instrument was also performed to GOME-2B and GOME-2C, since there is a strong likelihood for this to occur also at the end of the lifetimes for the remaining two instruments.

ID	Time period	Description
3	15 November	More L1b PDUs seem to be received than there were PDUs with status "reception confirmed". This offset is due to the deactivation of the Metop-A NRT processing on DLR side on 15 November during the course of the day and the non-availability of the sendlist of this specific day. Corrective action: N/A Preventive action: N/A
4	July	Regeneration of GOME.TC.AGG after exhaustive product reordering and reprocessing due to the reception system outage in July 2021 (see also ID1 in this table). Corrective action: Reordering of L1b orbits from EUMETSAT Order Client, which were either partially missing or completely missing due to the reception system outage. In addition, reprocessing the L2 products as well as regenerating the aggregated products. Peventive action: Switch to new reception chain as per ID 1
5	September	Late generation of GOME.TC.AGG by wrongly configured timer setting for triggering the product generation. The timer setting has not been checked and adapted after rebooting the processing machine. Corrective action: The timer was set correctly manually in order to ensure product triggering at correct time Preventive action: The regular check of the timer setting has been included in the operations procedures
6	December	Late generation of GOME.TC.AGG due to temporal performance related issues on the processing machine. After the shutdown of the processing instances for Metop-A a resource adaption has been performed to adapt for the repealed mission. However, it turned out that temporarily the processing machine was affected by performance issues. There was also a relation to frequent execution of a monitoring script on this machine. Corrective action: The resources on the processing machine were increased. In addition, the execution interval of the monitoring script was adapted to a reasonable value in order to reduce the load on the machine. Preventive action: N/A (the system is well balanced after the resource adaption and adaption of execution interval of the monitoring script)

4. Processing centre: KNMI

4.1. NRT and offline ozone profiles, absorbing aerosol height and index, global tropospheric ozone

4.1.1. Availability

For Level 1b products, the availability is defined as the number of unique L1b PDUs received either via EUMETCast Satellite or EUMETCast Terrestrial (demonstrational dissemination service), divided by the number of L1b PDUs not marked as "not sent" in the EUMETCast Satellite sendlist. This approximation presumes that all PDUs marked as "sent not confirmed" are still available via EUMETCast Terrestrial.

Availability for offline L2 products has been defined in Section 1.4. The availability statistics of KNMI products are presented in Table 4.1 and Table 4.2. If the availability requirements have been violated, those values are marked with red colour, identified by numbers and reported in Table 4.11.

Tropospheric ozone products are included in the ozone profile products and have the same statistics. The same applies to scattering aerosol index products which are included in the absorbing aerosol index products.

Note: Statistics for December 2021 are missing due to Metop-A de-commissioning.

Table 4.1. Availability of Metop-A L1b PDUs, ozone profile products and aerosol products during the reporting period

Product Identifier	Product Name	7/2021	8/2021	9/2021	10/2021	11/2021	12/2021
EUMETCast							
L1b	PDUs received / sent	14879/14880 100 %	14874/14874 100 %	14396/14397 100 %	14778/14806 99.8 %	6912/6720 103 %	
O3M-38.1	NRT high-resolution ozone profile	100 %	100 %	99.9 %	99.7 %	100 %	
O3M-68	NRT absorbing aerosol height	100 %	100 %	99.9 %	99.4 %	100 %	
O3M-62.1	NRT absorbing aerosol index from PMDs	100 %	100 %	99.9 %	99.4 %	100 %	
WMO/GTS							
O3M-38.1	NRT high-resolution ozone profile	100 %	100 %	99.9 %	100 %	100 %	
FMI archive							
O3M-39.1	Offline high-resolution ozone profile	100 %	100 %	100 %	100 %	100 %	
O3M-69	Offline absorbing aerosol height	100 %	100 %	100 %	100 %	100 %	

Product Identifier	Product Name	7/2021	8/2021	9/2021	10/2021	11/2021	12/2021
O3M-63.1	Offline absorbing aerosol index from PMDs	100 %	100 %	100 %	100 %	100 %	

Table 4.2. Availability of Metop-B L1b PDUs, ozone profile products and aerosol products during the reporting period

Product Identifier	Product Name	7/2021	8/2021	9/2021	10/2021	11/2021	12/2021
EUMETCast							
L1b	PDUs received / sent	14879/14880 100 %	14880/14880 100 %	14400/14400 100 %	14855/14880 99.8 %	14399/14399 100 %	14878/14878 100 %
O3M-47.1	NRT high-resolution ozone profile	100 %	100 %	100 %	99.7 %	100 %	100 %
O3M-78	NRT absorbing aerosol height	100 %	100 %	100 %	99.7 %	100 %	100 %
O3M-72.1	NRT absorbing aerosol index from PMDs	100 %	100 %	100 %	99.7 %	100 %	100 %
WMO/GTS							
O3M-47.1	NRT high-resolution ozone profile	100 %	100 %	100 %	100 %	100 %	100 %
FMI archive							
O3M-48.1	Offline high-resolution ozone profile	100 %	100 %	100 %	100 %	100 %	100 %
O3M-79	Offline absorbing aerosol height	100 %	100 %	100 %	100 %	100 %	100 %
O3M-73.1	Offline absorbing aerosol index from PMDs	100 %	100 %	100 %	100 %	100 %	100 %

Table 4.3. Availability of Metop-C L1b PDUs, ozone profile products and aerosol products during the reporting period

Product Identifier	Product Name	7/2021	8/2021	9/2021	10/2021	11/2021	12/2021
EUMETCast							
L1b	PDUs received / sent	14880/14880 100 %	14878/14880 100 %	14400/14400 100 %	14867/14867 100 %	14400/14400 100 %	14804/14804 100 %
O3M-311	NRT high-resolution ozone profile	100 %	100 %	100 %	99.9 %	100 %	100 %

Product Identifier	Product Name	7/2021	8/2021	9/2021	10/2021	11/2021	12/2021
O3M-364	NRT absorbing aerosol height	100 %	100 %	100 %	99.9 %	100 %	100 %
O3M-362	NRT absorbing aerosol index from PMDs	100 %	100 %	100 %	99.9 %	100 %	100 %
WMO/GTS							
O3M-311	NRT high-resolution ozone profile	100 %	100 %	100 %	99.9 %	100 %	100 %
FMI archive							
O3M-312	Offline high-resolution ozone profile	100 %	100 %	100 %	100 %	100 %	100 %
O3M-365	Offline absorbing aerosol height	100 %	100 %	100 %	100 %	100 %	100 %
O3M-363	Offline absorbing aerosol index from PMDs	100 %	100 %	100 %	100 %	100 %	100 %

4.1.2. Timeliness

Timeliness indicates the elapsed time between sensing and product dissemination. Timeliness requirements are 3 hours for NRT products and 15 days for offline products. If the requirements have been violated, those values are marked with red colour. In addition, the violations are identified by numbers and reported in Table 4.11 if they have caused the availability values to drop below the allowed limits.

Note: timeliness violations are not listed as anomalies if the availability is above the limit.

The values in Table 4.4 and Table 4.5 indicate elapsed times (days, hours and minutes in the format [ddT]hh:mm) from sensing to EUMETCast and WMO/GTS (NRT) or archive upload (offline). In each cell, the values from top to bottom represent observed monthly average, minimum and maximum times.

Tropospheric ozone products are included in the ozone profile products and have the same statistics.

Note: Statistics for December 2021 are missing due to Metop-A de-commissioning.

Table 4.4. Timeliness of Metop-A ozone profile and aerosol products during the reporting period

Product Identifier	Product Name	7/2021	8/2021	9/2021	10/2021	11/2021	12/2021
EUMETCast							
O3M-38.1	NRT high-resolution ozone profile	avg: 01:32 min: 00:39 max: 02:07	avg: 01:35 min: 00:36 max: 02:21	avg: 01:37 min: 00:32 max: 03:21	avg: 01:38 min: 00:32 max: 02:14	avg: 01:37 min: 01:07 max: 01:58	
O3M-68	NRT absorbing aerosol height	avg: 01:26 min: 00:35 max: 01:54	avg: 01:27 min: 00:33 max: 02:43	avg: 01:29 min: 00:32 max: 03:21	avg: 01:32 min: 00:32 max: 04:33	avg: 01:30 min: 01:07 max: 01:50	

O3M-62.1	NRT absorbing aerosol index from PMDs	avg: 01:26 min: 00:35 max: 01:54	avg: 01:27 min: 00:33 max: 02:05	avg: 01:29 min: 00:32 max: 03:22	avg: 01:32 min: 00:32 max: 04:33	avg: 01:30 min: 01:07 max: 01:51	
WMO/GTS							
O3M-38.1	NRT high-resolution ozone profile	avg: 01:33 min: 00:39 max: 02:09	avg: 01:36 min: 00:37 max: 02:32	avg: 01:38 min: 00:33 max: 03:24	avg: 01:39 min: 00:33 max: 02:15	avg: 01:38 min: 01:07 max: 01:59	
FMI archive							
O3M-39.1	Offline high-resolution ozone profile	avg: 08:03 min: 07:20 max: 02T03:20	avg: 08:02 min: 07:20 max: 02T03:25	avg: 07:57 min: 07:11 max: 02T02:37	avg: 07:47 min: 07:05 max: 08:50	avg: 07:42 min: 07:05 max: 08:23	
O3M-69	Offline absorbing aerosol height	avg: 07:58 min: 07:15 max: 08:36	avg: 08:00 min: 07:18 max: 02T03:15	avg: 07:57 min: 07:18 max: 02T02:27	avg: 07:47 min: 07:09 max: 08:54	avg: 07:40 min: 07:00 max: 08:18	
O3M-63.1	Offline absorbing aerosol index from PMDs	avg: 07:55 min: 07:19 max: 08:37	avg: 07:58 min: 07:13 max: 02T02:25	avg: 07:54 min: 07:10 max: 02T02:37	avg: 07:44 min: 07:07 max: 08:55	avg: 07:40 min: 07:07 max: 08:13	

Table 4.5. Timeliness of Metop-B ozone profile and aerosol products during the reporting period

Product Identifier	Product Name	7/2021	8/2021	9/2021	10/2021	11/2021	12/2021
EUMETCast							
O3M-47.1	NRT high-resolution ozone profile	avg: 01:03 min: 00:32 max: 02:08	avg: 01:05 min: 00:30 max: 02:05	avg: 01:04 min: 00:30 max: 02:11	avg: 01:08 min: 00:30 max: 02:06	avg: 01:09 min: 00:30 max: 02:12	avg: 01:07 min: 00:41 max: 02:09
O3M-78	NRT absorbing aerosol height	avg: 00:49 min: 00:30 max: 01:48	avg: 00:52 min: 00:29 max: 01:48	avg: 00:51 min: 00:27 max: 02:06	avg: 00:52 min: 00:29 max: 01:52	avg: 00:53 min: 00:29 max: 01:50	avg: 00:51 min: 00:26 max: 01:47
O3M-72.1	NRT absorbing aerosol index from PMDs	avg: 00:49 min: 00:30 max: 01:48	avg: 00:52 min: 00:29 max: 01:48	avg: 00:51 min: 00:26 max: 02:06	avg: 00:52 min: 00:29 max: 01:52	avg: 00:53 min: 00:29 max: 01:50	avg: 00:51 min: 00:26 max: 01:47
WMO/GTS							
O3M-47.1	NRT high-resolution ozone profile	avg: 01:04 min: 00:34 max: 02:09	avg: 01:06 min: 00:31 max: 02:06	avg: 01:05 min: 00:31 max: 02:09	avg: 01:09 min: 00:31 max: 02:07	avg: 01:10 min: 00:31 max: 02:14	avg: 01:08 min: 00:41 max: 02:10
FMI archive							
O3M-48.1	Offline high-resolution ozone profile	avg: 07:23 min: 06:32 max: 02T03:04	avg: 07:25 min: 06:35 max: 08:07	avg: 07:29 min: 06:41 max: 09:11	avg: 07:34 min: 06:50 max: 02T03:10	avg: 07:55 min: 06:53 max: 01T06:37	avg: 07:26 min: 06:50 max: 08:11
O3M-79	Offline absorbing aerosol height	avg: 07:15 min: 06:33 max: 08:15	avg: 07:21 min: 06:36 max: 08:00	avg: 07:26 min: 06:45 max: 09:06	avg: 07:33 min: 06:51 max: 02T03:00	avg: 07:51 min: 06:54 max: 01T06:37	avg: 07:24 min: 06:51 max: 08:06

Product Identifier	Product Name	7/2021	8/2021	9/2021	10/2021	11/2021	12/2021
O3M-73.1	Offline absorbing aerosol index from PMDs	avg: 07:12 min: 06:33 max: 08:03	avg: 07:21 min: 06:36 max: 08:15	avg: 07:23 min: 06:36 max: 08:00	avg: 07:30 min: 06:42 max: 02T02:30	avg: 07:49 min: 06:45 max: 01T06:37	avg: 07:22 min: 06:45 max: 08:09

Table 4.6. Timeliness of Metop-C ozone profile and aerosol products during the reporting period

Product Identifier	Product Name	7/2021	8/2021	9/2021	10/2021	11/2021	12/2021
EUMETCast							
O3M-311	NRT high-resolution ozone profile	avg: 01:51 min: 00:37 max: 02:24	avg: 01:56 min: 00:33 max: 02:37	avg: 01:54 min: 00:32 max: 02:54	avg: 01:57 min: 00:36 max: 03:53	avg: 01:54 min: 01:09 max: 02:21	avg: 01:52 min: 01:08 max: 02:32
O3M-364	NRT absorbing aerosol height	avg: 01:37 min: 00:34 max: 02:05	avg: 01:43 min: 00:33 max: 02:16	avg: 01:41 min: 00:32 max: 02:54	avg: 01:43 min: 00:35 max: 03:44	avg: 01:40 min: 01:09 max: 02:00	avg: 01:39 min: 01:08 max: 02:10
O3M-362	NRT absorbing aerosol index from PMDs	avg: 01:37 min: 00:34 max: 02:05	avg: 01:43 min: 00:33 max: 02:15	avg: 01:41 min: 00:32 max: 02:56	avg: 01:43 min: 00:35 max: 03:44	avg: 01:40 min: 01:09 max: 02:00	avg: 01:39 min: 01:08 max: 02:10
WMO/GTS							
O3M-311	NRT high-resolution ozone profile	avg: 01:51 min: 00:37 max: 02:25	avg: 01:57 min: 00:34 max: 02:39	avg: 01:54 min: 00:33 max: 02:57	avg: 01:57 min: 00:36 max: 03:52	avg: 01:55 min: 01:10 max: 02:22	avg: 01:53 min: 01:09 max: 02:32
FMI archive							
O3M-312	Offline high-resolution ozone profile	avg: 08:13 min: 07:32 max: 02T02:47	avg: 08:09 min: 07:29 max: 08:47	avg: 08:04 min: 07:22 max: 08:46	avg: 08:01 min: 07:17 max: 09:23	avg: 08:32 min: 07:10 max: 02T02:53	avg: 07:55 min: 07:17 max: 09:02
O3M-365	Offline absorbing aerosol height	avg: 08:05 min: 07:30 max: 08:39	avg: 08:10 min: 07:30 max: 08:48	avg: 08:00 min: 07:18 max: 08:36	avg: 08:01 min: 07:12 max: 09:18	avg: 08:26 min: 07:12 max: 02T02:48	avg: 07:54 min: 07:15 max: 08:57
O3M-363	Offline absorbing aerosol index from PMDs	avg: 08:02 min: 07:27 max: 08:50	avg: 08:07 min: 07:30 max: 08:44	avg: 07:58 min: 07:06 max: 08:35	avg: 07:57 min: 07:15 max: 08:48	avg: 08:28 min: 07:09 max: 02T02:54	avg: 07:51 min: 07:09 max: 09:00

4.2. Services, main events and anomalies

Tropospheric ozone products are included in the ozone profile products and have the same statistics.

Table 4.7. Number of products sent to FMI archive[1]

Product Identifier	Product Name	Metop satellite	7/2021	8/2021	9/2021	10/2021	11/2021	12/2021
O3M-39.1	Offline high-resolution ozone profile	A	439	440	425	437	205	
O3M-48.1		B	439	440	425	438	426	439
O3M-312		C	440	439	423	440	425	435
O3M-69	Offline absorbing aerosol height	A	439	440	425	437	205	
O3M-79		B	439	440	425	438	426	439
O3M-365		C	440	439	423	440	425	435
O3M-63.1	Offline absorbing aerosol index from PMDs	A	439	440	425	437	205	
O3M-73.1		B	439	440	425	438	426	439
O3M-363		C	440	439	423	440	425	435

Table 4.8. Number of products stored locally at KNMI[2]

Product Identifier	Product Name	Metop satellite	7/2021	8/2021	9/2021	10/2021	11/2021	12/2021
O3M-38.1	NRT high-resolution ozone profile	A	8166	8246	8051	8308	3876	
O3M-47.1		B	8198	8238	8022	8257	8046	8348
O3M-311		C	8206	8234	7959	8298	8035	8255
O3M-68	NRT absorbing aerosol height	A	8167	8246	8051	8308	3876	
O3M-78		B	8199	8238	8022	8257	8046	8348
O3M-364		C	8207	8234	7959	8298	8035	8255
O3M-62.1	NRT absorbing aerosol index from PMDs	A	8167	8246	8051	8308	3876	
O3M-72.1		B	8199	8238	8022	8257	8046	8348
O3M-362		C	8207	8234	7959	8298	8035	8255
O3M-39.1	Offline high-resolution ozone profile	A	439	440	425	437	205	
O3M-48.1		B	439	440	425	438	426	439
O3M-312		C	440	439	423	440	425	435
O3M-69	Offline absorbing aerosol height	A	439	440	425	437	205	
O3M-79		B	439	440	425	438	426	439
O3M-365		C	440	439	423	440	425	435

Product Identifier	Product Name	Metop satellite	7/2021	8/2021	9/2021	10/2021	11/2021	12/2021
O3M-63.1	Offline absorbing aerosol index from PMDs	A	439	440	425	437	205	
O3M-73.1		B	439	440	425	438	426	439
O3M-363		C	440	439	423	440	425	435

Table 4.9. EUMETCast and WMO/GTS uploads[3]

Product Identifier	Product Name	Metop satellite	7/2021	8/2021	9/2021	10/2021	11/2021	12/2021
O3M-38.1	NRT high-resolution ozone profile	A	8166/8166	8246/8246	8043/8042	8308/8308	3876/3876	
O3M-47.1		B	8198/8198	8238/8238	8022/8022	8257/8257	8046/8046	8348/8348
O3M-311		C	8206/8206	8234/8234	7959/7959	8289/8289	8035/8035	8255/8255
O3M-68	NRT absorbing aerosol height	A	8167	8246	8043	8289	3876	
O3M-78		B	8199	8238	8022	8257	8046	8348
O3M-364		C	8207	8234	7959	8290	8035	8255
O3M-62.1	NRT absorbing aerosol index from PMDs	A	8167	8246	8043	8289	3876	
O3M-72.1		B	8199	8238	8022	8257	8046	8348
O3M-362		C	8207	8234	7959	8290	8035	8255

[1] Products are archived in HDF5 format.

[2] Products are stored for 3 years (in HDF5 and BUFR formats).

[3] NRT high-resolution ozone profile is disseminated via EUMETCast and WMO/GTS in BUFR format. NRT absorbing aerosol index and NRT absorbing aerosol index from PMDs are disseminated only via EUMETCast (in HDF5 and BUFR formats).

Table 4.10 lists the main events (product/service/hardware/software updates etc.) at KNMI during the reporting period.

Table 4.10. Main events at KNMI during the reporting period

Date	Description
	Nothing to report.

Table 4.11 lists the main local and external anomalies at KNMI during the reporting period. Corrective and preventive actions should be provided also when applicable.

Table 4.11. Main local and external anomalies affecting KNMI systems and performance during the reporting period

ID	Time period	Description
		Nothing to report.

5. Processing centre: DMI

5.1. NRT clear-sky and cloud-corrected UV index

5.1.1. Availability

NUV product is required to be produced every day, either on the basis of new GOME ATO input or in the case of ATO delivery failure based on back-up total ozone data (ECMWF or climatology).

Availability requirement for NUV has been defined in Section 1.4. The availability statistics of DMI products are presented in Table 5.1. If the requirement is violated, those values are marked with red colour, identified by numbers and reported in Table 5.5.

Table 5.1. Availability of NRT UV products during the reporting period

Product Identifier	Product Name	7/2021	8/2021	9/2021	10/2021	11/2021	12/2021
O3M-409	NRT UV index, clear-sky	100 %	100 %	100 %	100 %	100 %	100 %
O3M-410	NRT UV index, cloud-corrected						

5.1.2. Timeliness

Timeliness requirement for NUV says that the final NUV product is to be delivered to users no later than two hours after receiving the ATO input and not later than 04:00 UTC. Processing is started at 02:45 UTC thus the maximum processing time allowed is 1 hour 15 min. If the timeliness requirement is violated, those values are marked with red colour. In addition, the violations are identified by numbers and reported in Table 5.5 if they have caused the availability values to drop below the allowed limits.

Days where no products are produced or could be delivered to users (as indicated in Table 5.1) are not included in Table 5.2.

Note: timeliness violations are not listed as anomalies if the availability is above the limit.

The values in Table 5.2 indicate elapsed processing times (hours, minutes and seconds in the format [hh:]mm:ss). In each cell, the values from top to bottom represent observed monthly average, minimum and maximum processing times.

Table 5.2. Timeliness of NRT UV products during the reporting period

Product Identifier	Product Name	7/2021	8/2021	9/2021	10/2021	11/2021	12/2021
O3M-409	NRT UV index, clear-sky	avg: 9:25 min: 7:21 max: 38:00	avg: 7:29 min: 7:22 max: 7:48	avg: 8:53 min: 7:23 max: 12:35	avg: 10:02 min: 9:09 max: 12:46	avg: 10:33 min: 9:11 max: 14:46	avg: 10:29 min: 9:06 max: 14:36
O3M-410	NRT UV index, cloud-corrected						

5.2. Services, main events and anomalies

Table 5.3. Number of products stored locally at DMI[1]

Description of service / event	7/2021	8/2021	9/2021	10/2021	11/2021	12/2021
Storage statistics						
Number of stored products (NRT UV index, clear-sky)	31	31	30	31	30	31
Number of stored products (NRT UV index, cloud-corrected)	31	31	30	31	30	31
Total size of stored products (MB)	248	248	240	248	240	248

[1] NUV products are stored at the DMI at least until the end of the Metop programs.

Table 5.4 lists the main events (product/service/hardware/software updates etc.) at DMI during the reporting period.

Table 5.4. Main events at DMI during the reporting period

Date	Event
	Nothing to report.

Table 5.5 lists the main local and external anomalies at DMI during the reporting period. Corrective and preventive actions should be provided also when applicable.

Table 5.5. Main local and external anomalies affecting DMI systems and performance during the reporting period

ID	Time period	Description
		Nothing to report.

6. Processing centre: EUMETSAT

6.1. NRT IASI CO, SO2, HNO3 and ozone profile

6.1.1. Availability

For Level 1c products, the availability is defined as the number of available PDUs divided by the number of maximum expected PDUs.

For NRT products, the availability requirement is 97.5 % and it is defined by the ratio of the number of in time processed and disseminated products to the number of maximum expected input products (L1c PDUs) per month.

The availability statistics of EUMETSAT products are presented in Table 6.1, Table 6.2 and Table 6.3. If the availability requirements have been violated, those values are marked with red colour, identified by numbers and reported in Table 6.9 and Table 6.10.

This reporting period also covers Metop-A end-of-life activities which have also been depicted in Table 6.9. Note that, in this frame, all IASI-A missions and services have been terminated, therefore IASI-A data and products were no longer available to the user after the 15th October.

Note that in the frame of this product processing centre being the EUMETSAT HQ in Darmstadt, the L1c data is directly available to the algorithm, i.e., its availability is not dependable of EUMETCast dissemination. Furthermore, since there is no relay of information from *Satellite* processing centres, the L2 product availability in the following tables concern the end-to-end availability as they were recorded in the EUMETSAT Reference Receiving Stations.

Metop-C based data have been added to this report given that they were operationally distributed during the reporting period, even if holding the "Demonstrational" status. The same happens to HNO3 and ozone profile products for all satellites.

Table 6.1. Availability of Metop-A L1c PDUs and IASI NRT products during the reporting period

Product Identifier	Product Name	7/2021	8/2021	9/2021	10/2021	11/2021	12/2021
L1c	PDUs available / PDUs expected	14853/14880	14860/14880	10806/14400	9791/14880		
L1c	Availability	99.82%	99.87%	75.0 % (5)	65.8 % (5)		
O3M-181	NRT IASI CO	98.61%	99.13%	73.4 % (5)	48.8 % (5)		
O3M-57	NRT IASI SO2	98.61%	99.13%	73.4 % (5)	48.8 % (5)		
O3M-81	NRT IASI HNO3	98.62%	99.13%	73.4 % (5)	48.8 % (5)		
O3M-49	NRT IASI ozone profile	98.62%	99.13%	73.4 % (5)	48.8 % (5)		

Table 6.2. Availability of Metop-B L1c PDUs and IASI NRT products during the reporting period

Product Identifier	Product Name	7/2021	8/2021	9/2021	10/2021	11/2021	12/2021
L1c	PDUs available / PDUs expected	13397/14880	14876/14880	14375/14400	14821/14880	14344/14400	14863/14880
L1c	Availability	90.0 % (2,3,6)	100 %	99.8 %	99.6 %	99.6 %	99.9 %
O3M-80	NRT IASI CO	89.7 % (2,3,6)	98.8 %	99.3 %	99.7 %	99.8 %	99.2 %
O3M-57	NRT IASI SO2	89.7 % (2,3,6)	98.8 %	99.3 %	99.7 %	99.8 %	99.2 %
O3M-81	NRT IASI HNO3	89.7 % (2,3,6)	98.8 %	99.3 %	99.7 %	99.8 %	99.2 %
O3M-49	NRT IASI ozone profile	89.7 % (2,3,6)	98.8 %	99.3 %	99.7 %	99.8 %	99.2 %

Table 6.3. Availability of Metop-C L1c PDUs and IASI NRT products during the reporting period

Product Identifier	Product Name	7/2021	8/2021	9/2021	10/2021	11/2021	12/2021
L1c	PDUs available / PDUs expected	14584/14880	14870/14880	14243/14400	14833/14880	14281/14400	14772/14880
L1c	Availability	98.0 %	99.9 %	98.9 %	99.7 %	99.2 %	99.3 %
O3M-352	NRT IASI CO	97.1 % (1,4)	98.8 %	98.9 %	99.2 %	99.4 %	99.1 %
O3M-377	NRT IASI SO2	97.1 % (1,4)	98.8 %	98.9 %	99.2 %	99.4 %	99.1 %
O3M-336	NRT IASI HNO3	97.1 % (1,4)	98.8 %	98.9 %	99.2 %	99.4 %	99.1 %
O3M-315	NRT IASI ozone profile	97.1 % (1,4)	98.8 %	98.9 %	99.2 %	99.4 %	99.1 %

6.1.2. Timeliness

Timeliness indicates the elapsed time between sensing and product dissemination. Timeliness requirement is 3 hours for NRT products. If the requirements have been violated, those values are marked with red colour. In addition, the violations are identified by numbers and reported in Table 6.10 if they have caused the availability values to drop below the allowed limits.

Note: timeliness violations are not listed as anomalies if the availability is above the limit.

The values in Table 6.4, Table 6.5 and Table 6.6 indicate elapsed times (hours and minutes in the format hh:mm) from sensing to EUMETCast Reference Receiving Station, i.e., end-to-end timeliness. In each cell, the values from top to bottom represent observed monthly average, minimum and maximum times.

Table 6.4. Timeliness of Metop-A IASI NRT products during the reporting period

Product Identifier	Product Name	7/2021	8/2021	9/2021	10/2021	11/2021	12/2021
O3M-181	NRT IASI CO	avg: 01:41 min: 00:53 max: 02:23	avg: 01:36 min: 00:52 max: 02:28	avg: 01:34 min: 00:38 max: 02:20	avg: 01:33 min: 00:42 max: 03:19		
O3M-57	NRT IASI SO2	avg: 01:41 min: 00:53 max: 02:23	avg: 01:36 min: 00:52 max: 02:28	avg: 01:34 min: 00:38 max: 02:20:	avg: 01:33 min: 00:42 max: 03:12		
O3M-81	NRT IASI HNO3	avg: 01:41 min: 00:53 max: 02:23	avg: 01:36 min: 00:52 max: 02:28	avg: 01:34 min: 00:38 max: 02:20	avg: 01:33 min: 00:42 max: 03:16		
O3M-49	NRT IASI ozone profile	avg: 01:41 min: 00:53 max: 02:23	avg: 01:36 min: 00:52 max: 02:28	avg: 01:34 min: 00:38 max: 02:20	avg: 01:33 min: 00:42 max: 03:15		

Table 6.5. Timeliness of Metop-B IASI NRT products during the reporting period

Product Identifier	Product Name	7/2021	8/2021	9/2021	10/2021	11/2021	12/2021
O3M-80	NRT IASI CO	avg: 01:07 min: 00:43 max: 02:12	avg: 01:07 min: 00:41 max: 01:54	avg: 01:06 min: 00:40 max: 02:10	avg: 01:06 min: 00:42 max: 03:07	avg: 01:06 min: 00:42 max: 03:15	avg: 01:03 min: 00:38 max: 01:55
O3M-57	NRT IASI SO2	avg: 01:07 min: 00:43 max: 02:12	avg: 01:07 min: 00:41 max: 01:54	avg: 01:06 min: 00:40 max: 02:10	avg: 01:06 min: 00:42 max: 03:07	avg: 01:06 min: 00:42 max: 03:15	avg: 01:03 min: 00:38 max: 01:55
O3M-81	NRT IASI HNO3	avg: 01:07 min: 00:43 max: 02:12	avg: 01:07 min: 00:41 max: 01:54	avg: 01:06 min: 00:40 max: 02:10	avg: 01:06 min: 00:42 max: 03:04	avg: 01:06 min: 00:42 max: 03:15	avg: 01:03 min: 00:38 max: 01:56
O3M-49	NRT IASI ozone profile	avg: 01:07 min: 00:43 max: 02:12	avg: 01:07 min: 00:41 max: 01:54	avg: 01:06 min: 00:40 max: 02:10	avg: 01:06 min: 00:42 max: 03:07	avg: 01:06 min: 00:42 max: 03:15	avg: 01:03 min: 00:38 max: 01:56

Table 6.6. Timeliness of Metop-C IASI NRT products during the reporting period

Product Identifier	Product Name	7/2021	8/2021	9/2021	10/2021	11/2021	12/2021
O3M-352	NRT IASI CO	avg: 01:42 min: 00:48 max: 02:28	avg: 01:44 min: 00:54 max: 02:30	avg: 01:41 min: 00:54 max: 02:27	avg: 01:44 min: 00:46 max: 03:46	avg: 01:37 min: 00:53 max: 02:47	avg: 01:38 min: 00:46 max: 02:39
O3M-377	NRT IASI SO2	avg: 01:42 min: 00:48 max: 02:28	avg: 01:44 min: 00:54 max: 02:31	avg: 01:41 min: 00:54 max: 02:27	avg: 01:44 min: 00:46 max: 03:46	avg: 01:37 min: 00:53 max: 02:47	avg: 01:38 min: 00:46 max: 02:39
O3M-336	NRT IASI HNO3	avg: 01:42 min: 00:48 max: 02:28	avg: 01:44 min: 00:54 max: 02:31	avg: 01:41 min: 00:54 max: 02:27	avg: 01:44 min: 00:46 max: 03:46	avg: 01:37 min: 00:53 max: 02:47	avg: 01:38 min: 00:46 max: 02:39
O3M-315	NRT IASI ozone profile	avg: 01:42 min: 00:48 max: 02:28	avg: 01:44 min: 00:54 max: 02:31	avg: 01:41 min: 00:54 max: 02:27	avg: 01:44 min: 00:46 max: 03:46	avg: 01:37 min: 00:53 max: 02:47	avg: 01:38 min: 00:46 max: 02:39

6.2. Services, main events and anomalies

Table 6.7. Number of products stored locally at EUMETSAT[1]

Product Identifier	Product Name	Metop satellite	7/2021	8/2021	9/2021	10/2021	11/2021	12/2021
O3M-181		A	14791	14781	10609	8648		
O3M-80	NRT IASI CO	B	13402	14710	14310	14854	14374	14781
O3M-352		C	14494	14727	14246	14774	14335	14774
O3M-57		A	14791	14781	10610	8648		
	NRT IASI SO2	B	13402	14711	14310	14854	14374	14781
O3M-377		C	14493	14727	14246	14774	14335	14774
O3M-81		A	14791	14781	10610	8648		
	NRT IASI HNO3	B	13402	14711	14310	14854	14374	14781
O3M-336		C	14493	14727	14246	14774	14335	14774
O3M-49		A	14791	14781	10610	8648		
	NRT IASI ozone profile	B	13402	14711	14310	14854	14374	14781
O3M-315		C	14493	14727	14246	14774	14335	14774

[1] PDUs are concatenated back to orbit-based products before being stored

Table 6.8. EUMETCast uploads[1]

Product Identifier	Product Name	Metop satellite	7/2021	8/2021	9/2021	10/2021	11/2021	12/2021
O3M-181	NRT IASI CO	A	14732	14743	10594	7256		
O3M-80		B	13363	14687	14256	14818	14362	14680
O3M-352		C	14456	14681	14205	14725	14306	14674
O3M-57	NRT IASI SO2	A	14734	14742	10595	7257		
		B	13365	14687	14255	14819	14362	14679
O3M-377		C	14454	14681	14205	14724	14305	14673
O3M-81	NRT IASI HNO3	A	14733	14742	10593	7259		
		B	13368	14688	14253	14819	14363	14679
O3M-336		C	14455	14681	14205	14724	14306	14676
O3M-49	NRT IASI ozone profile	A	14733	14743	10594	7259		
		B	13367	14688	14253	14818	14362	14678
O3M-315		C	14454	14681	14205	14725	14306	14675

[1] NRT IASI products are disseminated via EUMETCast (in BUFR format)

Table 6.9 lists the main events (product/service/hardware/software updates etc.) at EUMETSAT during the reporting period.

Table 6.9. Main planned activities at EUMETSAT during the reporting period

ID	Date	Description
1	19 July	Metop-C IASI external calibration
2	20 July	Metop-B IASI instrument maintenance
3	21 July	Metop-B/C external calibration. Lunar acquisition. CS2 campaign.
4	27 – 28 July	Metop-C IASI instrument maintenance
5	6 -7 September	Metop-A technology tests. Testing of IASI redundant components. Satellite maintenance. SSR recovery of latched partition.
	16 September – 15 October	Metop-A technology test. IASI will scan with oversampling causing data quality degradation.
	23 – 24 September	Metop-A external calibration (Moon intrusion)
	11 – 12 October	Metop-A technology test. Yaw bias test. Change of spacecraft altitude with geocentric pointing with the addition of -4 degrees yaw bias.
	13 – 14 October	Metop-A technology test. SHDESAT test. Test on reaction wheel management.
	15 October	Metop-A IASI end of all mission services

Table 6.10 lists the main local and external anomalies at EUMETSAT during the reporting period. Corrective and preventive actions should be provided also when applicable.

Table 6.10. Main local and external anomalies affecting EUMETSAT systems and performance during the reporting period

ID	Time period	Description
6	20 – 23 July	Metop-B (M01) memory error after reboot Corrective action: Bypass the self-test after initialising the ICU and command the ICU to RUN, RESET mode. Payload avionics will still communicate correctly with the ICU as the errors are IASI internal. Preventive action: Update contingency procedures

7. Validation and quality monitoring

This section describes the validation status and validation/quality monitoring activities of NRT and offline data products during the reporting period. Validation reports for data records are found from https://acsaf.org/valreps.html

Reference documents are listed in Section 1.3 and accuracy requirements in Section 1.5.

7.1. Total ozone column products

Table 7.1. Validation status of total ozone column products

Product Identifier	Product Name	Accuracy	Reference	Validating Institute	Correlative data sources
O3M-01.1	NRT total O3	Fulfils threshold accuracy requirement	RD5	AUTH	World Ozone Mapping Centre
O3M-41.1					
O3M-300			RD27		
O3M-06.1	Offline total O3	Fulfils threshold accuracy requirement	RD5	AUTH	World Ozone and Ultraviolet Radiation Data Center (WOUDC), of the World Meteorological Organization, (WMO), Global Atmosphere Watch, (GAW)
O3M-42.1					
O3M-301			RD27		

Validation results can be found in more detail on the AC SAF validation & quality assessment website at http://acsaf.physics.auth.gr/eumetsat/validation/near_real and http://acsaf.physics.auth.gr/eumetsat/validation/offline

7.1.1. GOME-2A, GOME-2B and GOME-2C total ozone column validation

This summary presents the validation activities for total ozone column products (TOCs), reported by the GOME-2/Metop-A, GOME-2/Metop-B and GOME-2/Metop-C instruments. Members of the Laboratory of Atmospheric Physics of the Aristotle University of Thessaloniki (LAP/AUTH), Thessaloniki, Greece, involved in the validation activities include Professor, Dr. Dimitris Balis, Special Teaching Fellow & Researcher, Dr. Katerina Garane and Research Associate, Dr. MariLiza Koukouli.

During the reporting period, the operational validation of offline total ozone and NRT total ozone products continued as per previous periods.

7.1.1.1 Update of database for reference ground-based data

For the nominal validation, the ground-based TOCs from Brewer, Dobson and M-124 instruments reported to the World Ozone and Ultraviolet Radiation Data Centre (WOUDC), are employed. WOUDC is one of the World Data Centres which are part of the Global Atmosphere Watch (GAW) programme of the World Meteorological Organization (WMO). For the quality of the reference ground-based data used for the validation of the total ozone products, updated information were extracted from recent inter-comparisons and calibration records. This continuously updated selection of ground-based measurements has already been used numerous times in the validation and analysis of global total ozone records such as the inter-comparison between the OMI/Aura TOMS and OMI/Aura DOAS algorithms [Balis *et al.*, 2007a], the validation of ten years of GOME/ERS-2 ozone record [Balis *et al.*, 2007b], the validation of the updated version of the

OMI/Aura TOMS algorithm [Antón *et al.*, 2009], the GOME-2/Metop-A validation [Loyola *et al.*, 2011; Koukouli *et al.*, 2012], the GOME-2/Metop-B validation [Hao et al., 2014] and the evaluation of the European Space Agency's Ozone Climate Change Initiative project [O$_3$-CCI] TOCs [Koukouli *et al.*, 2015, Garane *et al.*, 2018], as well as in TROPOMI/S5P TOCs validation [Garane et al., 2019]. In all the aforementioned works, LAP/AUTH assumes the leading role in the validation efforts. The number of WOUDC ground-based stations used in the full operational periods of the two instruments, alongside the mean difference between ground- and space-based TOC estimates is given in Table 7.2.

7.1.1.2   GOME-2A, GOME-2B and GOME-2C TOC validation | The Dobson comparisons

GOME-2A, GOME-2B and GOME-2C OTO data for the period January 2007 to December 2022 have been downloaded, quality assured and pre-processed in order to perform the validation strategies. The GDP-4.8 algorithm is the latest version of the GDP-4.x suite of algorithms that have been used for the operational processing of GOME-2A and GOME-2B total ozone columns. GOME-2C is processed with GDP-4.9. The main differences between GDP-4.8 and GDP-4.9 concern the SO$_2$ vertical column retrieval. For ozone only minor updates have been performed, such as the optimization of the slit function, the introduction of a pseudo absorber for possible orbital variations of the resolution etc. Therefore, the ozone columns from GOME-2C can be assumed to be similar to the respective data from GOME-2 on Metop-B and Metop-A, analyzed with the previous version of the algorithm.

This period's satellite-to-ground-based measurements comparisons were performed and were added to the existing time series. The majority of the quality-assured ground-based Brewer and Dobson TOCs are reported to the WOUDC repository between 3 and 6 months after measurement, which accounts for the last couple of months missing from the comparative plots shown below. This is a common reporting feature, quite unavoidable.

The plots shown in Figure 7.1 show the status of the GOME-2A and GOME-2B since the beginning of each individual mission in the form of a monthly mean time-series of the percentage differences between each sensor and the Dobson stations (Northern Hemisphere stations to the left and Southern Hemisphere stations to the right). Focusing on the monthly mean time series, both for the Northern (NH-left) as well as the Southern Hemisphere (SH -right), the differences appear well-stable in time and within -1 to +2.5 % to the ground network, depending on the season.

This seasonality in the differences between satellite and ground-based Dobson observations is a well-known feature which appears in most operational and scientific satellite TOC comparisons, see for e.g. the validation of the OMI/Aura products [Balis *et al.*, 2007a], the GOME/ERS-2 product [Balis *et al.*, 2007b] and even the recent GOME/ERS-2, SCIAMACHY/Envisat and GOME-2/Metop-A ESA products [Koukouli *et al.*, 2015, Garane *et al.*, 2018]. The reasons have to do with the treatment of the variability of the stratospheric temperature and how that affects the ozone absorption coefficients used in the different algorithms [Fragkos *et al.*, 2013; Serdyuchenko *et al.*, 2014]. Hence, when the assumed stratospheric temperature deviates strongly from what is assumed by the algorithms, which is usually the case during the winter months, the differences between ground and satellite increase. See the work of Koukouli *et al.*, 2016, and discussion therein, on this topic.

The plots shown in the upper part of Figure 7.2 are as per Figure 7.1, but for the common time period of operation of the GOME-2A and GOME-2B sensors, hence since the beginning of year 2013 onwards. There appear to be periods where the two instruments deviate in both the NH (upper left) and the SH (upper right); for the NH, a difference of ~ 1 % is seen for year 2013 as well as from mid-2015 onwards which manifests as a GOME-2A over-estimation in the former and under-

estimation in the latter period. For the SH, the 2013 differences are observed, again at the ~1 % difference level, extending up until mid-2014.
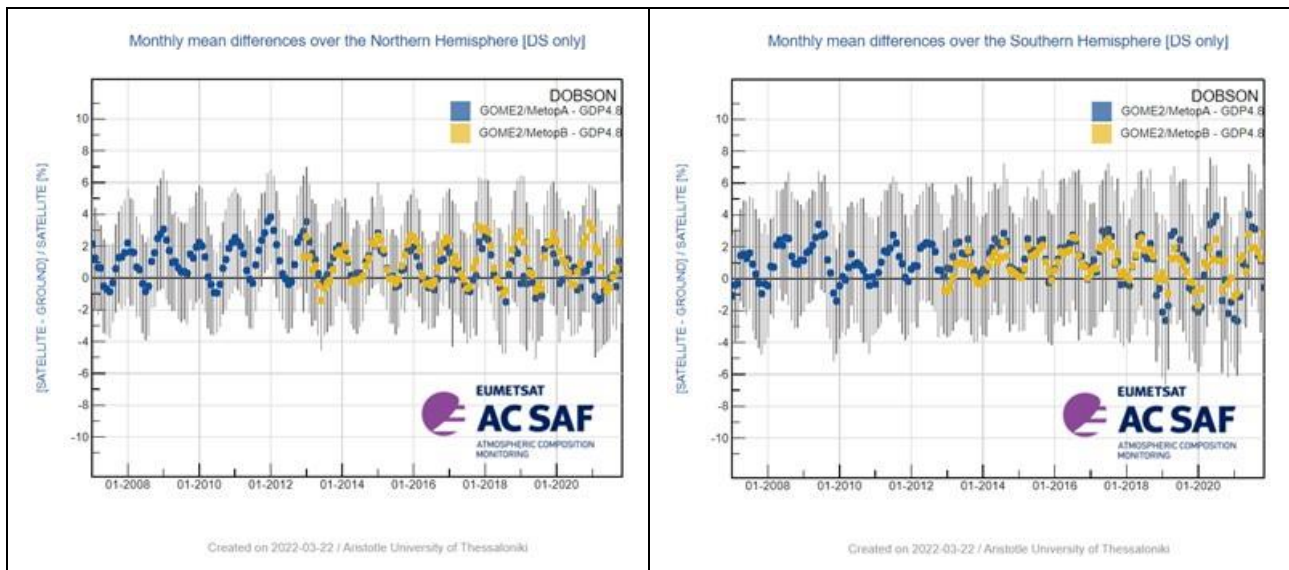

Figure 7.1. Time-series of the monthly mean percentage differences between GOME-2A GDP-4.8 (blue symbols) and GOME-2B GDP-4.8 (orange symbols) against the Dobson Northern Hemisphere stations (left panel) and the Dobson Southern Hemisphere stations (right panel).
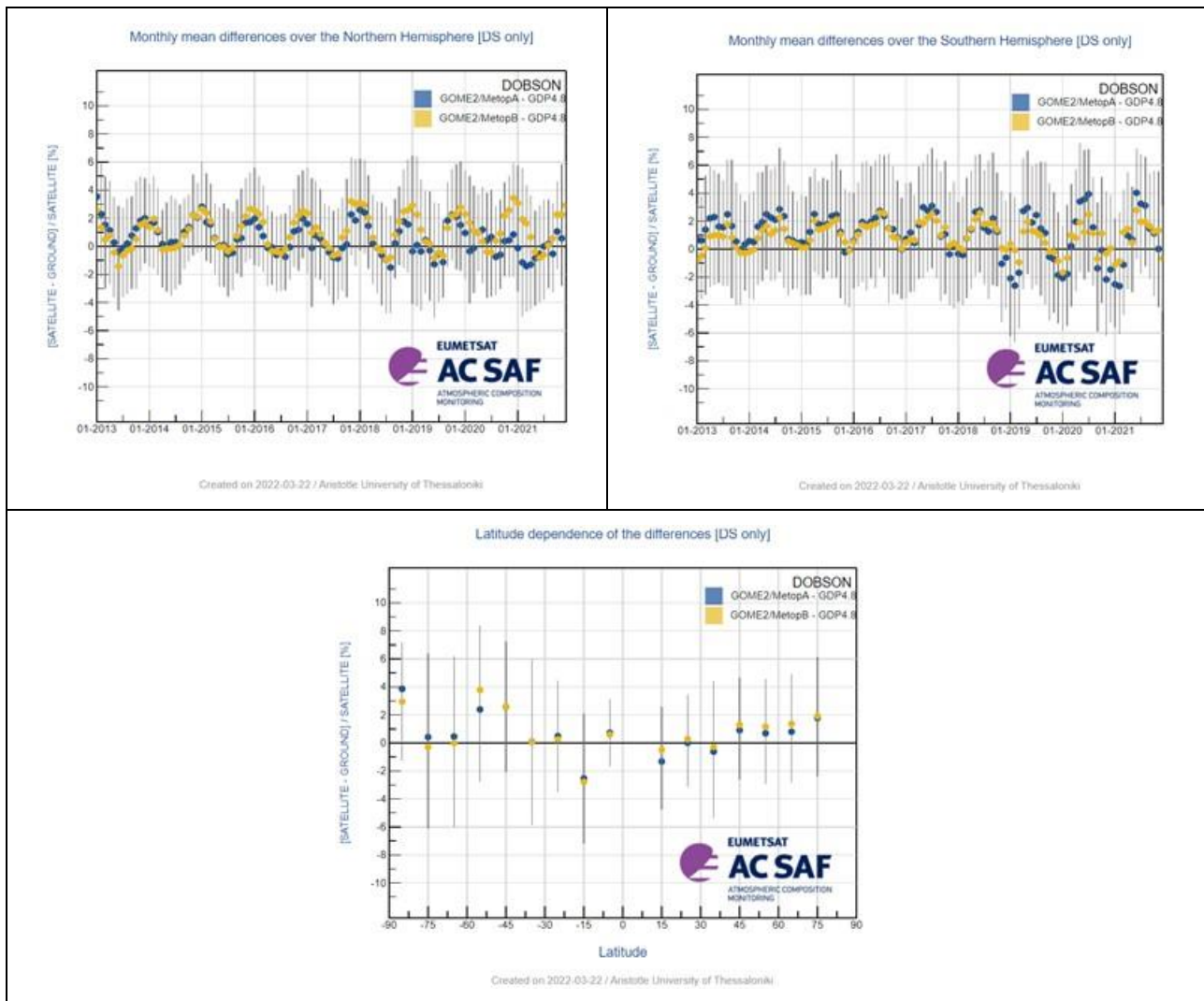
Figure 7.2. Upper plots as in Figure 7.1. The common time period of operation is shown here. The latitudinal dependency of the differences for the Dobson network are shown at the bottom panel.

The very good agreement between the two sensors is only interrupted between January and mid-March 2019, between mid-November 2019 and mid-April 2020, and since July 2020 due to the loss of solar visibility for GOME-2A. During these periods, a switch to the empirical solar model took place to substitute the sensor's normal measurements.

- For the period **January – March 2019**, the solar model deviated from GOME-2B by about -2 to -3 % in both Hemispheres
- For the period **November 2019 – April 2020** the deviation was about -2 % for the NH and -0.5 % for the SH
- GOME-2A was switched to the solar model again in **mid-July 2020** until it's end of operation in November 2021. Its performance was almost the same as it was for in 2019, since the observed deviations between the two sensors go up to -3 %. The same feature is shown in Brewer comparisons.

From the latitudinal variability plot, Figure 7.2 bottom panel, it can be seen that in the high southern latitudes, GOME-2A slightly (<1 %) over-estimates TOCs compared to GOME-2B, whereas in the NH their correlation is inverted. It must be stressed, though, that the periods of the switch to the solar model are included in these comparisons, increasing the deviation between the two sensors.

In Figure 7.3 the time-series of the monthly mean percentage differences for both hemispheres (above) and the pole-to-pole graph of the GOME-2B and GOME-2C comparisons are shown (below), for their common time period of operation (since January 2019). The agreement between the two sensors in the NH is different before and after the spring of 2020:

- Before this point, the two sensors deviate by ~ 0 – 1 %
- Since about April 2020, their deviation gradually increases up to 2 % with GOME-2C reporting higher TOCs than GOME-2B. The increased difference extends to the spring and summer months (NH) and decreases again since October 2020. The same seasonal effect is already seen during 2021, with a higher deviation up to 2.5 % occurring during summer. In the SH, for the spring-summer months an increased difference is also seen, going up to 2 – 2.5 %, with GOME-2C reporting higher O_3 values than GOME-2B. Additionally, the percentage differences of GOME-2C with respect to ground-based measurements stays positive ~ +2 % throughout 2020 and 2021 at the SH. For the latter part of 2021, the number of ground-based measurements is still limited, especially for the SH, so this is expected to be confirmed when more data are available.

This seasonal pattern in the deviation between the two sensors was not that visible during the NH and SH spring-summer months of 2019. Therefore, it is suggested that one to two more years of observations have to become available until this pattern is confirmed (or not).

In the latitudinal plot (Figure 7.3, below), it is shown that the TOC overestimation of GOME-2C with respect to GOME-2B is global and up to now it is more evident for the mid-latitudes and the tropics, where GOME-2C reports higher TOCs by about 1 – 2 % with respect to GOME-2B.

Nevertheless, the overall agreement of both sensors to the ground-based measurements is very good, within 0 – 2 % in the tropics and the mid-latitudes.
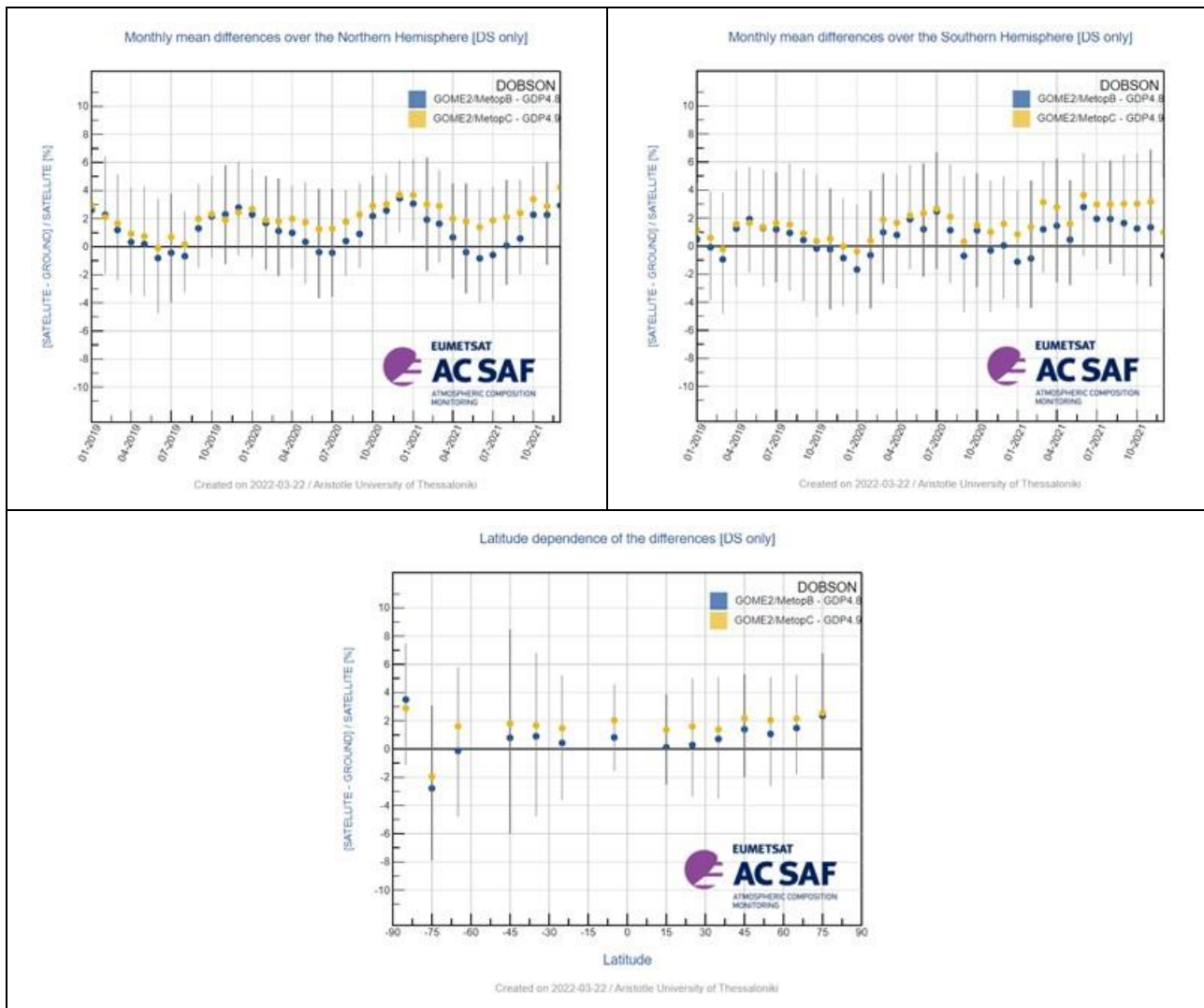
Figure 7.3. As in Figure 7.2 for the common time period of operation of GOME-2B and GOME-2C.

7.1.1.3   GOME-2A, GOME-2B and GOME-2C TOC validation | The Brewer comparisons

In Figure 7.4, the time-series of the comparisons between GOME-2A and GOME-2B and Brewer TOCs are shown for the Northern Hemisphere (upper plots). To the left the whole time series for each sensor is shown and to the right only the common period of operation, between 2013 and June 2021, is used. A very similar behaviour is observed in the latter plot (upper right), as per Figure 7.2 left panel for the Dobson comparisons. The respective deviations by ~ 2 – 3 % between the two sensors during the switches to the empirical solar model are also seen here. In the lower panel of Figure 7.4, the latitudinal variability of the differences is presented, which shows a very good agreement between the two sensors for the years of common operation.
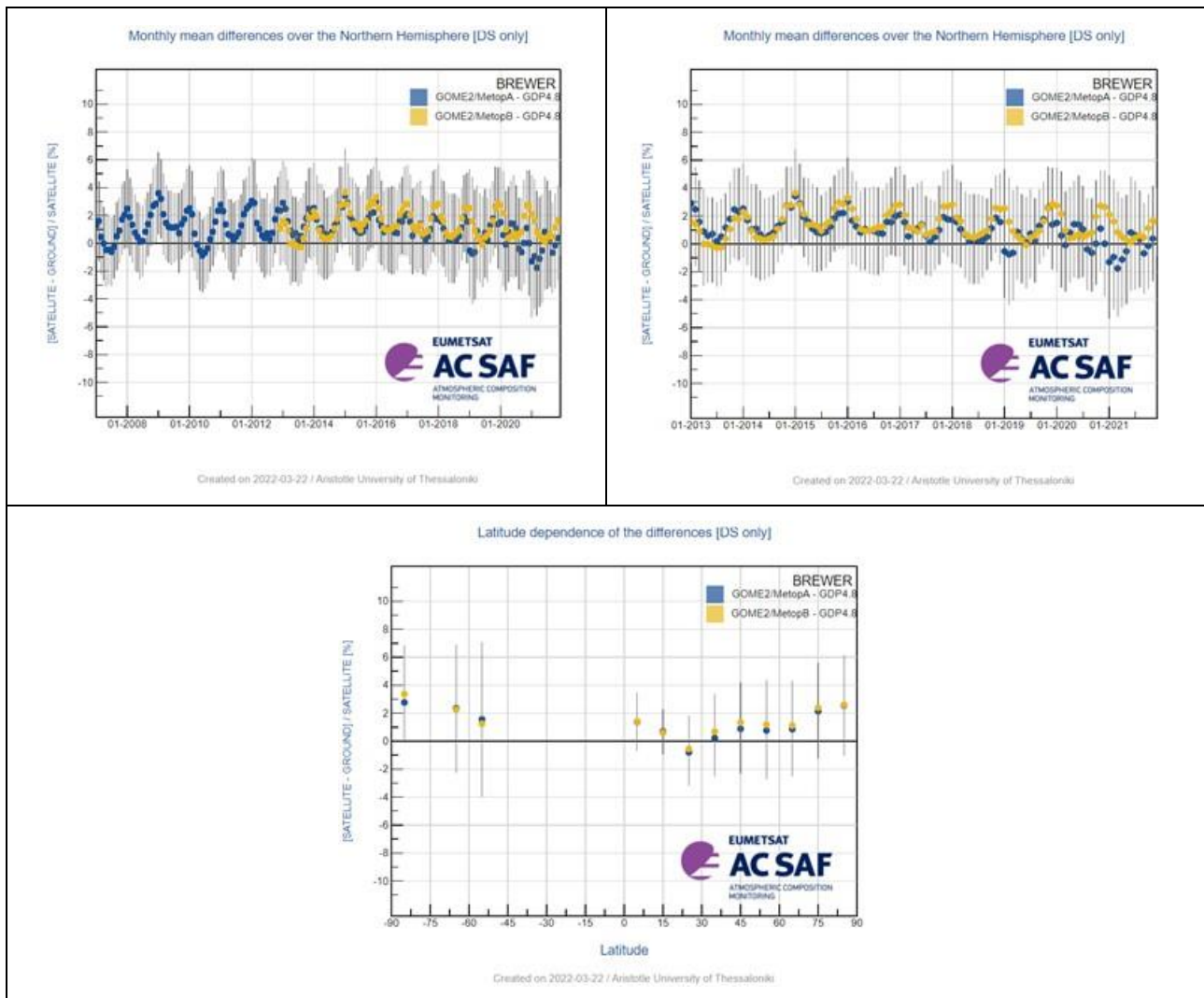
Figure 7.4. Time-series of the monthly mean percentage differences between GOME-2A GDP-4.8 (blue symbols) and GOME-2B GDP-4.8 (orange symbols) against the Brewer reported TOCs between January 2007 and June 2021.

Figure 7.5 shows the same time series and latitudinal plot as shown in Figure 7.4, for the GOME-2B and GOME-2C common time period of operations, thus since January 2019. The higher deviation between the two sensors for the spring-summer months is also seen here, and is again more enhanced during 2020 and early 2021. In the latitudinal plot, it is seen that for the Northern high latitude Brewer comparisons GOME-2C has an almost constant positive bias with respect to GOME-2B of about 0.5 %, which is increased to 1 % for the co-locations within the tropics. Nevertheless, a longer time period of operation need to become available for these conclutions to be solid.

Figure 7.5. As in Figure 7.4 but for the GOME-2B and GOME-2C common time period of operation. At the right panel, the latitudinal dependency of the differences is seen.

7.1.1.4 GOME-2A, GOME-2B and GOME-2C TOC validation | Tables of statistics

In Table 7.2, the summary statistics for the comparisons presented in Sections 7.1.1.2 and 7.1.1.3, for the Dobson and the Brewer stations, are enumerated.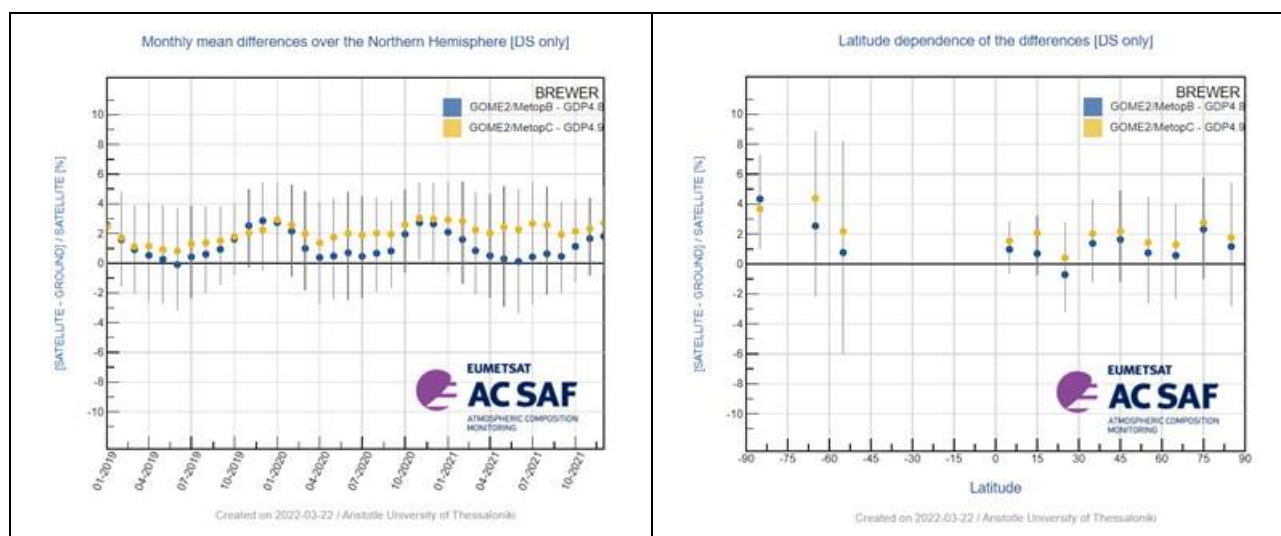 The number of individual daily common observations for the Dobsons hence apply to the entire globe, whereas the Brewer comparisons depict only the NH. As can be noted, the relative differences between GOME-2A and GOME-2B against Brewer and Dobson stations are very stable, with an average mean difference of less than $+1 \pm 4.5$ %. GOME-2C has a higher mean relative bias with respect to ground-based measurements, of $+1.5 \pm 4.0$ %.

Table 7.2. Summary statistics for the respective time period of operation of each sensor, based on GOME-2A, GOME-2B & GOME-2C OTO data compared to WOUDC Brewer & Dobson observations

		Brewer	**Dobson**
GOME-2/Metop-A 01/2007 – 11/2021	# stations:	76	68
	# obs:	211091	146366
	Mean Rel. Bias (%):	0.76 ± 4.40	0.75 ± 4.73
GOME-2/Metop-B 01/2013 – 12/2021	# stations:	66	64
	# obs:	147492	96555
	Mean Rel. Bias (%):	0.93 ± 4.12	0.78 ± 4.49
GOME-2/Metop-C 01/2019 – 12/2021	# stations:	50	46
	# obs:	45303	23349
	Mean Rel. Bias (%):	1.53 ± 3.63	1.65 ± 4.32

7.1.2. Validation website update

The AC SAF Ozone Validation & Quality Assessment was launched on the initiation of the project's CDOP 2 phase in 2013. The validation webpages host the validation results of GOME-2A

GDP-4.8, GOME-2B GDP4.8 and GOME-2C GDP4.9 near real-time and offline total ozone data. Currently, the validation results are available until December 2021.

The website and the processing algorithms that run behind it are routinely inspected and quality controlled. All the necessary actions, needed to keep it at its current good state, are taken by the LAP/AUTH team.

In Figure 7.6 and Figure 7.7 some example statistics about the website traffic are shown for the period 1 July 2021 – 31 December 2021, as extracted from Google Analytics.
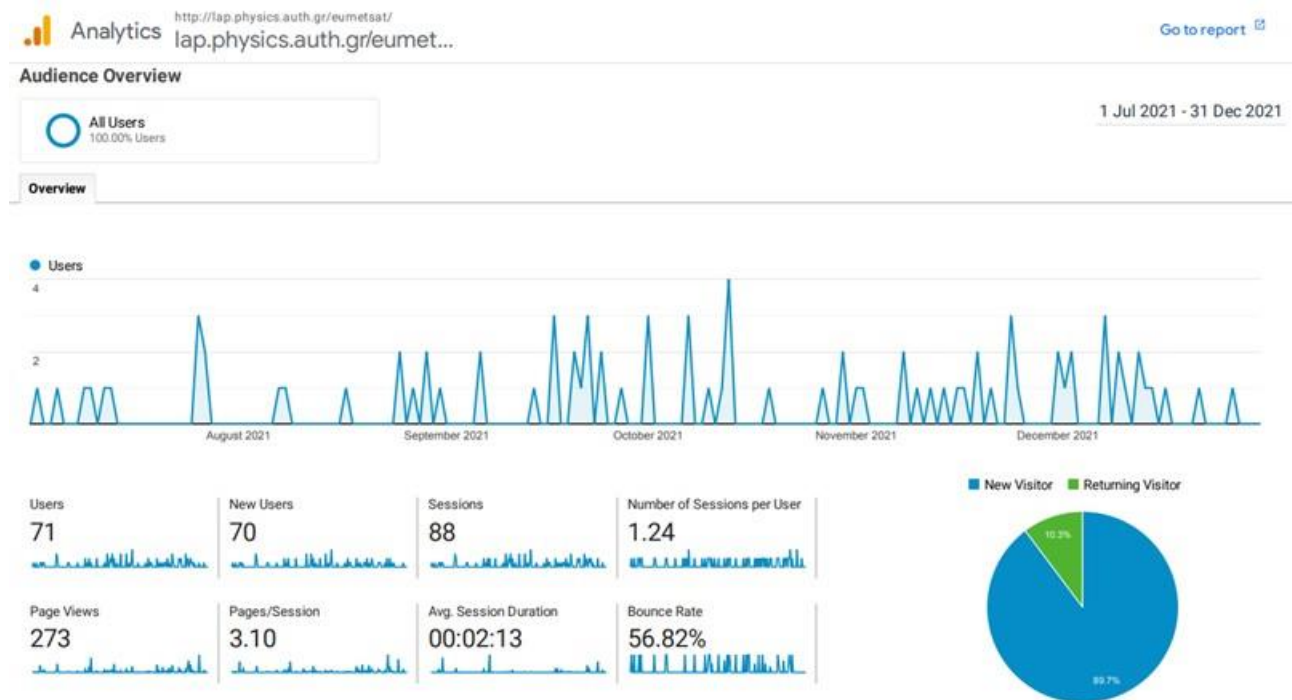
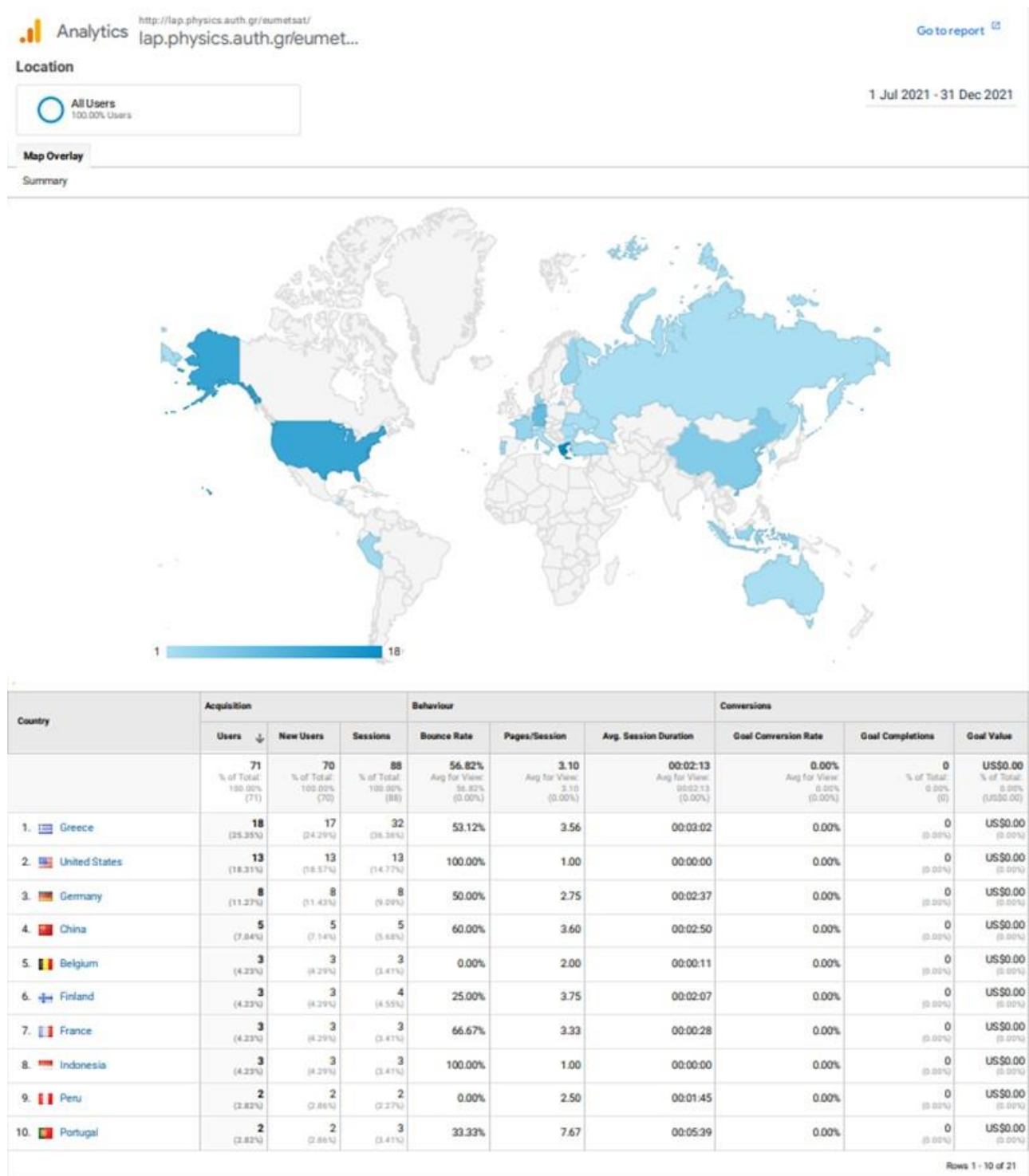**Figure 7.6. The activity of the users of the AC SAF validation web pages.**

Figure 7.7. The location of the website visitors.

References:

Antón, M., Loyola, D., López, M., Vilaplana, J. M., Bañón, M., Zimmer, W., and Serrano, A.: Comparison of GOME-2/MetOpA total ozone data with Brewer spectroradiometer data over the Iberian Peninsula, Annales Geophysicae, 27, 1377–1386, 2009. https://doi.org/10.5194/angeo-27-1377-2009

Balis, D., Kroon M., Koukouli, M.E., Brinksma, E. J., Labow, G., Veefkind, J. P., and McPeters, R. D.: Validation of Ozone Monitoring Instrument total ozone column measurements using Brewer and Dobson spectrophotometer ground-based observations, J. Geophys. Res., 112, D24S46, 2007a. https://doi.org/10.1029/2007JD008796

Balis, D., Lambert, J-C., Van Roozendael, M., Spurr, R., Loyola, D., Livschitz, Y., Valks, P., Amiridis, V., Gerard, P., Granville, J., and Zehner, C.: Ten years of GOME/ERS-2 total ozone data – The new GOME data processor (GDP) version 4: 2. Ground-based validation and comparisons with TOMS V7/V8, J. Geophys. Res., vol. 112, D07307, 2007b. https://doi.org/10.1029/2005JD006376

Fragkos, K., Bais, A. F., Balis, D., Meleti, C., and Koukouli, M. E.: The effect of three different absorption cross-sections and their temperature dependence on total ozone measured by a mid-latitude Brewer spectrophotometer, Atmos. Ocean, 53, 2015. https://doi.org/10.1080/07055900.2013.847816

Hao, N., Koukouli, M. E., Inness, A., Valks, P., Loyola, D. G., Zimmer, W., Balis, D. S., Zyrichidou, I., Van Roozendael, M., Lerot, C., and Spurr, R. J. D.: GOME-2 total ozone columns from MetOp-A/MetOp-B and assimilation in the MACC system, Atmos. Meas. Tech., 7, 2937-2951, 2014. https://doi.org/10.5194/amt-7-2937-2014

Koukouli, M. E., Balis, D. S., Loyola, D., Valks, P., Zimmer, W., Hao, N., Lambert, J.-C., Van Roozendael, M., Lerot, C., and Spurr, R. J. D.: Geophysical validation and long-term consistency between GOME-2/MetOp-A total ozone column and measurements from the sensors GOME/ERS-2, SCIAMACHY/ENVISAT and OMI/Aura, Atmos. Meas. Tech., 5, 2169-2181, 2012. https://doi.org/10.5194/amt-5-2169-2012

Koukouli, M. E., Lerot, C., Granville, J., Goutail, F., Lambert, J.-C., Pommereau, J.-P., Balis, D., Zyrichidou, I., Van Roozendael, M., Coldewey-Egbers, M., Loyola, D., Labow, G., Frith, S., Spurr, S., and Zehner, C.: Evaluating a new homogeneous total ozone climate data record from GOME/ERS-2, SCIAMACHY/Envisat and GOME-2/MetOp-A, J. Geophys. Res. Atmos., 120, 12296-12312, 2015. https://doi.org/10.1002/2015JD023699

Koukouli, M. E., Zara, M., Lerot, C., Fragkos, K., Balis, D., van Roozendael, M., Allart, M. A. F., and van der A, R. J.: The impact of the ozone effective temperature on satellite validation using the Dobson spectrophotometer network, Atmos. Meas. Tech., 9, 2055-2065, 2016. https://doi.org/10.5194/amt-9-2055-2016

Loyola, D. G., Koukouli, M. E., Valks, P., Balis, D. S., Hao, N., Van Roozendael, M., Spurr, R. J. D., Zimmer, W., Kiemle, S., Lerot, C., and Lambert, J.-C.: The GOME-2 total column ozone product: Retrieval algorithm and ground-based validation, J. Geophys. Res., 116, 2011. https://doi.org/10.1029/2010JD014675

Serdyuchenko, A., Gorshelev, V., Weber, M., Chehade, W., and Burrows, J. P.: High spectral resolution ozone absorption cross-sections – Part 2: Temperature dependence, Atmos. Meas. Tech.,7, 625–636, 2014. https://doi.org/10.5194/amt-7-625-2014

Garane, K., Lerot, C., Coldewey-Egbers, M., Verhoelst, T., Koukouli, M. E., Zyrichidou, I., Balis, D. S., Danckaert, T., Goutail, F., Granville, J., Hubert, D., Keppens, A., Lambert, J.-C., Loyola, D., Pommereau, J.-P., Van Roozendael, M., and Zehner, C.: Quality assessment of the Ozone_cci

Climate Research Data Package (release 2017) – Part 1: Ground-based validation of total ozone column data products, Atmos. Meas. Tech., 11, 1385-1402, 2018.
https://doi.org/10.5194/amt-11-1385-2018

Garane, K., Koukouli, M.-E., Verhoelst, T., Lerot, C., Heue, K.-P., Fioletov, V., Balis, D., Bais, A., Bazureau, A., Dehn, A., Goutail, F., Granville, J., Griffin, D., Hubert, D., Keppens, A., Lambert, J.-C., Loyola, D., McLinden, C., Pazmino, A., Pommereau, J.-P., Redondas, A., Romahn, F., Valks, P., Van Roozendael, M., Xu, J., Zehner, C., Zerefos, C., and Zimmer, W.: TROPOMI/S5P total ozone column data: global ground-based validation and consistency with other satellite missions, Atmos. Meas. Tech., 12, 5263–5287, 2019.
https://doi.org/10.5194/amt-12-5263-2019

7.1.3. Online quality monitoring

The online quality monitoring tool is operational and consists of the continuous generation of plots showing the slant column density (SCD) distribution, the vertical column density (VCD) distribution as well as the root mean square (RMS) as histograms per sensing day as well as time series per sensing month. These plots are generated for three different geographic regions, the pacific ocean (25-15S, 210-250E), the Sahara desert (20-30N, 0-30E) and global, in order to represent typical extremes of ground reflectivity and atmospheric conditions as well as the global mean. The plots are generated per sensing instrument (GOME-2A, GOME-2B, GOME-2C) and per product (O_3, NO_2, BrO, HCHO, SO_2, H_2O).

The online quality monitoring plots are published in PDF format on the DLR AC SAF FTP server (acsaf.eoc.dlr.de) using the following directory schemes:

/oq/GOME-2[ABC]/[O3 NO2 BrO HCHO SO2 H2O]/daily/YYYY/MM/DD/[global sahara pacific]/*.[vcd scd rms]_hist.pdf
/oq/GOME-2[ABC]/[O3 NO2 BrO HCHO SO2 H2O]/monthly/YYYY/MM/[global sahara pacific]/ *.[vcd scd rms]_series.pdf

More information about quality monitoring of the operational GOME-2 total ozone columns by other AC SAF and external partners is available at the following websites:
https://acsaf.org → Validation & QA → QM websites
http://acsaf.physics.auth.gr/eumetsat/validation/near_real
http://acsaf.physics.auth.gr/eumetsat/validation/offline
https://www.temis.nl/acsaf/vod.php
https://www.ecmwf.int/en/forecasts/charts/obstat/?facets=Parameter,Ozone;Instrument,GOME2

7.2. Tropospheric ozone products

Table 7.3. Validation status of tropospheric ozone products

Product Identifier	Product Name	Accuracy	Reference	Validating Institute	Correlative data sources
O3M-35	Offline tropical tropospheric ozone	Fulfils target accuracy requirement	RD18	KMI	Ozonesonde data from SHADOZ, NDACC, NILU and WOUDC
O3M-43					
O3M-302			RD24		

Product Identifier	Product Name	Accuracy	Reference	Validating Institute	Correlative data sources
O3M-172	NRT global tropospheric ozone	Fulfils target accuracy requirement	RD19	KMI	Ozonesonde data from SHADOZ, NDACC, NILU and WOUDC
O3M-174					
O3M-304			RD25		
O3M-173	Offline global tropospheric ozone	Fulfils target accuracy requirement	RD19	KMI	Ozonesonde data from SHADOZ, NDACC, NILU and WOUDC
O3M-175					
O3M-305			RD25		

Validation activities summary for global tropospheric ozone:

This summary contains validation results of the GOME-2A, GOME-2B and GOME-2C high resolution (HR) global tropospheric ozone column (TrOC) products, retrieved by the Ozone Profile Retrieval Algorithm (OPERA) at KNMI. It covers the time period January – December 2021. Validation results are shown from two TrOC products, i.e. the tropopause related product and a fixed altitude TrOC product. The TrOC products are derived from the daily operational ozone profile product. Also here, we consider now the time period where the updated algorithm with degradation correction is active.

Since these TrOC products are derived from the OPERA ozone profile product, OPERA averaging kernel smoothing has been applied to the ground-based reference profiles before calculating comparison statistics. This AVK smoothing is expected to reduce the vertical smoothing difference error between satellite and ground-based measurements. The outcome is summarized at the end of this section.

The global tropospheric ozone column (TrOC) product has the following user requirements:

- Threshold accuracy: within 50 %
- Target accuracy: within 20 %
- Optimal accuracy: within 15 %

This summary was made available by Dr. Andy Delcloo from KMI. More information on how these values are extracted is available in the Metop-A/B validation report and Metop-C validation report. The collocation data used are the same as for the ozone profiles (Figure 7.24).

The statistics on the accuracy of the GOME-2A, GOME-2B and GOME-2C HR tropospheric ozone column products (tropopause related) for different latitude belts, validated against $X_{AVK\text{-}sonde}$, are shown in Table 7.4, Table 7.5 and Table 7.6.

Table 7.4. Relative differences (RD) and standard deviation (STDEV) are shown (in percent) together with the absolute difference (DU) on the accuracy of the GOME-2A HR tropospheric ozone column products (tropopause related) for five different latitude belts, validated against $X_{AVK-sonde}$

January – December 2021	GOME-2A HR			
	RD (%)	STDEV (%)	AD (DU)	STDEV (DU)
Northern Polar Region	-	-	-	-
Northern Mid-Latitudes	**58.9**	61.0	16.9	18.1
Tropical region	**66.4**	49.1	16.0	11.6
Southern Mid-Latitudes	17.1	29.8	2.67	5.12
Southern Polar Region	15.3	25.4	1.79	3.00

Table 7.5. Relative differences (RD) and standard deviation (STDEV) are shown (in percent) together with the absolute difference (DU) on the accuracy of the GOME-2B HR tropospheric ozone column products (tropopause related) for five different latitude belts, validated against $X_{AVK-sonde}$

January – December 2021	GOME-2B HR			
	RD (%)	STDEV (%)	AD (DU)	STDEV (DU)
Northern Polar Region	-	-	-	-
Northern Mid-Latitudes	1.97	5.59	0.57	1.42
Tropical region	-3.75	18.3	-1.28	5.30
Southern Mid-Latitudes	13.6	35.6	2.90	7.82
Southern Polar Region	-1.23	17.7	-0.20	3.62

Table 7.6. Relative differences (RD) and standard deviation (STDEV) are shown (in percent) together with the absolute difference (DU) on the accuracy of the GOME-2C HR tropospheric ozone column products (tropopause related) for five different latitude belts, validated against $X_{AVK-sonde}$

January – December 2021	GOME-2C HR			
	RD (%)	STDEV (%)	AD (DU)	STDEV (DU)
Northern Polar Region	-	-	-	-
Northern Mid-Latitudes	16.6	22.0	4.82	6.66
Tropical region	**53.5**	50.2	12.3	7.93
Southern Mid-Latitudes	5.20	22.7	1.25	5.24
Southern Polar Region	-17.4	33.3	-1.99	4.33

The statistics on the accuracy of the GOME-2A, GOME-2B and GOME-2C HR tropospheric ozone column products (fixed altitude) for different latitude belts, validated against $X_{AVK-sonde}$, are shown in Table 7.7, Table 7.8 and Table 7.9.

Table 7.7. Relative differences (RD) and standard deviation (STDEV) are shown (in percent) together with the absolute difference (DU) on the accuracy of the GOME-2A HR tropospheric ozone column products (fixed altitude) for five different latitude belts, validated against X$_{AVK\text{-}sonde}$

January – December 2021	GOME-2A HR			
	RD (%)	STDEV (%)	AD (DU)	STDEV (DU)
Northern Polar Region	-	-	-	-
Northern Mid-Latitudes	35.6	37.4	6.20	6.65
Tropical region	**68.0**	54.1	8.22	6.04
Southern Mid-Latitudes	9.46	15.7	0.87	1.55
Southern Polar Region	9.60	8.43	0.67	0.59

Table 7.8. Relative differences (RD) and standard deviation (STDEV) are shown (in percent) together with the absolute difference (DU) on the accuracy of the GOME-2B HR tropospheric ozone column products (fixed altitude) for five different latitude belts, validated against X$_{AVK\text{-}sonde}$

January – December 2021	GOME-2B HR			
	RD (%)	STDEV (%)	AD (DU)	STDEV (DU)
Northern Polar Region	-	-	-	-
Northern Mid-Latitudes	-2.84	10.6	-0.52	1.88
Tropical region	5.09	29.8	0.56	3.68
Southern Mid-Latitudes	-1.41	9.72	-0.13	1.02
Southern Polar Region	-17.1	11.4	-1.11	0.83

Table 7.9. Relative differences (RD) and standard deviation (STDEV) are shown (in percent) together with the absolute difference (DU) on the accuracy of the GOME-2C HR tropospheric ozone column products (fixed altitude) for five different latitude belts, validated against X$_{AVK\text{-}sonde}$

January – December 2021	GOME-2C HR			
	RD (%)	STDEV (%)	AD (DU)	STDEV (DU)
Northern Polar Region	-	-	-	-
Northern Mid-Latitudes	8.82	11.6	1.52	2.06
Tropical region	40.3	36.7	5.26	3.93
Southern Mid-Latitudes	1.57	12.0	0.18	1.34
Southern Polar Region	-13.1	10.2	-0.94	0.92

The quality on the GOME-2A TrOC products doesn't comply anymore with the threshold accuracy for all stations. Only for the Southern polar and mid-latitude region, the target accuracy (20 %) is met. This is the last time we are reporting on Metop-A results. The final degradation correction will be necessary for all sensors.

For the GOME-2B and GOME-2C TrOC products, most of these products comply with the target accuracy requirement. Only for the tropical region (GOME-2C), this is not the case. Between all sensors, there is a clear offset visible in the results. Also here, a degradation correction will be necessary to correct for this offset.

Validation activities summary for tropical tropospheric ozone:

At the time of writing this report (rev. 1), there was no new TTrOC reference data available from DLR. Therefore, all the results are as in AC SAF Operations Report 1/2021.

This summary contains validation results of the GOME-2A, GOME-2B and GOME-2C tropical tropospheric ozone column (TTrOC) products, using the cloud slicing method. The tropospheric ozone retrieval is based on the GOME-2 ozone columns as derived by the GOME Data Processor (GDP, version 4.8) and covers the tropical latitude belt (20S – 20N). This product is available on a monthly basis and has a resolution of 1.25° latitude x 2.5° longitude.

The tropical tropospheric ozone column product has the following user requirements:

- Threshold accuracy: within 50 %
- Target accuracy: within 25 %
- Optimal accuracy: within 15 %

This summary was made available by Dr. Andy Delcloo from KMI. More information on how these values are extracted is available in the validation report. The collocation data used are the same as for the ozone profiles (Figure 7.24).

The time period covered is January 2019 – December 2020 for GOME-2A, GOME-2B and GOME-2C offline TtrOC products.

In Table 7.10, Table 7.11 and Table 7.12, the statistics on the accuracy of the GOME-2A/B/C tropical tropospheric ozone column products for different stations under consideration are shown, showing some general statistics for each dataset. It is shown that most of the stations are within the target accuracy (25 %). The correlation varies between 0.3 and 0.9 with a RMSE between 2.6 – 8.2 DU. There is also an offset present between GOME-2A/GOME-2C and GOME-2B/GOME-2C as described in the validation report. These TtrOC products still fulfill the user requirements.

Table 7.10. Relative Differences (RD), standard deviation (STDEV), correlation, bias and RMSE are shown on the accuracy of the GOME-2A TtrOC product for the time period January 2019 – December 2020

Station	RD (%)	STDEV (%)	Correlation	Bias (DU)	RMSE (DU)
Paramaribu	8.84	21.9	0.48	1.61	4.05
Alajuela	18.7	17.0	0.72	3.15	4.25
Samoa	12.1	27.4	0.75	1.86	4.14
Ascension Island	4.06	11.7	0.64	0.94	3.38
Kuala Lumpur	-4.73	12.5	0.72	-1.31	2.85
Nairobi	28.0	6.40	0.99	4.93	5.30
Natal	6.85	19.6	0.51	1.28	4.32
Hilo	14.9	16.8	0.86	3.72	5.55

Table 7.11. Relative Differences (RD), standard deviation (STDEV), correlation, bias and RMSE are shown on the accuracy of the GOME-2B TtrOC product for the time period January 2019 – December 2020

Station	RD (%)	STDEV (%)	Correlation	Bias (DU)	RMSE (DU)
Paramaribu	10.7	23.3	0.58	2.01	4.45
Alajuela	25.1	24.2	0.32	4.03	5.68
Samoa	8.52	22.8	0.76	1.35	3.65
Ascension Island	7.08	13.7	0.56	1.73	4.02
Kuala Lumpur	-2.35	15.5	0.76	-0.92	2.57
Nairobi	21.3	15.7	0.76	3.35	3.82
Natal	4.50	15.9	0.69	0.89	3.51
Hilo	20.0	10.4	0.89	4.22	4.66

Table 7.12. Relative Differences (RD), standard deviation (STDEV), correlation, bias and RMSE are shown on the accuracy of the GOME-2C TtrOC product for the time period January 2019 – December 2020

Station	RD (%)	STDEV (%)	Correlation	Bias (DU)	RMSE (DU)
Paramaribu	8.71	22.2	0.44	1.57	4.15
Alajuela	21.8	23.2	0.43	3.47	5.20
Samoa	16.0	20.4	0.76	2.29	3.76
Ascension Island	11.3	14.5	0.56	3.05	4.99
Kuala Lumpur	-2.57	25.1	0.07	-1.41	4.31
Nairobi	19.8	14.7	0.73	3.20	3.75
Natal	2.98	15.7	0.71	0.62	3.63
Hilo	29.2	21.5	0.65	6.73	8.22

7.3. Trace gas products

Table 7.13. Validation status of trace gas products

Product Identifier	Product Name	Accuracy	Reference	Validating Institute	Correlative data sources
O3M-02.1	NRT total NO2	Fulfils threshold accuracy requirement	RD6	BIRA-IASB	NDACC zenithSky measurements
O3M-50.1					
O3M-338			RD28		
O3M-36.1	NRT tropospheric NO2	Fulfils threshold accuracy requirement	RD6	BIRA-IASB	BIRA-IASB MAXDOAS stations
O3M-52.1					
O3M-341			RD28		

Product Identifier	Product Name	Accuracy	Reference	Validating Institute	Correlative data sources
O3M-54.1	NRT total SO2	Fulfils threshold accuracy requirement	RD10	BIRA-IASB	BIRA-IASB Xianghe MAXDOAS station
O3M-55.1					
O3M-176.0	NRT total HCHO	Fulfils threshold accuracy requirement	RD12	BIRA-IASB	BIRA-IASB MAXDOAS stations
O3M-177.0					
O3M-344			RD29		
O3M-07.1	Offline total NO2	Fulfils threshold accuracy requirement	RD6	BIRA-IASB	NDACC zenithSky measurements
O3M-51.1					
O3M-339			RD28		
O3M-37.1	Offline tropospheric NO2	Fulfils threshold accuracy requirement	RD6	BIRA-IASB	BIRA-IASB MAXDOAS stations
O3M-53.1					
O3M-342			RD28		
O3M-09.1	Offline total SO2	Fulfils threshold accuracy requirement	RD10	BIRA-IASB	BIRA-IASB Xianghe MAXDOAS station
O3M-56.1					
O3M-08.1	Offline total BrO	Fulfils threshold accuracy requirement	RD11	BIRA-IASB	BIRA-IASB Harestua zenithSky station
O3M-82.1					
O3M-317			RD30		
O3M-10.1	Offline total HCHO	Fulfils target accuracy requirement	RD12	BIRA-IASB	BIRA-IASB MAXDOAS stations
O3M-58.1					
O3M-345			RD29		
O3M-12.1	Offline total H2O	Fulfils threshold accuracy requirement	RD13	FMI, DLR	IGRA, COSMIC-SuomiNet, SSM/I
O3M-86.1					
O3M-386			RD31		Comparison against GOME-2B water vapour data

Validation activities summary:

This summary presents validation activities for offline total and tropospheric NO_2, total HCHO, total BrO and SO_2 data products of GOME-2A/B/C as performed at BIRA-IASB.

The authors of this summary are Gaia Pinardi (for tropospheric NO_2, HCHO and SO_2 validation), Jean-Christopher Lambert, José Granville and Tijl Verhoelst (for total/stratospheric NO_2 validation), François Hendrick (for BrO validation) and Jeroen van Gent (for quality assessment).

Validation exercises are performed following the protocols described in the original Metop-A, Metop-B and Metop-C validation reports and updated in Pinardi *et al*. (AMT 2020) and Verhoelst *et al*. (AMT 2021), and the results presented in this report are based on updates of the correlative

datasets with the last available – and sometimes improved – versions. While illustrations at a few stations are included in this report, all the updated figures are reported on the [BIRA-IASB trace gases validation server](#).

Update of database for reference data

The validation database was updated with ground-based BIRA-IASB MAXDOAS NO_2 and HCHO data, BIRA-IASB ZenithSky BrO data at Harestua, NDACC UVVIS ZenithSky NO_2 data, Xianghe MAXDOAS SO_2 data and Xianghe DirectSun NO_2 and SO_2 data, in order to cover as much as possible of the period until the end of 2021.

ZenithSky NO_2 total columns are collected from the NDACC Data Host Facility (to where the data have to be uploaded by instrument Pis within 1 year after data acquisition) and from the SAOZ rapid delivery operational facility operated by LATMOS. The ground-based data are then quality assessed and post-processed at BIRA-IASB in preparation for the data comparisons. This preparation includes calculation of the effective ground-based airmasses with which GOME-2 data co-locations will be sought.

The BIRA-IASB MAXDOAS ground-based dataset are automatically retrieved with an improved version of the bePRO profiling algorithm (Clémer *et al.*, 2010; Hendrick *et al.*, 2014, Vlemmix *et al.*, 2015) developed within the EU FP7 NORS and QA4ECV projects (aiming at rapid delivery of improved NO_2 and HCHO profiles), and is progressively shifting to the FRM4DOAS analysis chain. Datasets from the following ground-based stations have been used: OHP (from June 2007 to July 2014 with the geometrical approximation, and since August 2014 to March 2017 with the bePRO profiling tool), Beijing (from June 2008 to April 2009), Uccle (from April 2011 to March 2016 with a miniMAXDOAS instrument (Uccle-miniDOAS) and from end of January 2017 to February 2020 with a scientific grade MAXDOAS: Uccle-SG), Bujumbura (from November 2013 to July 2017; since then the instrument had a power failure and only limited data transfer was possible, so no new data are included in this report) and LePort, on Reunion Island (from April 2016 to 10 January 2018). The instrument in Reunion Island has been reinstalled in June 2018 on the Maido site, and data analysis from the FRM4DOAS analysis chain is under test, but it is not adapted for tropospheric (NO_2, HCHO) gases validation at this mountaneous site and is not used for this report. Xianghe (from March 2010 to July 2018 and since October 2019) is thus the only MAX-DOAS station measuring during this report period.

Ground-based BrO columns are derived at Harestua from vertical profiles retrieved by applying an OEM (Optimal Estimation Method)-based profiling technique to zenith-sky measurements at sunrise (Hendrick *et al.*, 2007).

The Xianghe SO_2 MAXDOAS profiles dataset have been reanalysed after the instrumental break, and SO_2 validation wrt. ground-based data is performed in this report, although the SO_2 levels are very low now in China.

Status of GOME-2A, GOME-2B and GOME-2C tropospheric NO_2

Comparisons with ground-based MAXDOAS instruments is performed similarly as in previous [validation report](#). In Pinardi *et al*. (2020) it is shown that best results are achieved by filtering out the largest pixels and selecting only pixels covering the stations. For GOME-2, the selection includes keeping only pixels with a size of less than 100 km, while selecting pixels over the station, only slightly changes the results, as generally pixels with their center within 50 km, are covering the station. This improvement of the biases comes at the expenses of a strongly reduced number of pixels (see AC SAF Operations Report 1/2020).

For this report only Xianghe has data until the end of 2021, and Figure 7.8 shows example of results for GOME-2B and GOME-2C for Xianghe. Monthly mean differences are calculated for every year and for the whole time-series in order to see the evolution in time of the bias. Table 7.14 reports the median differences and the spread (half the percentile 68) at the stations, with and without the smoothing, and the figures for all the stations can be found on the BIRA-IASB validation web server.
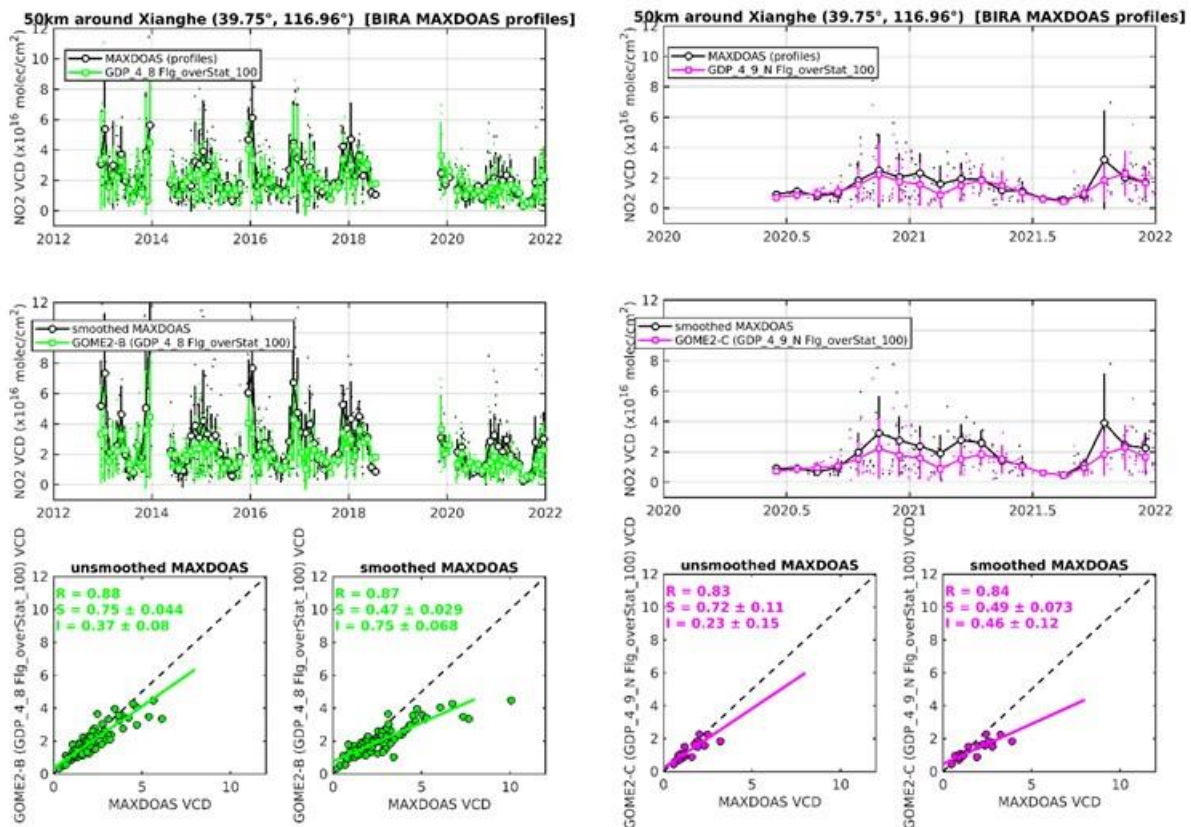

Figure 7.8. Illustration for the Xianghe MAXDOAS versus GOME-2B GDP-4.8 (left) and GOME-2C GDP-4.9 (right) tropospheric NO₂ comparisons, of the application of the satellite averaging kernels on MAXDOAS profiles.

Table 7.14. Median Absolute Differences (AD, in 10^{15} molec/cm²), Relative Differences (RD, in %) and spread (0.5*IP68) on the accuracy of GOME-2A, GOME-2B and GOME-2C tropospheric NO₂ products when comparing to MAXDOAS data (NOT cloud filtered). Values for the last 12 months are given, and the values for the whole time-series are reported in brackets for comparison. Results for both the original comparisons (pixels over the station, for pixels smaller than 100 km side) and for the smoothed comparisons are reported. <u>Only Xianghe data covers up to the end of 2021. Note that GOME-2A mission ends 15 November 2021.</u>

	GOME-2A			GOME-2B			GOME-2C		
	AD ($\times 10^{15}$)	RD (%)	SPREAD (%)	AD ($\times 10^{15}$)	RD (%)	SPREAD (%)	AD ($\times 10^{15}$)	RD (%)	SPREAD (%)
Uccle SG **last 12 months:** **03/2019 – 02/2020** **[whole period:** **02/2017 – 02/2020]**	-2.1 [-1.6]	-29 [-20]	40 [30]	-1.2 [-1.4]	-16 [-20]	33 [36]	-	-	-
Uccle SG smoothed	-3.7 [-2.3]	-51 [-24]	36 [28]	-2.5 [-2.7]	-26 [-29]	38 [36]	-	-	-
Reunion Maido **(last 12 months:** **12/2018 – 11/2019)** **[whole period:** **06/2018 – 11/2019]**	-0.09 [-0.01]	2 [37]	175 [201]	-0.02 [-0.02]	-4.2 [-4.3]	76 [93]	-	-	-
Reunion Maido **smoothed**	-0.08 [-0.03]	33 [13]	288 [237]	-0.03 [-0.01]	-1.4 [-9]	85 [115]	-	-	-
Xianghe **(last 12 months:** **12/2020 – 12/2021)** **[whole period:** **03/2010 – 12/2021]**	-7.2 [-2.21]	-51 [-13]	45 [23]	-0.7 [-1.1]	-8.3 [-6]	20 [25]	-0.8 [-1.2]	-6.2 [-10]	27 [22]
Xianghe smoothed	-15 [-6.2]	-59 [-24]	28 [32]	-2.7 [-3.9]	-17 [-18]	33 [36]	-5.8 [-3.1]	-22 [-26]	26 [27]
Beijing **[whole period:** **06/2008 – 04/2009]**	[-17]	[-47]	[21]	-	-	-	-	-	-
Beijing smoothed	[-15]	[-47]	[32]	-	-	-	-	-	-
Bujumbura **(last 12 months:** **07/2016 – 07/2017)** **[whole period:** **11/2013 – 07/2017]**	-3.2 [-3.4]	-80 [-77]	32 [35]	-3.4 [-3.2]	-83 [-81]	42 [28]	-	-	-
Bujumbura **smoothed**	-2.5 [-2]	-68 [-71]	31 [45]	-2 [-1.8]	-70 [-74]	21 [35]	-	-	-

OHP (last 12months: 03/2016 – 03/2017) [whole period: 08/2014 – 03/2017]	-0.9 [-0.8]	-51 [-42]	66 [44]	-0.7 [-0.6]	-37 [-28]	34 [36]	-	-	-
OHP smoothed	-1.1 [-0.8]	-51 [-42]	60 [51]	-0.5 [-0.4]	-36 [-24]	41 [39]	-	-	-
Reunion LePort Last 12 months: 12/2016 – 12/2017) [whole period: 04/2016 – 12/2017]	-1.5 [-1.6]	-84 [-86]	29 [28]	-1.4 [-1.4]	-83 [-84]	25 [25]	-	-	-
Reunion LePort smoothed	-0.5 [-0.5]	-62 [-67]	29 [31]	-0.41 [-0.42]	-59 [-60]	22 [25]	-	-	-
Uccle minDOAS (last 12 months: 03/2015 – 03/2016) [whole period: 04/2011 – 03/2016]	-3.2 [-3.9]	-27 [-37]	29 [30]	-2.6 [-3]	-26 [-31]	25 [24]	-	-	-
Uccle minDOAS smoothed	-4.5 [-5]	-36 [-44]	31 [34]	-3.6 [-3.3]	-29 [-33]	20 [30]	-	-	-

For GOME-2C, scatter plot results are similar to what obtained with GOME-2B in Xianghe (slopes around 0.72 and 0.75, respectively), probably due to the absence of large NO_2 columns ($>4\times10^{15}$ molec/cm²) that strongly influence the regression analysis (Pinardi *et al*., 2020). The absolute and relative differences are similar tio what obtained with GOME-2B in the last year. For both GOME-2A and GOME-2B sensors, the biases increase in the last year wrt. To the whole time-series, with large spread for GOME-2A, reached its end-of-life in November 2021, with increasing RMS (as shown in AC SAF Operations Report 2/2020) and bias around the target accuracy requirement limit of 30 %.

Generally, the results are within the requirements (target accuracy requirement of 30 % in polluted conditions and optimal accuracy of 20 %) for Xianghe and Uccle. Beijing and OHP report about 50 % biases, while larger values are found for Bujumbura and Reunion, as previously (Pinardi *et al.*, 2014; NO_2 Validation Report 2015; Pinardi *et al*., 2020). As before, smoothing the MAXDOAS profiles with the satellite averaging kernels is not always reducing the mean comparison differences, with an impact of ~10-20 % depending on the station (AC SAF Operations Report 1/2018, PT meeting of May 2018). In term of stability most of the stations report differences over time up to 10 %, which is also about the level of difference between GOME-2A and GOME-2B (10 to 15 %). These biases could be reduced in the future with GDP-4.9 GOME-2 data (Liu *et al.*, 2019) showing improved validation results e.g for Xianghe.

Status of GOME-2A, GOME-2B and GOME-2C total (stratospheric) NO2

Quality monitoring of the GOME-2 NO_2 total (stratospheric) column data is regularly carried out using correlative ground-based measurements collected from about 20 Zenith-Scattered-Light DOAS UV-visible (ZSL-DOAS) instruments affiliated with the Network for the Detection of Atmospheric Composition Change (NDACC). The NO_2 column validation protocol has already been described in previous AC SAF validation reports with its latest updates published in Verhoelst

et al. (AMT 2021). This protocol includes the selection of GOME-2/NDACC co-located data pairs based on the air-mass matching technique, a model-based photochemical correction compensating for significant solar local time differences between GOME-2 mid-morning and NDACC twilight observations in polar summer, and a cloud-based filtering of NO_2 data over polluted stations aiming at the removal of pollution-affected pixels. At some stations real-time processing of the ground-based observations still uses NO_2 absorption cross-sections at room temperature instead of stratospheric temperature. As a result, the retrieved total NO_2 column is affected by a negative systematic bias of 15 – 20 %, thus a seasonally varying bias in total NO_2: such data are removed. Thanks to this strict protocol, data comparisons can be carried out within a residual uncertainty of maximum $2 - 3 \times 10^{14}$ molec/cm^2 combining both the ground-based data uncertainty and comparison errors, which is indicated by the shaded area on the pole-to-pole graphs.

GOME-2A (GDP 4.8) NO2 VCD vs. CNRS SAOZ at Dumont d'Urville (66.67°S, 140.02°E)

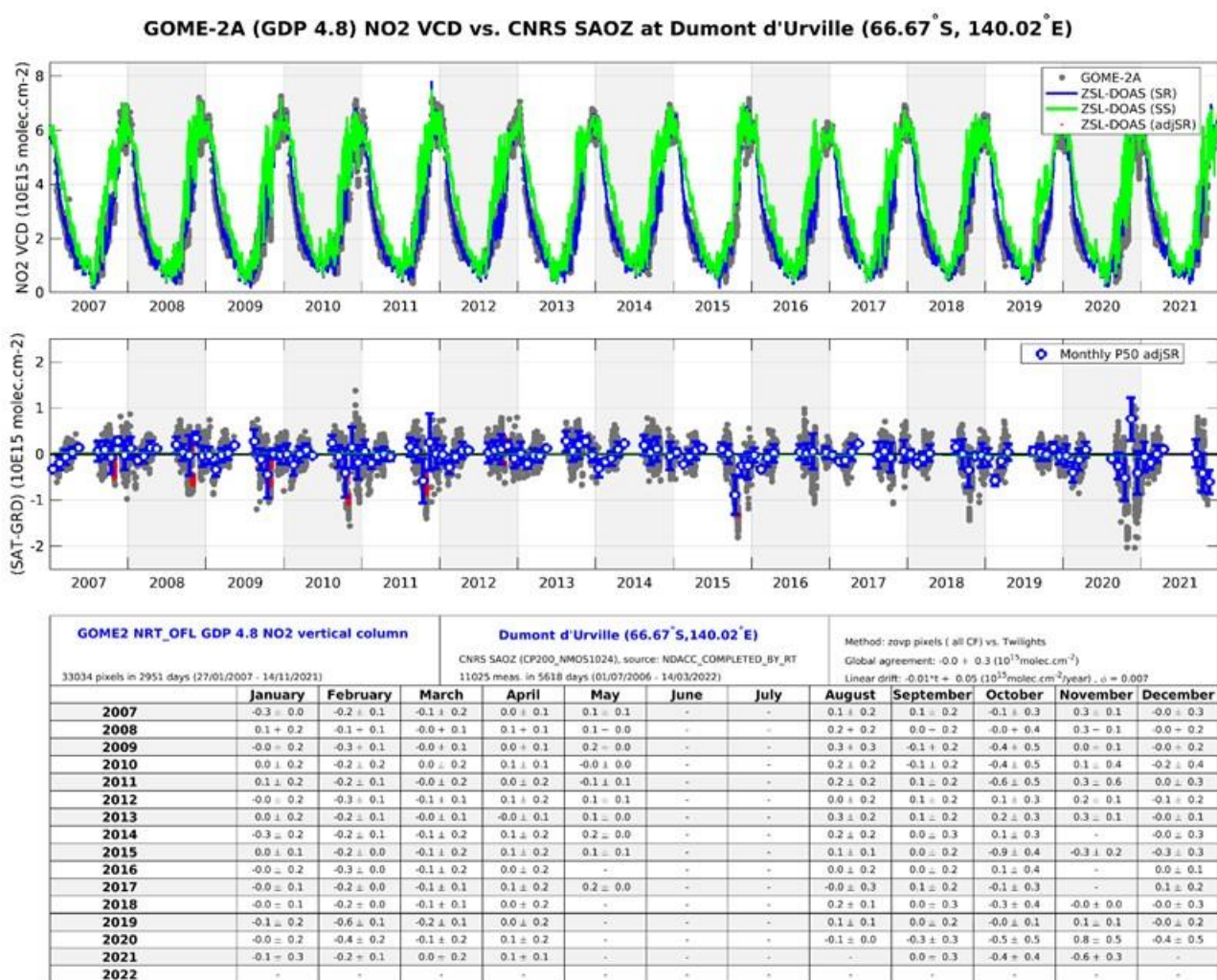| GOME2 NRT_OFL GDP 4.8 NO2 vertical column
33034 pixels in 2951 days (27/01/2007 - 14/11/2021) | | | | Dumont d'Urville (66.67°S,140.02°E)
CNRS SAOZ (CP200_NMOS1024), source: NDACC_COMPLETED_BY_RT
11025 meas. in 5618 days (01/07/2006 - 14/03/2022) | | | | Method: zovp pixels (all CF) vs. Twilights
Global agreement: -0.0 ± 0.3 (10^{15} molec.cm^{-2})
Linear drift: -0.01*t + 0.05 (10^{15}molec.cm^{-2}/year) , φ = 0.007 | | | | |
	January	February	March	April	May	June	July	August	September	October	November	December
2007	-0.3 ± 0.0	-0.2 ± 0.1	-0.1 ± 0.2	0.0 ± 0.1	0.1 ± 0.1	-	-	0.1 ± 0.2	0.1 ± 0.2	-0.1 ± 0.3	0.3 ± 0.1	-0.0 ± 0.3
2008	0.1 ± 0.2	-0.1 ± 0.1	-0.0 ± 0.1	0.1 ± 0.1	0.1 ± 0.0	-	-	0.2 ± 0.2	0.0 ± 0.2	-0.0 ± 0.4	0.3 ± 0.1	-0.0 ± 0.2
2009	-0.0 ± 0.2	-0.3 ± 0.1	-0.0 ± 0.1	0.0 ± 0.1	0.2 ± 0.0	-	-	0.3 ± 0.3	-0.1 ± 0.2	-0.4 ± 0.5	0.0 ± 0.1	-0.0 ± 0.2
2010	0.0 ± 0.2	-0.2 ± 0.2	0.0 ± 0.2	0.1 ± 0.1	-0.0 ± 0.0	-	-	0.2 ± 0.2	-0.1 ± 0.2	-0.4 ± 0.5	0.1 ± 0.4	-0.2 ± 0.4
2011	0.1 ± 0.2	-0.2 ± 0.1	-0.0 ± 0.2	0.0 ± 0.2	-0.1 ± 0.1	-	-	0.2 ± 0.2	0.1 ± 0.2	-0.6 ± 0.5	0.3 ± 0.6	0.0 ± 0.3
2012	-0.0 ± 0.2	-0.3 ± 0.1	-0.1 ± 0.1	0.1 ± 0.1	0.1 ± 0.1	-	-	0.0 ± 0.2	0.1 ± 0.2	0.1 ± 0.3	0.2 ± 0.1	0.1 ± 0.2
2013	0.0 ± 0.2	-0.2 ± 0.1	-0.0 ± 0.1	-0.0 ± 0.1	0.1 ± 0.0	-	-	0.3 ± 0.2	0.1 ± 0.2	0.2 ± 0.3	0.3 ± 0.1	-0.0 ± 0.1
2014	-0.3 ± 0.2	-0.2 ± 0.1	-0.1 ± 0.2	0.1 ± 0.2	0.2 ± 0.0	-	-	0.2 ± 0.2	0.0 ± 0.3	0.1 ± 0.3	-	-0.0 ± 0.3
2015	0.0 ± 0.1	-0.2 ± 0.0	-0.1 ± 0.2	0.1 ± 0.2	0.1 ± 0.1	-	-	0.1 ± 0.1	0.0 ± 0.2	-0.9 ± 0.4	-0.3 ± 0.2	-0.3 ± 0.3
2016	-0.0 ± 0.2	-0.3 ± 0.0	-0.1 ± 0.2	0.0 ± 0.2	-	-	-	0.0 ± 0.2	0.0 ± 0.2	0.1 ± 0.4	-	0.0 ± 0.1
2017	-0.0 ± 0.1	-0.2 ± 0.0	-0.1 ± 0.1	0.1 ± 0.2	0.2 ± 0.0	-	-	-0.0 ± 0.3	0.1 ± 0.2	-0.1 ± 0.3	-	0.1 ± 0.2
2018	-0.0 ± 0.1	-0.2 ± 0.0	-0.1 ± 0.1	0.0 ± 0.2	-	-	-	0.2 ± 0.1	0.0 ± 0.3	-0.3 ± 0.4	-0.0 ± 0.0	-0.0 ± 0.3
2019	-0.1 ± 0.2	-0.6 ± 0.1	-0.2 ± 0.1	0.0 ± 0.2	-	-	-	0.1 ± 0.1	0.0 ± 0.2	-0.0 ± 0.1	0.1 ± 0.1	-0.0 ± 0.2
2020	-0.0 ± 0.2	-0.4 ± 0.2	-0.1 ± 0.2	0.1 ± 0.2	-	-	-	-0.1 ± 0.0	-0.3 ± 0.3	-0.5 ± 0.5	0.8 ± 0.5	-0.4 ± 0.5
2021	-0.1 ± 0.3	-0.2 ± 0.1	0.0 ± 0.2	0.1 ± 0.1	-	-	-	-	0.0 ± 0.3	-0.4 ± 0.4	-0.6 ± 0.3	-
2022	-	-	-	-	-	-	-	-	-	-	-	-

Figure 7.9. Comparison of NO₂ column data measured at the NDACC Antarctic station of Dumont d'Urville by GOME-2A (GDP-4.8) and by the CNRS/LATMOS ZSL-DOAS spectrometer. Top: time series of NO₂ column data; centre: time series of NO₂ column difference; bottom (table): monthly median value (and its ±1σ scatter) of the difference between GOME-2A GDP-4.8 and the NDACC ZSL-DOAS NO₂ column data.

Figure 7.9 (for GOME-2A), Figure 7.10 (for GOME-2B) and Figure 7.11 (for GOME-2C) show the comparison of NO₂ column data at the NDACC Antarctic station of Dumont d'Urville, a station

located on the polar circle, in a pristine environment without any known source of tropospheric NO_2. Comparison results at this station are representative of the validation of purely stratospheric data series, at moderate and large solar zenith angle, and over the full range of NO_2 stratospheric column values from winter lows of about 10^{14} molec/cm^2 (wintertime denoxification episodes) up to summer highs of 7×10^{15} molec/cm^2 (complete depletion of N_2O_5 into NO_2 due to polar midnight Sun). On a monthly median basis, and over the 14 years of GOME-2A operation and 9 years of GOME-2B operation, the target bias of $3 - 5\times10^{14}$ molec/cm^2 has never been exceeded, except occasionally in October when the station is overpassed frequently by the border of the polar vortex, thus when atmospheric variability contributes significant co-location mismatch noise and bias to the difference in stratospheric NO_2. The ground dataset shown in this figure is a composite dataset consisting of the NDACC reprocessed dataset extended through the last year by the near-real-time dataset (latmos_rt).
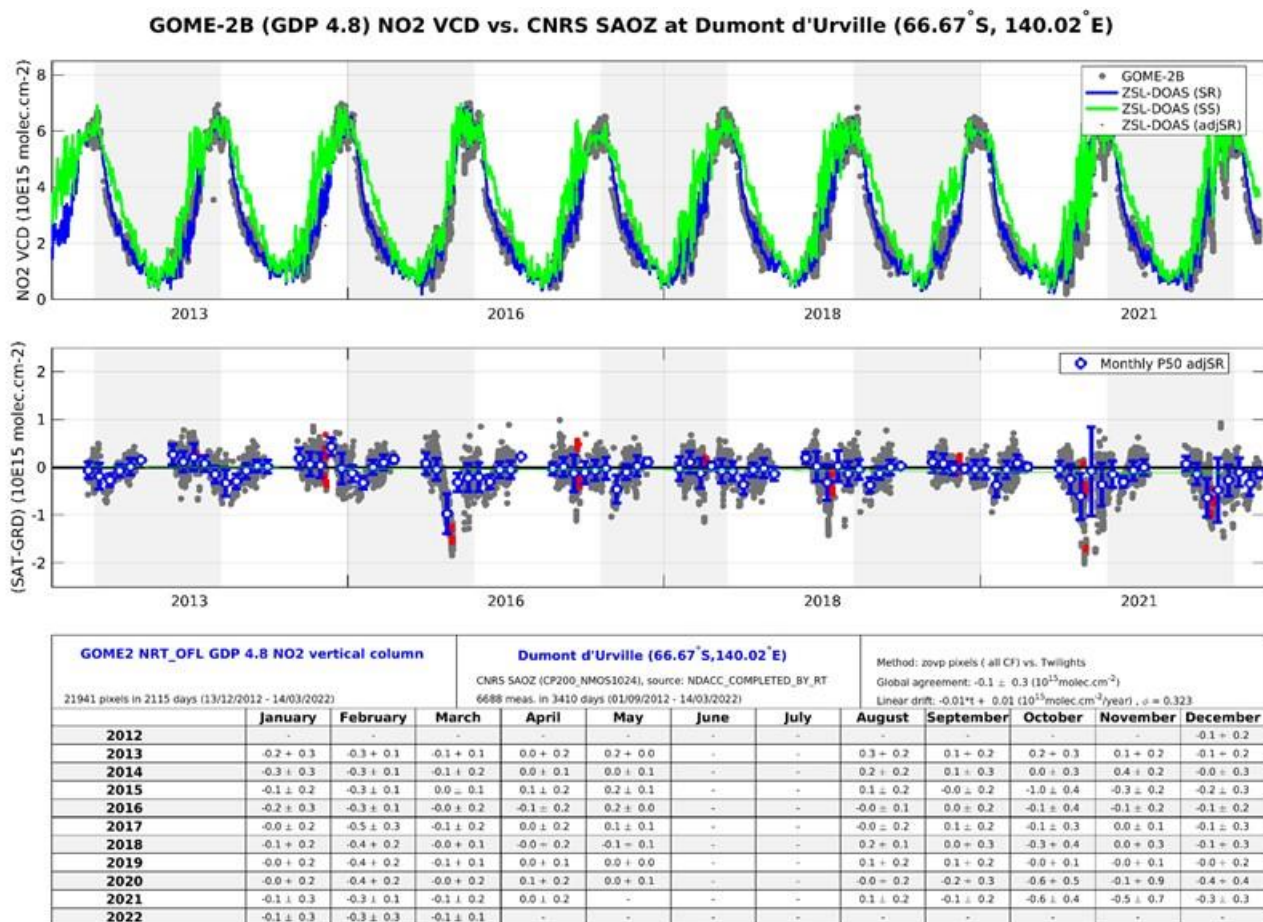

GOME-2B (GDP 4.8) NO2 VCD vs. CNRS SAOZ at Dumont d'Urville (66.67°S, 140.02°E)

	January	February	March	April	May	June	July	August	September	October	November	December
2012	-	-	-	-	-	-	-	-	-	-	-	-0.1 + 0.2
2013	-0.2 + 0.3	-0.3 + 0.1	-0.1 + 0.1	0.0 + 0.2	0.2 + 0.0	-	-	0.3 + 0.2	0.1 + 0.2	0.2 + 0.3	0.1 + 0.2	-0.1 + 0.2
2014	-0.3 + 0.3	-0.3 + 0.1	-0.1 + 0.2	0.0 + 0.1	0.0 + 0.1	-	-	0.2 + 0.2	0.1 + 0.3	0.0 + 0.3	0.4 + 0.2	-0.0 + 0.3
2015	-0.1 ± 0.2	-0.3 ± 0.1	0.0 ± 0.1	0.1 ± 0.2	0.2 ± 0.1	-	-	0.1 ± 0.2	-0.0 ± 0.2	-1.0 ± 0.4	-0.3 ± 0.2	-0.2 ± 0.3
2016	-0.2 ± 0.3	-0.3 ± 0.1	-0.0 ± 0.2	-0.1 ± 0.2	0.2 ± 0.0	-	-	-0.0 ± 0.1	0.0 ± 0.2	-0.1 ± 0.4	-0.1 ± 0.2	-0.1 ± 0.2
2017	-0.0 ± 0.2	-0.5 ± 0.3	-0.1 ± 0.2	0.0 ± 0.2	0.1 ± 0.1	-	-	-0.0 ± 0.2	0.1 ± 0.2	-0.1 ± 0.3	0.0 ± 0.1	-0.1 ± 0.3
2018	-0.1 + 0.2	-0.4 + 0.2	-0.0 + 0.1	-0.0 + 0.1	-0.1 + 0.1	-	-	0.2 + 0.1	0.0 + 0.3	-0.3 + 0.4	0.0 + 0.3	-0.1 + 0.3
2019	-0.0 + 0.2	-0.4 + 0.2	-0.1 + 0.1	0.0 + 0.1	0.0 + 0.0	-	-	0.1 + 0.2	0.1 + 0.2	-0.0 + 0.1	-0.0 + 0.1	-0.0 + 0.2
2020	-0.0 + 0.2	-0.4 + 0.2	-0.0 + 0.2	0.1 + 0.2	0.0 + 0.1	-	-	-0.0 + 0.2	-0.0 + 0.2	-0.6 + 0.5	-0.1 + 0.9	-0.4 + 0.4
2021	-0.1 0.3	-0.3 ± 0.1	-0.1 ± 0.2	0.0 ± 0.2	-	-	-	0.1 ± 0.2	-0.1 ± 0.2	-0.6 ± 0.4	-0.5 ± 0.7	-0.3 ± 0.3
2022	-0.1 ± 0.3	-0.3 ± 0.3	-0.1 ± 0.1	-	-	-	-	-	-	-	-	-

Figure 7.10. Same as Figure 7.9 but with GOME-2 on Metop-B (GDP4.8), from December 2012 to March 2022.
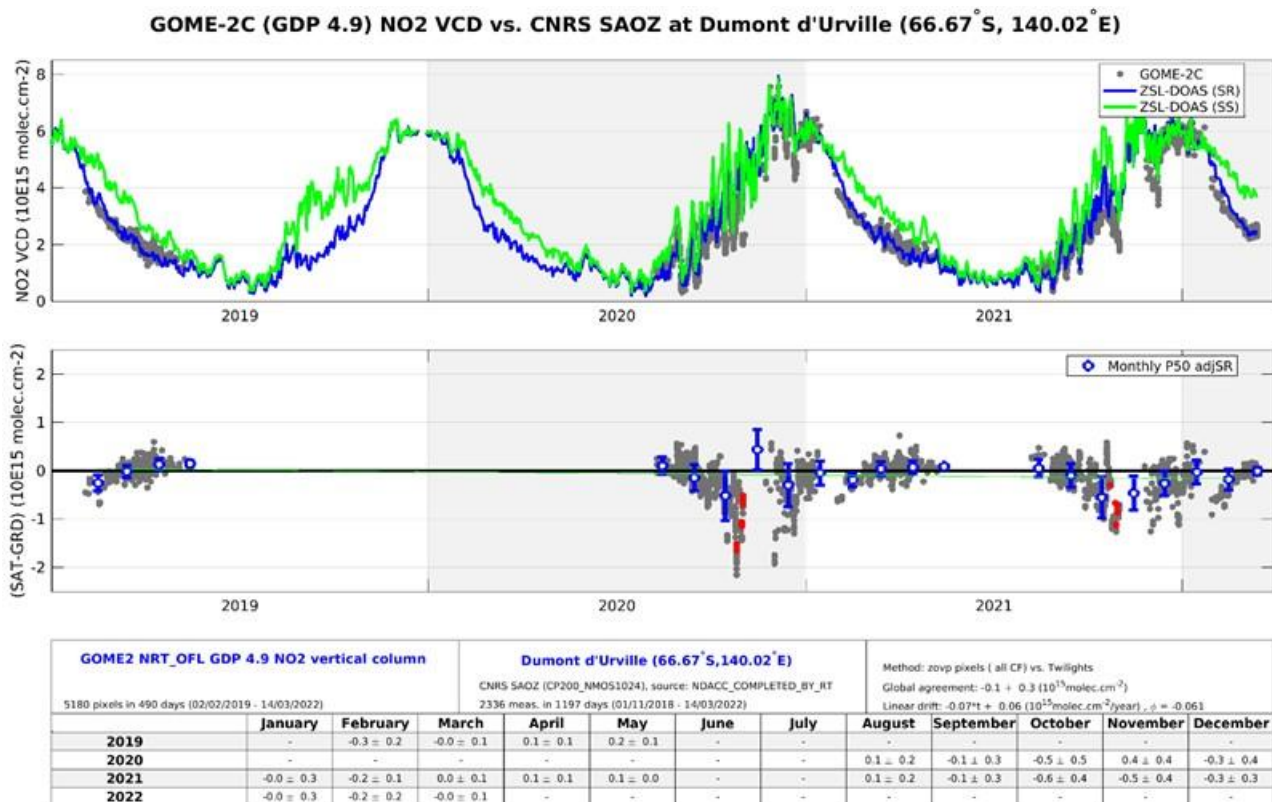
Figure 7.11. Same as Figure 7.9 but with GOME-2 on Metop-C (GDP4.9), from February 2019 to March 2022.

Figure 7.12 and Figure 7.13 display similar results obtained at the NDACC Alpine station of Observatoire de Haute Provence in Southern France and the NDACC Southern Tropic station of Saint-Denis de la Réunion, thus in occasional presence of pollution and over a wider range of solar zenith angle. Again, the target bias of $3 - 5 \times 10^{14}$ molec/cm^2 has rarely been exceeded, except in very few cases.
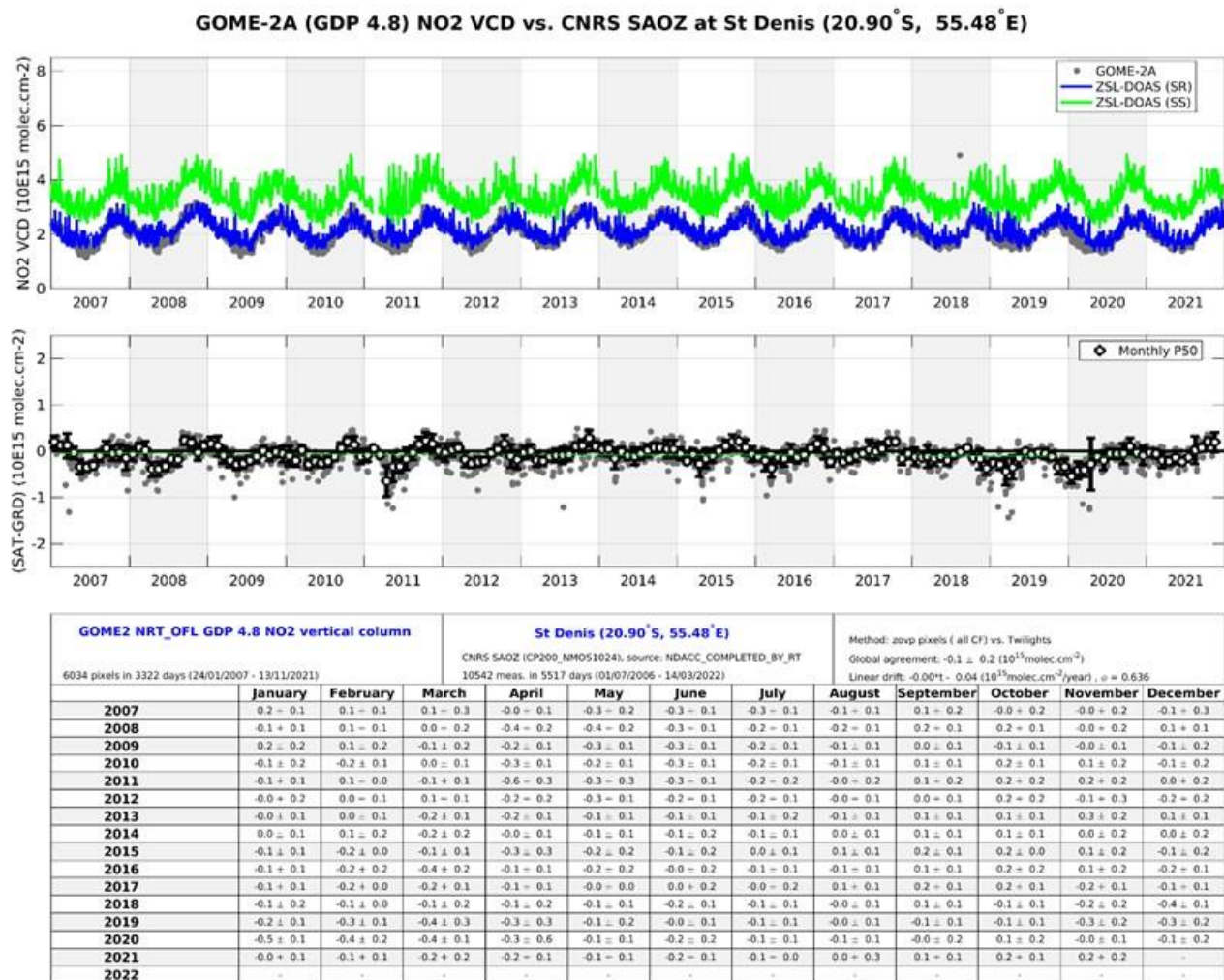
GOME-2A (GDP 4.8) NO2 VCD vs. CNRS SAOZ at Observatoire de Haute-Provence (43.94°N, 5.71°E)

GOME2 NRT_OFL GDP 4.8 NO2 vertical column		Observatoire de Haute-Provence (43.94°N, 5.71°E)			Method: zovp pixels (CF>25%) vs. Twilights							
11805 pixels in 3920 days (23/01/2007 - 15/11/2021)		CNRS SAOZ (CP200_NMOS1024), source: NDACC_COMPLETED_BY_RT 10885 meas. in 5626 days (01/07/2006 - 14/03/2022)			Global agreement: -0.1 ~ 0.3 (10^{15}molec.cm^{-2}) Linear drift: -0.01*t - 0.05 (10^{15}molec.cm^{-2}/year), σ = 0.452							
	January	February	March	April	May	June	July	August	September	October	November	December
2007	0.4 ± 0.1	-0.1 ± 0.2	-0.1 ± 0.2	0.0 ~ 0.2	-0.2 ± 0.2	-0.0 ~ 0.3	-0.0 ~ 0.2	0.0 ± 0.1	-0.0 ± 0.2	-0.5 ± 0.3	-0.4 ± 0.6	-0.1 ± 0.2
2008	-0.3 ± 0.2	-0.1 ± 0.1	-0.1 ± 0.3	-0.1 ± 0.2	0.0 ± 0.3	-0.1 ± 0.3	0.1 ± 0.2	0.1 ± 0.1	-0.0 ± 0.2	-0.3 ± 0.3	-0.3 ± 0.2	-0.4 ± 0.4
2009	-0.0 ± 0.2	-0.0 ± 0.4	0.0 ± 0.4	-0.0 ± 0.2	-0.0 ± 0.1	-0.0 ± 0.3	0.1 ± 0.3	0.1 ± 0.1	-0.1 ± 0.3	-0.2 ± 0.3	-0.2 ± 0.2	-0.1 ± 0.3
2010	-0.2 ± 0.3	-0.2 ± 0.3	-0.2 ± 0.2	-0.0 ± 0.2	-0.2 ± 0.3	-0.1 ± 0.2	0.1 ± 0.1	0.0 ± 0.3	0.0 ± 0.1	-0.2 ± 0.5	-0.2 ± 0.3	-0.1 ± 0.4
2011	-0.0 ± 0.2	0.0 ± 0.2	-0.2 ± 0.2	-0.0 ± 0.2	-0.2 ± 0.2	-0.1 ± 0.3	-0.1 ± 0.1	0.2 ± 0.1	-0.1 ± 0.2	-0.2 ± 0.1	-0.2 ± 0.5	-0.3 ± 0.2
2012	-0.2 ± 0.4	-0.1 ± 0.2	-0.0 ± 0.2	0.0 ± 0.2	-0.0 ± 0.3	0.1 ± 0.1	-0.1 ± 0.2	0.1 ± 0.3	0.0 ± 0.2	-0.2 ± 0.4	-0.1 ± 0.5	-0.2 ± 0.3
2013	-0.1 ± 0.5	0.1 ± 0.3	0.1 ± 0.3	-0.0 ± 0.3	-0.1 ± 0.1	0.2 ± 0.1	0.1 ± 0.2	0.4 ± 0.1	-0.1 ± 0.2	-0.1 ± 0.4	-0.6 ± 0.9	-0.1 ± 0.3
2014	-0.3 ± 0.3	-0.2 ± 0.1	0.1 ± 0.2	-0.0 ± 0.2	-0.0 ± 0.2	0.2 ± 0.3	0.1 ± 0.2	0.3 ± 0.1	-0.0 ± 0.6	-0.2 ~ 0.1	-0.3 ± 0.1	-0.3 ± 0.7
2015	-0.0 ± 0.6	-0.3 ± 0.3	-0.3 ± 0.3	0.0 ~ 0.1	0.0 ~ 0.1	0.0 ± 0.3	0.3 ± 0.1	0.1 ± 0.2	-0.0 ± 0.3	-0.3 ± 0.2	-0.3 ± 0.1	-0.1 ± 0.2
2016	-0.3 ± 0.5	-0.7 ± 0.4	-0.1 ± 0.1	0.0 ± 0.2	0.0 ± 0.2	-0.1 ± 0.3	0.2 ± 0.2	0.2 ± 0.3	-0.1 ± 0.3	-0.4 ± 0.2	-0.1 ± 0.2	0.0 ± 0.2
2017	-0.1 ± 0.3	-0.2 ± 0.3	-0.0 ± 0.1	-0.2 ± 0.1	0.1 ± 0.2	0.1 ± 0.2	0.1 ± 0.1	0.2 ± 0.1	-0.0 ± 0.2	-0.1 ± 0.1	-0.3 ± 0.2	-0.3 ± 0.3
2018	-0.3 ± 0.2	-0.2 ± 0.3	-0.1 ± 0.2	-0.1 ± 0.2	-0.2 ± 0.4	-0.2 ± 0.2	0.1 ± 0.5	0.0 ± 0.2	-0.3 ± 0.1	-0.4 ± 0.1	-0.5 ± 0.3	-0.1 ± 0.2
2019	-0.1 ± 0.3	-0.4 ± 0.0	-0.2 ± 0.2	-0.1 ± 0.3	-0.1 ± 0.1	0.1 ± 0.1	0.1 ± 0.1	0.1 ± 0.4	-0.2 ± 0.3	-0.2 ± 0.3	-0.3 ± 0.3	-0.4 ± 0.3
2020	-0.3 ~ 0.3	-0.4 ± 0.2	-0.2 ± 0.1	-0.2 ± 0.1	-0.1 ± 0.2	0.1 ± 0.2	0.1 ± 0.1	0.1 ± 0.1	-0.2 ± 0.4	-0.3 ± 0.1	-0.3 ± 0.1	-0.1 ± 0.1
2021	-0.3 ± 0.3	-0.2 ± 0.3	-0.1 ± 0.1	-0.2 ± 0.2	-0.1 ± 0.2	-0.0 ± 0.1	0.0 ± 0.2	0.1 ± 0.1	-0.1 ± 0.2	-0.2 ± 0.1	-0.2 ± 0.2	-
2022	-	-	-	-	-	-	-	-	-	-	-	-

Figure 7.12. Same as Figure 7.9 but at the NDACC Alpine station of Observatoire de Haute Provence by GOME-2A (GDP-4.8) and by the LATMOS ZSL-DOAS spectrometer (NDACC and latmos_rt). Top: time series of NO₂ column data; centre: time series of NO₂ column difference; bottom (table): monthly median value (and its ±1σ scatter) of the difference between GOME-2A GDP-4.8 and the NDACC NO₂ column data.

GOME-2A (GDP 4.8) NO2 VCD vs. CNRS SAOZ at St Denis (20.90°S, 55.48°E)

GOME2 NRT_OFL GDP 4.8 NO2 vertical column		St Denis (20.90°S, 55.48°E)		Method: zovp pixels (all CF) vs. Twilights		
6034 pixels in 3322 days (24/01/2007 - 13/11/2021)		CNRS SAOZ (CP200_NMOS1024), source: NDACC_COMPLETED_BY_RT		Global agreement: -0.1 ± 0.2 (10¹⁵molec.cm⁻²)		
		10542 meas. in 5517 days (01/07/2006 - 14/03/2022)		Linear drift: -0.00*t - 0.04 (10¹⁵molec.cm⁻²/year) , e = 0.636		

	January	February	March	April	May	June	July	August	September	October	November	December
2007	0.2 – 0.1	0.1 – 0.1	0.1 – 0.3	-0.0 – 0.1	-0.3 – 0.2	-0.3 – 0.1	-0.3 – 0.1	-0.1 ÷ 0.1	0.1 ÷ 0.2	-0.0 ÷ 0.2	-0.0 ÷ 0.2	-0.1 ÷ 0.3
2008	-0.1 + 0.1	0.1 – 0.1	0.0 – 0.2	-0.4 – 0.2	-0.4 – 0.2	-0.3 – 0.1	-0.2 – 0.1	-0.2 – 0.1	0.2 – 0.1	0.2 – 0.1	-0.0 – 0.2	0.1 + 0.1
2009	0.2 – 0.2	0.1 – 0.2	-0.1 ± 0.2	-0.2 – 0.1	-0.3 – 0.1	-0.3 – 0.1	-0.2 – 0.1	-0.1 – 0.1	0.0 – 0.1	-0.1 ± 0.1	-0.0 ± 0.1	-0.1 ± 0.2
2010	-0.1 ± 0.2	-0.2 ± 0.1	0.0 – 0.1	-0.3 – 0.1	-0.2 – 0.1	-0.3 – 0.1	-0.2 – 0.1	-0.1 – 0.1	0.1 – 0.1	0.2 – 0.1	0.1 ± 0.2	-0.1 ± 0.2
2011	-0.1 + 0.1	0.1 – 0.0	-0.1 + 0.1	0.6 – 0.3	-0.3 – 0.3	-0.3 – 0.1	-0.2 – 0.2	-0.0 – 0.2	0.1 – 0.2	0.2 + 0.2	0.2 + 0.2	0.0 + 0.2
2012	-0.0 + 0.2	0.0 – 0.1	0.1 – 0.1	-0.2 – 0.2	-0.3 – 0.1	-0.2 – 0.1	-0.2 – 0.1	-0.0 – 0.1	0.0 – 0.1	0.2 – 0.2	-0.1 – 0.3	-0.2 – 0.2
2013	-0.0 ± 0.1	0.0 – 0.1	-0.2 ± 0.1	-0.2 – 0.1	-0.1 – 0.1	-0.1 – 0.1	-0.1 – 0.2	-0.1 – 0.1	0.1 – 0.1	0.1 ± 0.1	0.3 ± 0.2	0.1 ± 0.1
2014	0.0 ± 0.1	0.1 ± 0.2	-0.2 ± 0.2	-0.0 ± 0.1	-0.1 – 0.1	-0.1 – 0.2	-0.1 – 0.1	0.0 ± 0.1	0.1 ± 0.1	0.1 ± 0.1	0.0 ± 0.2	0.0 ± 0.2
2015	-0.1 ± 0.1	-0.2 ± 0.0	-0.1 ± 0.1	-0.3 ± 0.3	-0.2 ± 0.2	-0.1 ± 0.2	0.0 ± 0.1	0.1 ± 0.1	0.2 ± 0.1	0.2 ± 0.0	0.1 ± 0.2	-0.1 ± 0.2
2016	-0.1 ± 0.1	-0.2 + 0.2	-0.4 ± 0.2	-0.1 – 0.1	-0.2 – 0.2	-0.0 – 0.2	-0.1 – 0.1	-0.1 – 0.1	0.1 – 0.1	0.2 ± 0.2	0.1 ± 0.2	-0.2 ± 0.1
2017	-0.1 + 0.1	-0.2 + 0.0	-0.2 + 0.1	-0.1 – 0.1	-0.0 – 0.0	0.0 + 0.2	-0.0 – 0.2	0.1 + 0.1	0.2 – 0.1	0.2 ± 0.1	-0.2 ± 0.1	-0.1 + 0.1
2018	-0.1 ± 0.2	-0.1 ± 0.0	-0.1 ± 0.2	-0.1 ± 0.2	-0.1 ± 0.1	-0.2 ± 0.1	-0.1 ± 0.1	-0.0 ± 0.1	0.1 ± 0.1	-0.1 ± 0.1	-0.2 ± 0.2	-0.4 ± 0.1
2019	-0.2 ± 0.1	-0.3 ± 0.1	-0.4 ± 0.3	-0.3 ± 0.3	-0.1 ± 0.2	-0.0 ± 0.1	-0.1 ± 0.1	-0.0 ± 0.1	-0.1 ± 0.1	-0.1 ± 0.1	-0.3 ± 0.2	-0.3 ± 0.2
2020	-0.5 ± 0.1	-0.4 ± 0.2	-0.4 ± 0.1	-0.3 ± 0.6	-0.1 ± 0.1	-0.2 ± 0.2	-0.1 ± 0.1	-0.1 ± 0.1	-0.0 ± 0.2	0.1 ± 0.2	-0.0 ± 0.1	-0.1 ± 0.2
2021	-0.0 + 0.1	0.1 ± 0.1	0.2 ± 0.2	0.2 – 0.1	0.1 – 0.1	0.2 – 0.1	0.1 – 0.0	0.0 + 0.3	0.1 – 0.1	0.2 ± 0.1	0.2 ± 0.2	-
2022	-	-	-									

Figure 7.13. Same as Figure 7.9 and Figure 7.10, but at the NDACC Southern Tropic station of Saint-Denis de la Réunion by GOME-2A (GDP-4.8) and by LATMOS ZSL-DOAS spectrometer (NDACC and latmos_rt). Top: time series of NO₂ column data; centre: time series of NO₂ column difference; bottom (table): monthly median value (and its ±1σ scatter) of the difference between GOME-2A GDP-4.8 and the NDACC NO₂ column data.

Figure 7.14 reports from pole to pole the median value of the systematic bias between GOME-2 and NDACC ZSL-DOAS data, assessed on the basis of all co-located data pairs available so far with the entire GOME-2A/B/C time-series until March 2022, while Figure 7.15 displays, again from pole to pole, the linear drift between GOME-2A/B/C and NDACC data. Those graphs show the good long-term stability of both the GOME-2A and GOME-2B GDP-4.8 NO₂ column data with respect to NDACC ZSL-DOAS data at all stations.

They also show that the target bias of $3 - 5 \times 10^{14}$ molec/cm^2 in unpolluted conditions is achieved for both satellites. Figure 7.13 also confirms the slight difference already noticed in previous validation reports between the biases observed respectively in the Southern and Northern hemispheres. Averaging median differences separately over the Northern and Southern Hemispheres concludes to an inter-hemispheric bias of about $2 - 3 \times 10^{14}$ molec/cm^2.
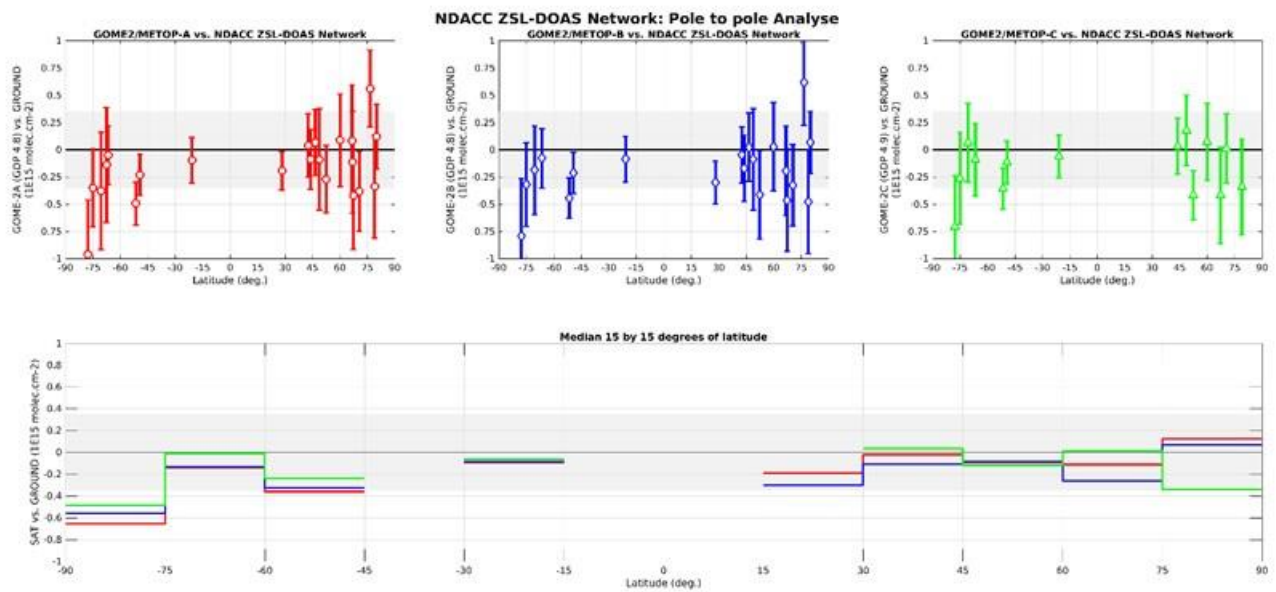
Figure 7.14. From pole to pole, median difference between the NO₂ column data reported by GOME-2A/B/C (red/ blue/ green) GDP-4.8 (GDP 4.9 for GOME-2C) and by ground-based ZSL-DOAS spectrometers at about 20 NDACC stations, calculated over 2007 – March 2022 for GOME-2A, 2012 – March 2022 for GOME-2B and 2019 – March 2022 for GOME-2C. Top: median difference at individual stations. Bottom: median difference averaged over 15° latitude bins.
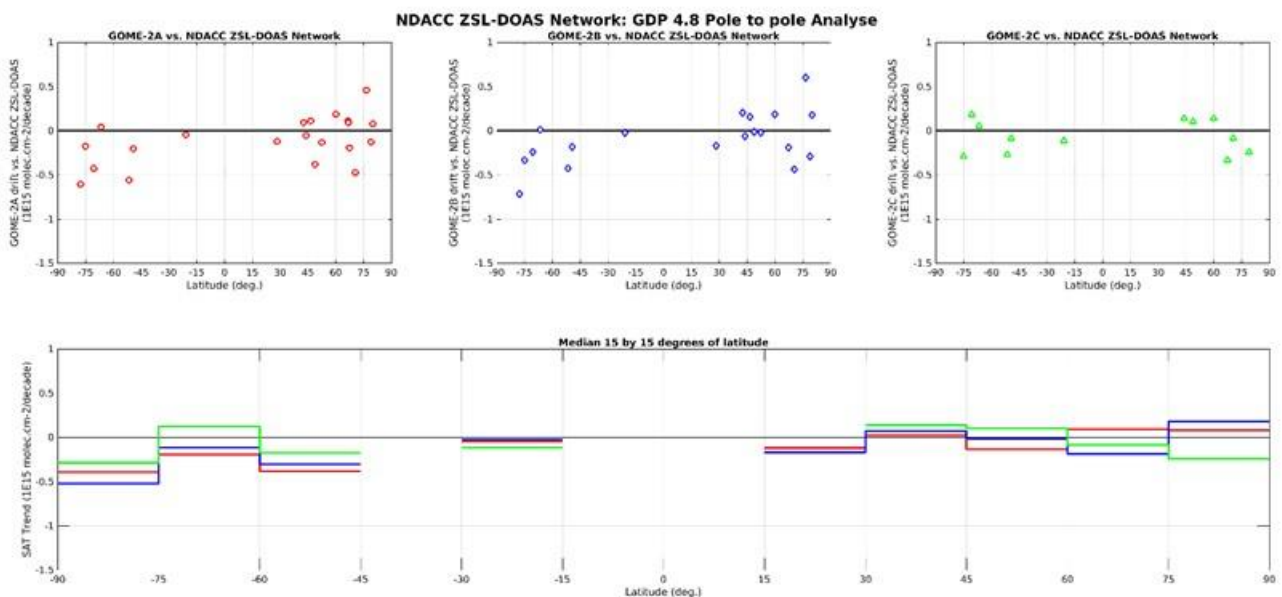
Figure 7.15. From pole to pole, linear drift (in percent by decade) of the difference between the NO₂ column data reported by GOME 2A/B/C (red/ blue/ green) GDP 4.8 (GDP 4.9 for GOME-2C) and by ground-based ZSL-DOAS spectrometers at about 20 NDACC stations, calculated over 2007 – March 2022 for GOME-2A, 2012 – March 2022 for GOME-2B and 2019 – March 2022 for GOME-2C. Top: linear drift estimates at individual stations. Bottom: same linear drift estimates but averaged over 15° latitude bins.

Status of GOME-2A, GOME-2B and GOME-2C total HCHO

This validation exercise is an extension of what is presented in the HCHO GDP-4.8 validation report, relying on correlative observations from MAX-DOAS instruments operated by BIRA-IASB at

Xianghe, Bujumbura, Uccle (miniDOAS and SG), OHP and Reunion (Le Port and Maido). Only data from Xianghe station are available for the last 6 months' time period.

The satellite and ground-based data selections are as in the validation report, and the updated comparisons figures until the end of 2021 can be found on the BIRA validation web server.

An illustration of the results for Xianghe is shown in Figure 7.16 for the GOME-2B and GOME-2C time-series and the scatter plots of both original comparisons and when smoothing MAXDOAS profiles with satellite averaging kernels. Absolute and relative difference plots can be found on the validation web server and mean bias values and correlation coefficients are summarized in Table 7.15.
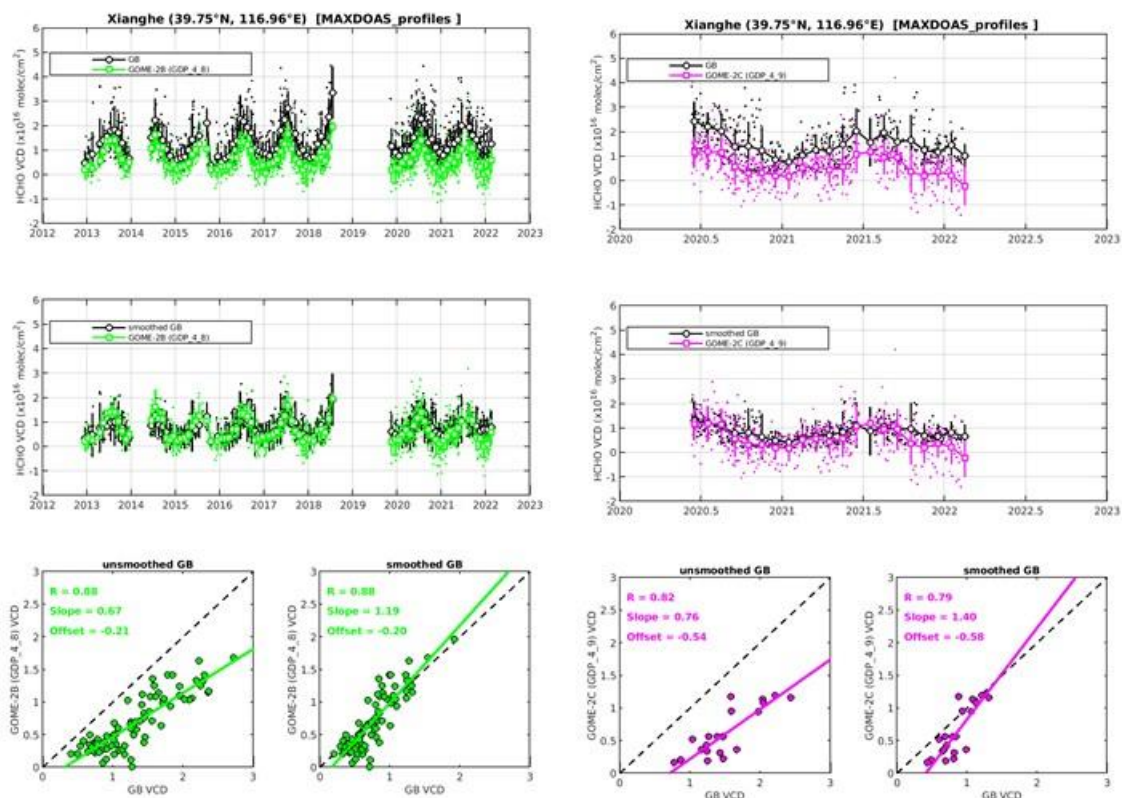
Figure 7.16. Comparison between GOME-2B GDP-4.8 (left), GOME-2C GDP 4.9 (right) and MAX-DOAS HCHO VCDs at Xianghe.

Table 7.15. Summary of the mean biases (in 10^{15} molec/cm^2) between GOME-2A/B/C and MAX-DOAS HCHO VCDs. The values in parentheses correspond to the mean relative biases and R is the correlation coefficients and S the slope of the linear regression of the monthly mean points. <u>Only Xianghe has been updated in this report, and for GOME-2A only until the end-of-life in November 2021</u>

	GOME-2A	GOME-2B	GOME-2C
UCCLE-SG **(50.8°N, 4.3°E)** **(whole period: 02/2017 – 12/2019)**	1.3 ± 2.0 (29 ± 56) R = 0.33, S = 0.29	0.3 ± 1.6 (7 ± 52) R = 0.75, S = 0.96	-
With smoothing	2.5 ± 1.8 (74 ± 81) R = 0.32, S = 0.38	1.6 ± 1.7 (49 ± 75) R = 0.76, S = 1.34	-
REUNION MAIDO **(20.9°S, 55.3°E)** **(whole period: 06/2018 – 11/2019)**	0.3 ± 1.6 (15 ± 78) R = 0.71, S = 2.32	2.1 ± 0.8 (94 ± 54) R = 0.84, S = 1.17	-
With smoothing	0.0 ± 1.5 (-0.04 ± 68) R = 0.77, S = 2.36	1.7 ± 0.8 (68 ± 43) R = 0.69, S = 1.29	-
XIANGHE **(39.7°N, 117.0°E)** **(whole period: 03/2010 – 12/2021)**	-5.3 ± 3.2 (-43 ± 18) R = 0.84, S = 0.51	-6.4 ± 2.7 (-48 ± 16) R = 0.88, S = 0.67	-8.9 ± 2.6 (-60 ± 21) R = 0.82, S = 0.76
With smoothing	-0.20 ± 2.0 (-2.7 ± 31) R = 0.85, S = 0.85	0.59 ± 2.2 (-8 ± 31) R = 0.88, S = 1.19	-2.4 ± 2.7 (-29 ± 37) R = 0.79, S = 1.40
BUJUMBURA **(3.0°S, 29.0°E)** **(whole period: 11/2013 – 07/2017)**	-6.3 ± 2.4 (-44 ± 10) R = 0.83, S = 0.46	-4.4 ± 2.2 (-32 ± 10) R = 0.88, S = 0.52	-
With smoothing	-1.6 ± 2.4 (-17 ± 24) R = 0.50, S = 0.43	0.3 ± 2.0 (3.2 ± 25) R = 0.72, S = 0.65	-
OHP **(whole period: 08/2014 – 03/2017)**	-0.1 ± 2.5 (1.7 ± 40) R = 0.42, S = 0.29	0.3 ± 1.1 (4.2 ± 21) R = 0.90, S = 0.75	-
With smoothing	0.9 ± 2.3 (16 ± 42) R = 0.39, S = 0.32	103.51 ± 1.0 (17 ± 22) R = 0.86, S = 1.01	-
REUNION LEPORT **(20.9°S, 55.3°E)** **(whole period: 04/2016 – 12/2017)**	-0.3 ± 1.0 (-10 ± 43) R = 0.66, S = 1.23	103.51 ± 0.8 (39 ± 26) R = 0.80, S = 1.56	-
With smoothing	103.51 ± 1.1 (71 ± 99) R = 0.59, S = 1.56	2.6 ± 0.1 (180 ± 56) R = 0.78, S = 2.83	-
UCCLE-miniDOAS **(50.8°N, 4.3°E)** **(whole period: 04/2011 – 05/2015)**	-0.5 ± 2.6 (-8.3 ± 49) R = 0.21, S = 0.25	-0.6 ± 1.6 (-9.4 ± 29) R = 0.76, S = 0.89	-
With smoothing	0.8 ± 2.7 (14 ± 81) R = 0.11, S = 0.13	-0.4 ± 1.7 (7.1 ± 34) R = 0.73, S = 0.88	-

In general, the results confirm that both satellite instruments capture well the HCHO VCD seasonality. In Reunion the signal is very small (less than ~0.5×10^{16} molec/cm²) and is more difficult to have firm conclusions. Differences with the newly installed Reunion Maido station need to be further investigated. In Uccle and OHP, the signal from GOME-2A is quite noisy, and the results are better with GOME-2B, which is probably related to GOME-2A degradation. A significant bias exists between GOME-2A/B and MAX-DOAS observations at the four stations (up to 50 %), but as already shown in the GDP-4.8 validation report, for some stations this bias can be significantly reduced when smoothing the MAX-DOAS profiles with the satellite column averaging kernels (see also values with smoothing in Table 7.15). The different figures for each stations can also be found on the BIRA validation web server.

For GOME-2C, scatter plot results are similar to what obtained with GOME-2B in Xianghe (slopes around 0.67/0.79 before smoothing). The absolute and relative differences are slightly larger than GOME-2B.

Monthly mean differences are calculated for every year and for the whole time-series in order to see the evolution in time of the bias. The differences are overall quite coherent over time (although larger values are found for GOME-2A compared to GOME-2B). Comparisons with GOME-2A could be performed until the Metop-A end-of-life in November 2021.

Status of GOME-2A, GOME-2B and GOME-2C total BrO

GOME-2A/B/C total columns of BrO from GDP-4.8 (4.9 in the case of GOME-2C) operational product are compared to ground-based UV-visible zenith-sky measurements at Harestua, Norway (60°N, 11°E). As done in previous validation report, the ground-based columns are derived from the vertical profiles retrieved by applying an OEM (Optimal Estimation Method) –based profiling technique to zenith-sky measurements at sunrise (Hendrick *et al.*, 2007).

The sensitivity of these measurements to the troposphere is increased by using a fixed reference spectrum corresponding to clear-sky noon summer conditions for the spectral analysis. In order to ensure the photochemical matching between satellite and ground-based observations, sunrise ground-based columns have been photochemically converted to the satellite overpass SZAs using a stacked box photochemical model (Hendrick *et al.*, 2007 and 2008).

Comparison results (150 km overpasses) for GOME-2A, GOME-2B and GOME-2C are shown in Figure 7.17, Figure 7.18 and Figure 7.19, respectively.

Mean biases values between GOME-2A/B/C and ground-based data are of -10 ± 12 %, -15 ± 11 % and -10 ± 10 %. GOME-2A/B/C BrO columns are thus all within the target accuracy of 30 % and also within the optimal accuracy of 15 %, except GOME-2B which is slightly above the required optimal accuracy threshold. Between 2013 and 2017, there is also an overall positive slope in the relative difference between GOME-2A and ground-based data. Given the fact that this slope is significantly less marked in GOME-2B comparisons, this indicates a possible drift in GOME-2A data likely related to the known degradation of the instrument. However, one cannot exclude that ground-based observations also partly contribute to this drift, due to the large uncertainty in the determination of the residual amount of BrO in the yearly selected reference spectra.
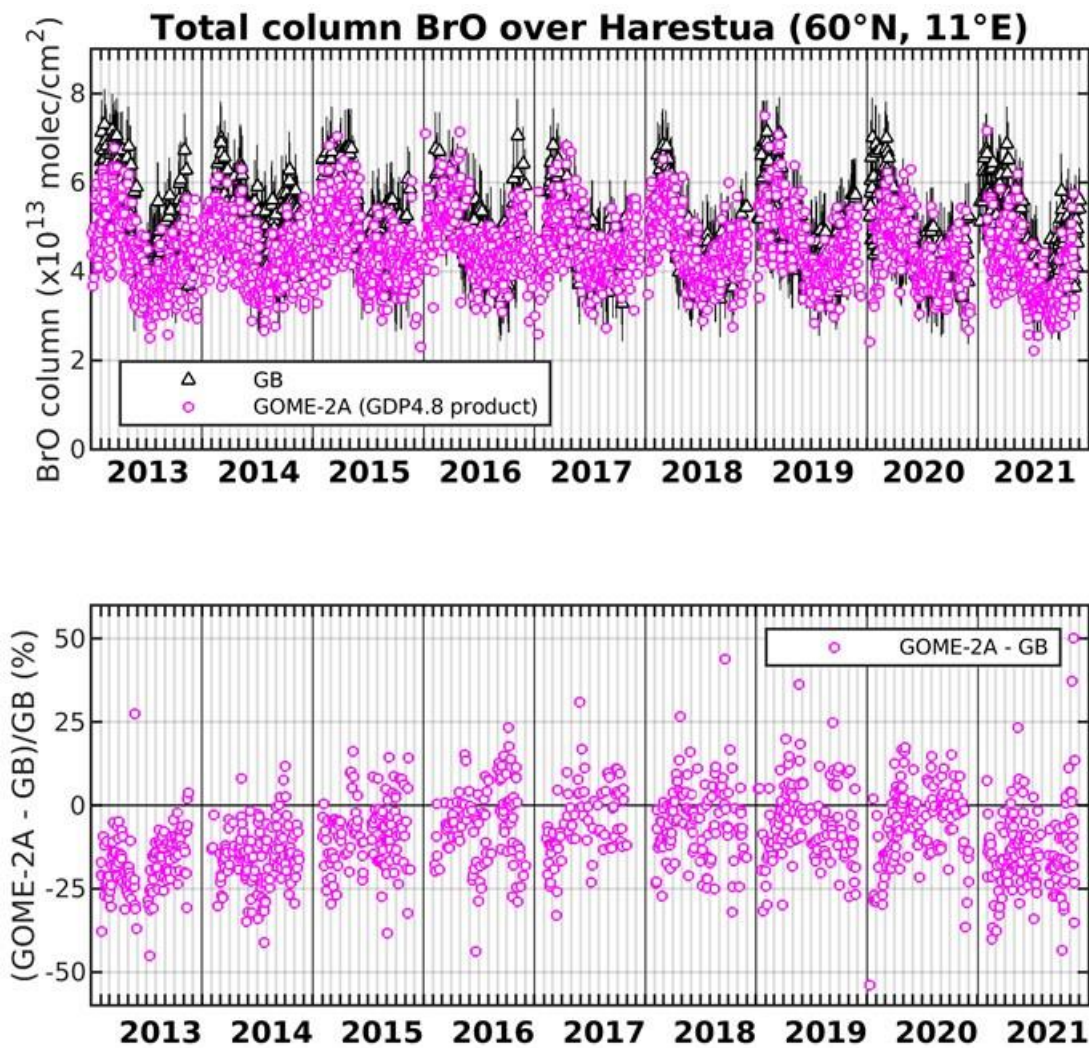
Figure 7.17. Comparison between GOME-2A GDP-4.8 and ground-based total BrO columns at Harestua (60°N, 11°E). The relative differences appear in the lower plot.
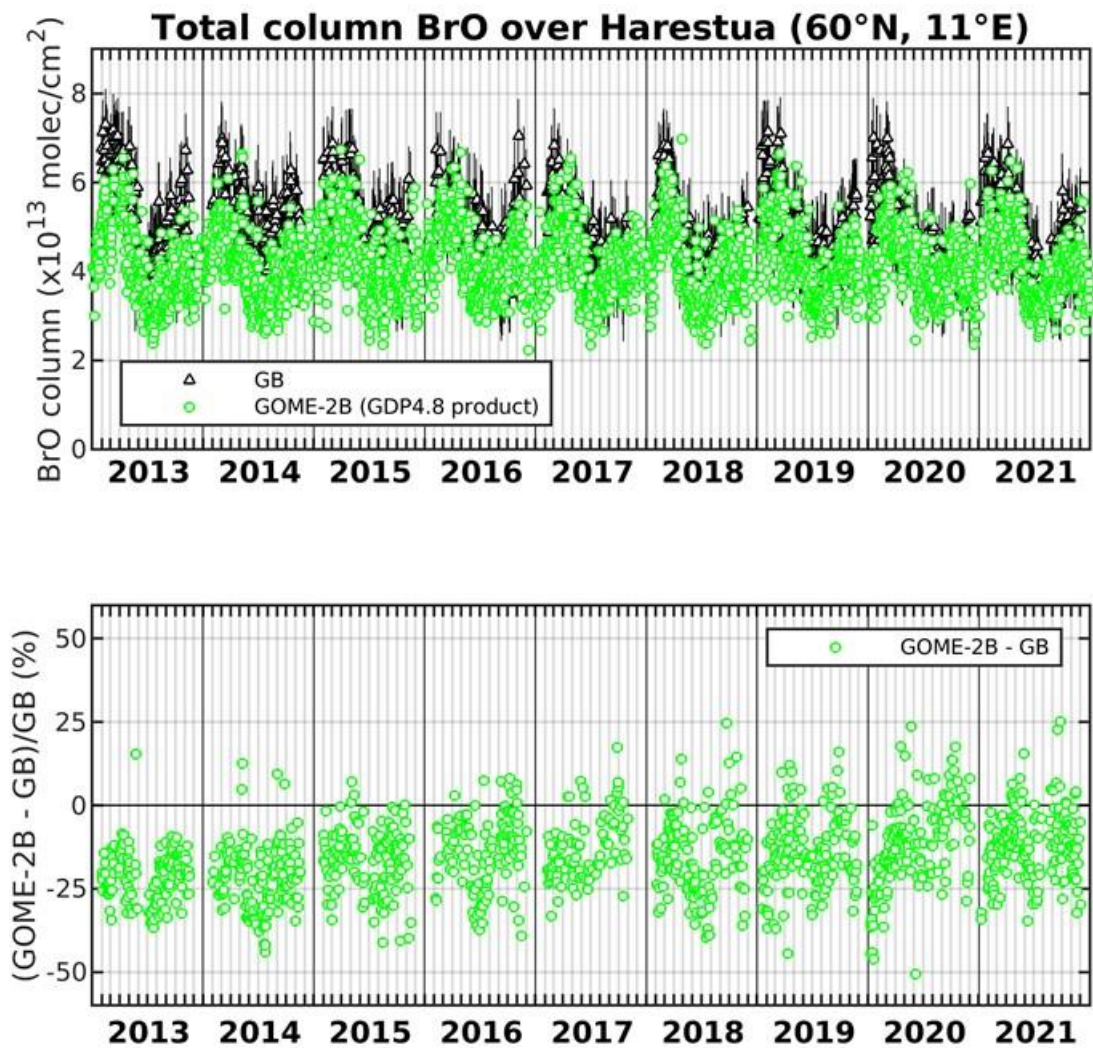
Figure 7.18. Comparison between GOME-2B GDP-4.8 and ground-based total BrO columns at Harestua (60°N, 11°E). The relative differences appear in the lower plot.
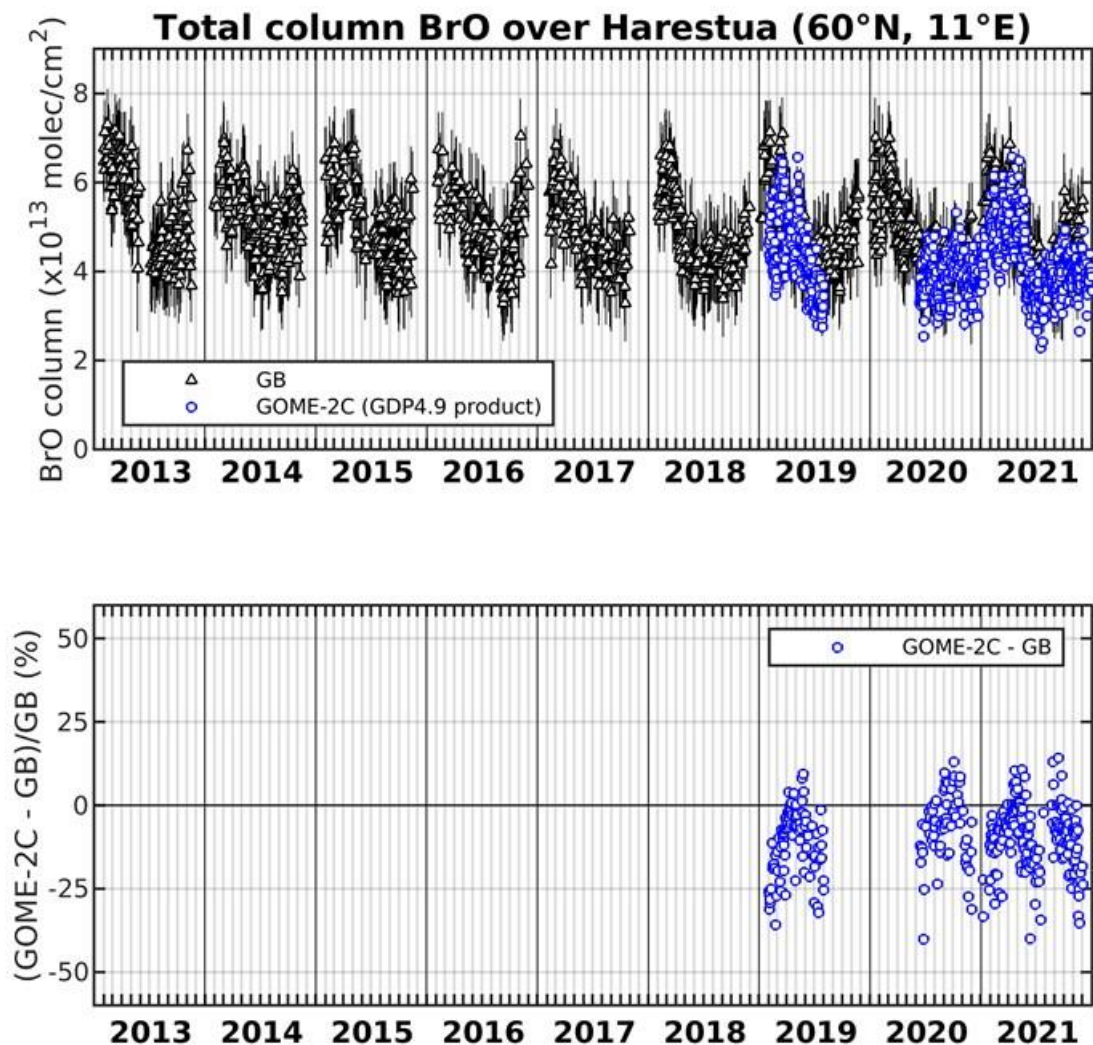
Figure 7.19. Comparison between GOME-2C GDP-4.9 and ground-based total BrO columns at Harestua (60°N, 11°E). The relative differences appear in the lower plot.

Status of GOME-2A, GOME-2B and GOME-2C SO₂

GOME-2 SO_2 GDP-4.8 continues to be used for the near-real-time observation of volcanic activity within the SACS service. The Support to Aviation Control Service (SACS) hosted by the Royal Belgian Institute for Space Aeronomy (BIRA-IASB) aims at supporting the Volcanic Ash Advisory Centers, like Toulouse VAAC and London VAAC. This is achieved by delivering near real-time data of SO_2 and aerosols derived from satellite measurements regarding volcanic emissions by UV-VIS (OMI, GOME-2A and GOME-2B composite until 31 March 2021 and GOME-2B and GOME-2C composite since then, OMPS, TROPOMI) and infrared (AIRS, IASI-A, IASI-B) instruments. In case of volcanic eruptions, notifications are sent out by email to interested parties. The SACS notification archive service gathers all the notifications; the results can be found here.

In the second half of 2021, SACS reported several clusters of cases where the maximum SO_2 detected by GOME-2 instruments was larger than 6 DU, as shown in Figure 7.20. These cover the Soufrière Saint-Vincent big eruption (9-12 April 2021) (regions 304 and 305) and the Etna paroxysms from the 21rst February 2021 to now (around region 207). Similar SO_2 levels and alerts are seen by GOME-2B and GOME-2C, with some small differences (end June and August 2021) due to small differences of the maximum SO_2 levels.

An example is shown in Figure 7.21 after the 19 September 2021 Cumbre Vieja eruption in La Palma (SACS region 205) and all the cases can be visualized on the SACS website by following the links found here. The coherence of the GOME-2B/C measurements with the other morning instruments (first line) is clear, as the temporal evolution with the afternoon platform instruments (second and third line).
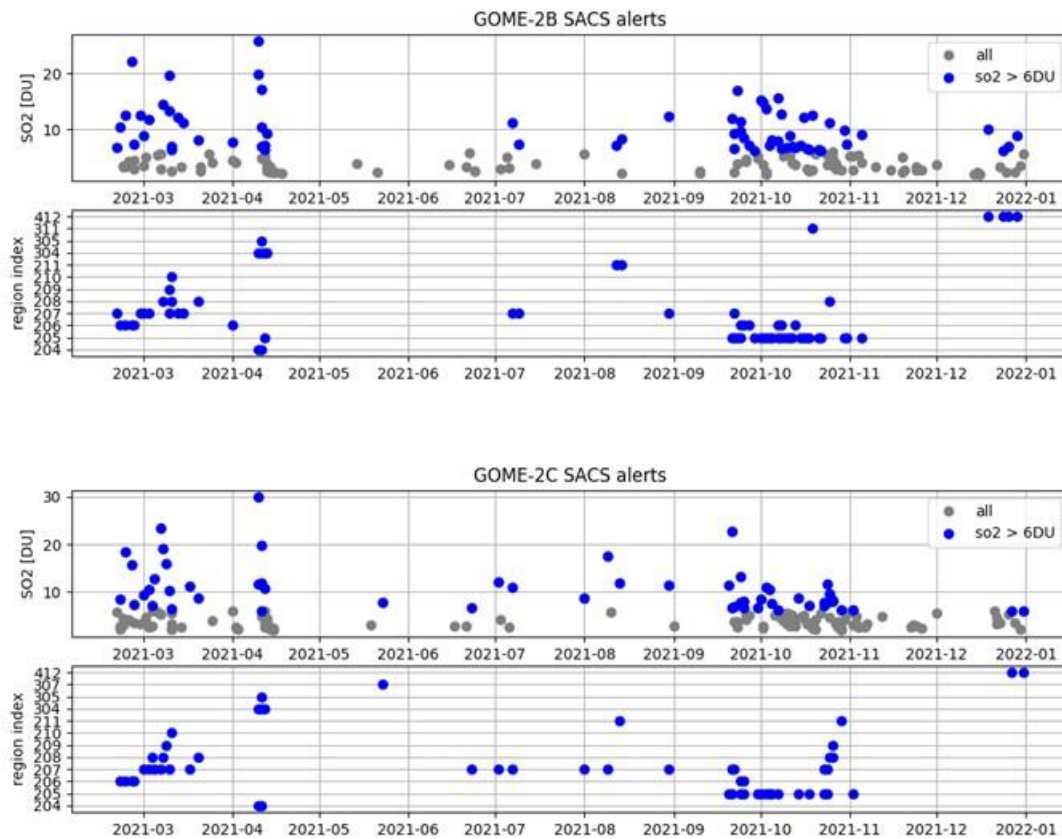
Figure 7.20. Illustration of the SACS alerts (with focus on alerts with SO2 VCD > 6 DU) for GOME-2B (top) and GOME-2C (bottom), for 2021. SO$_2$ amount and region numbers are indicated as a function of time.
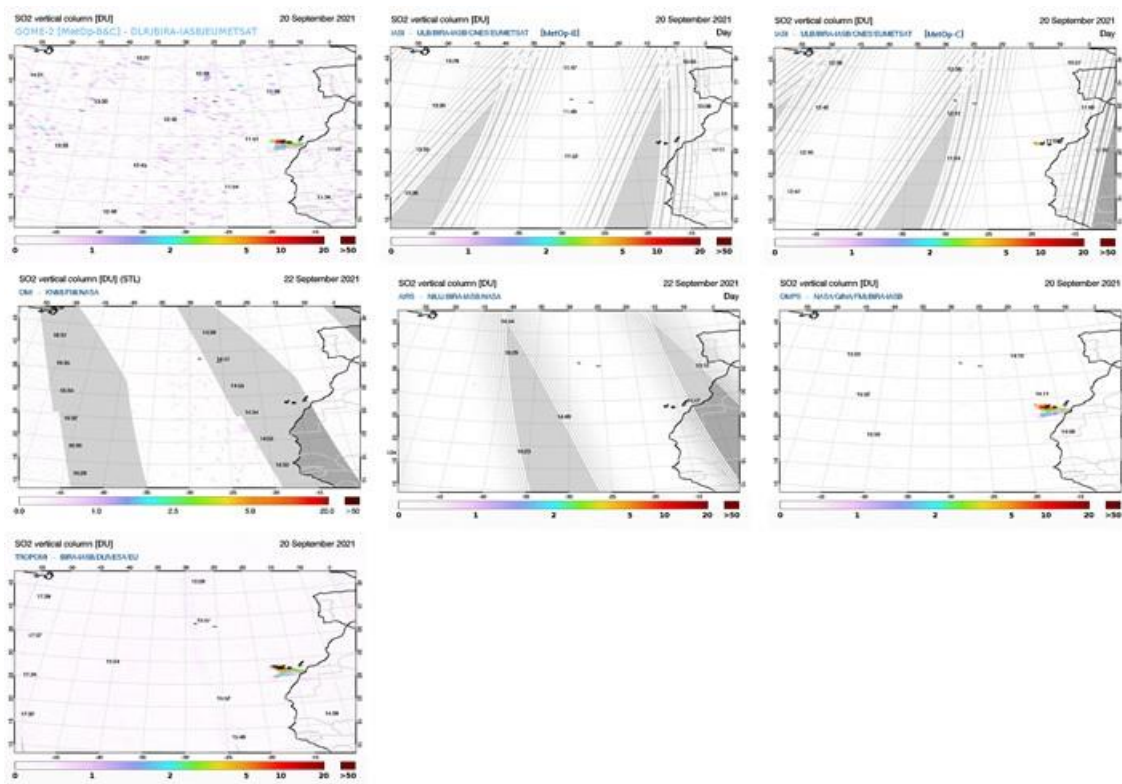
Figure 7.21. Illustration of the eruption of Cumbre Vieja in 19 September 2021 (La Palma, SACS region 205) as seen by GOME-2B and GOME-2C (composite), IASI-A and IASI-B, OMI, AIRS, OMPS and TROPOMI instruments.

GDP-4.8 also contains an anthropogenic SO_2 product that can be compared with ground-based MAXDOAS/DirectSun data from the Xianghe station, similarly to what is done in the SO$_2$ report. In this Operations Report however, the SO2 levels in China dropping from year to year, the levels of the PBL product are found to be so noisy that only time-series are shown (see Figure 7.22). Test validation had also been performed with respect to Mexico City (unam) Pandora data received from PGN team (A. Cede, M. Tiefengraben), but without much success (see AC SAF Operations Report 2/2020).
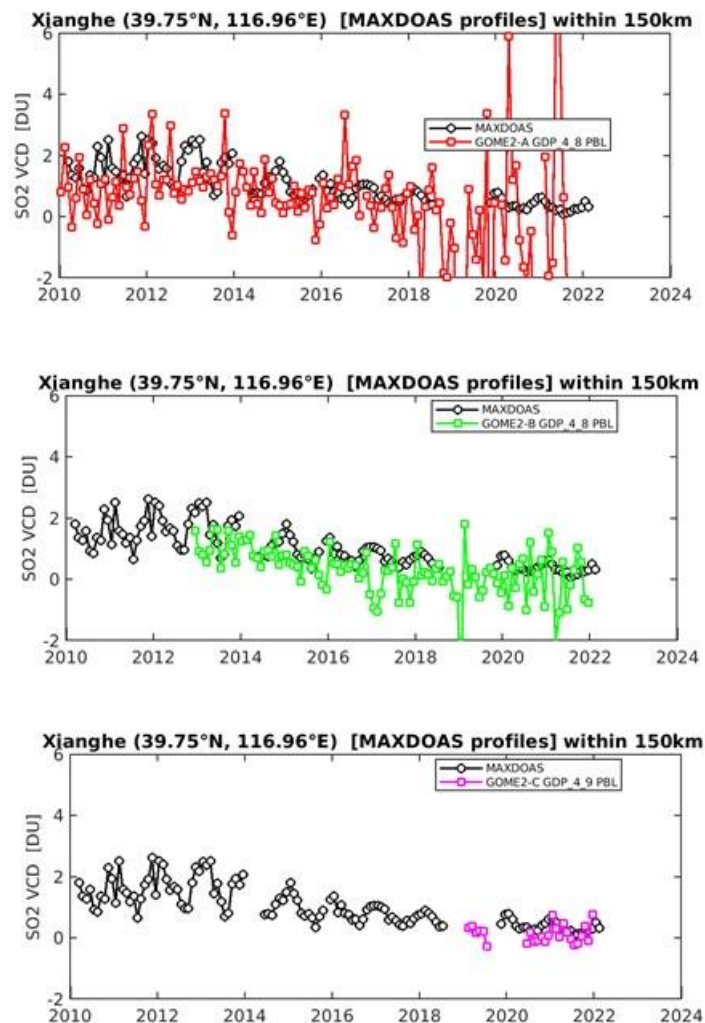
Figure 7.22. Time-series of the SO2 PBL around Xianghe for GOME-2A, GOME-2B, GOME-2C and MAXDOAS data. Left: daily points, right: monthly means.

As discussed in previous Operations Reports, the plan for the improvement of the SO_2 GOME-2 products is to follow BIRA-IASB recommendations and bring the GDP SO_2 algorithm consistent to the TROPOMI product (Theys *et al.*, 2017). This has been tested for the GOME-2C validation, with change of the DOAS wavelength fit region, but has been found not appropriate for GOME-2A and GOME-2B, due to issues with L1 data.

References:

Clémer, K., Van Roozendael, M., Fayt, C., Hendrick, F., Hermans, C., Pinardi, G., Spurr, R., Wang, P., and De Mazière, M.: Multiple wavelength retrieval of tropospheric aerosol optical properties from MAXDOAS measurements in Beijing, Atmos. Meas. Tech., 3, 863-878, 2010. https://doi.org/10.5194/amt-3-863-2010

De Smedt, I., Stavrakou, T., Hendrick, F., Danckaert, T., Vlemmix, T., Pinardi, G., Theys, N., Lerot, C., Gielen, C., Vigouroux, C., Hermans, C., Fayt, C., Veefkind, P., Müller, J.-F., and Van Roozendael, M.: Diurnal, seasonal and long-term variations of global formaldehyde columns

inferred from combined OMI and GOME-2 observations, Atmos. Chem. Phys., 15, 12519-12545, 2015.
https://doi.org/10.5194/acp-15-12519-2015

Gielen, C., Van Roozendael, M., Hendrick, F., Pinardi, G., Vlemmix, T., De Bock, V., De Backer, H., Fayt, C., Hermans, C., Gillotay, D., and Wang, P.: A simple and versatile cloud-screening method for MAX-DOAS retrievals, Atmos. Meas. Tech., 7, 3509–3527, 2014.
https://doi.org/10.5194/amt-7-3509-2014

Hendrick, F.M., Van Roozendael, M., Chipperfield, M.P., Dorf, M., Goutail, F., Yang, X., Fayt, C., Hermans, C., Pfeilsticker, K., Pommereau, J.-P., Pyle, J.A., Theys, N., and De Maziere, M.: Retrieval of stratospheric and tropospheric BrO profiles and columns using ground-based zenith-sky DOAS observations at Harestua, 60° N., Atmos. Chem. Phys., 7, 4869-4885, 2007.
https://doi.org/10.5194/acp-7-4869-2007

Hendrick, F., Johnston, P.V., De Mazière, M., Fayt, C., Hermans, C., Kreher, K., Theys, N., Thomas, A., and Van Roozendael, M.: One-decade trend analysis of stratospheric BrO over Harestua (60°N) and Lauder (45°S) reveals a decline, Geophys. Res. Letters, 35, L14801, 2008.
https://doi.org/10.1029/2008gl034154

Hendrick, F., Müller, J.-F., Clémer, K., Wang, P., De Mazière, M., Fayt, C., Gielen, C., Hermans, C., Ma, J.Z., Pinardi, G., Stavrakou, T., Vlemmix, T., and Van Roozendael, M.: Four years of ground-based MAX-DOAS observations of HONO and NO2 in the Beijing area, Atmos. Chem. Phys., 14, 765–781, 2014.
https://doi.org/10.5194/acp-14-765-2014

Pinardi, G., Van Roozendael, M., Lambert, J.-C., Granville, J., Hendrick, F., Tack, F., Yu, H., Cede, A., Kanaya, Y., Irie, I., Goutail, F., Pommereau, J.-P., Pazmino, A., Wittrock, F., Richter, A., Wagner, T., Gu, M., Remmers, J., Friess, U., Vlemmix, T., Piters, A., Hao, N., Tiefengraber, M., Herman, J., Abuhassan, N., Bais, A., Kouremeti, N., Hovila, J., Holla, R., Chong, J., Postylyakov, O., Ma, J.: GOME-2 total and tropospheric NO$_2$ validation based on zenith-sky, direct-sun and multi-axis DOAS network observations, Proceeding of the EUMETSAT conference, 22-26 September 2014, Geneva, Switzerland.

Pinardi, G., Van Roozendael, M., Hendrick, F., Theys, N., Abuhassan, N., Bais, A., Boersma, F., Cede, A., Chong, J., Donner, S., Drosoglou, T., Frieß, U., Granville, J., Herman, J. R., Eskes, H., Holla, R., Hovila, J., Irie, H., Kanaya, Y., Karagkiozidis, D., Kouremeti, N., Lambert, J.-C., Ma, J., Peters, E., Piters, A., Postylyakov, O., Richter, A., Remmers, J., Takashima, H., Tiefengraber, M., Valks, P., Vlemmix, T., Wagner, T., and Wittrock, F.: Validation of tropospheric NO2 column measurements of GOME-2A and OMI using MAX-DOAS and direct sun network observations, Atmos. Meas. Tech., 13, 6141-6174, 2020.
https://doi.org/10.5194/amt-13-6141-2020

Richter, A., Behrens, L., Hilboll, A., Munassar, S., Burrows, J.P., Pinardi, G., and Van Roozendael, M.: Cloud effects on satellite retrievals of tropospheric NO2 over China, oral presentation at the DOAS workshop, September 2017, Yokohama, Japan.

Theys, N., De Smedt, I., Yu, H., Danckaert, T., van Gent, J., Hörmann, C., Wagner, T., Hedelt, P., Bauer, H., Romahn, F., Pedergnana, M., Loyola, D., and Van Roozendael, M.: Sulfur dioxide retrievals from TROPOMI onboard Sentinel-5 Precursor: algorithm theoretical basis, Atmos. Meas. Tech., 10, 119-153, 2017.
https://doi.org/10.5194/amt-10-119-2017

Verhoelst, T., Compernolle, S., Pinardi, G., Lambert, J.-C., Eskes, H. J., Eichmann, K.-U., Fjæraa, A. M., Granville, J., Niemeijer, S., Cede, A., Tiefengraber, M., Hendrick, F., Pazmiño, A., Bais, A., Bazureau, A., Boersma, K. F., Bognar, K., Dehn, A., Donner, S., Elokhov, A., Gebetsberger, M., Goutail, F., Grutter de la Mora, M., Gruzdev, A., Gratsea, M., Hansen, G. H., Irie, H., Jepsen, N., Kanaya, Y., Karagkiozidis, D., Kivi, R., Kreher, K., Levelt, P. F., Liu, C., Müller, M., Navarro Comas, M., Piters, A. J. M., Pommereau, J.-P., Portafaix, T., Prados-Roman, C., Puentedura, O., Querel, R., Remmers, J., Richter, A., Rimmer, J., Rivera Cárdenas, C., Saavedra de Miguel, L., Sinyakov, V. P., Stremme, W., Strong, K., Van Roozendael, M., Veefkind, J. P., Wagner, T., Wittrock, F., Yela González, M., and Zehner, C.: Ground-based validation of the Copernicus Sentinel-5P TROPOMI NO2 measurements with the NDACC ZSL-DOAS, MAX-DOAS and Pandonia global networks, Atmos. Meas. Tech., 14, 481–510, 2021.
https://doi.org/10.5194/amt-14-481-2021

Vlemmix, T., Hendrick, F., Pinardi, G., Smedt, I., Fayt, C., Hermans, C., Piters, A., Wang, P., Levelt, P, and Van Roozendael, M.: MAX-DOAS observations of aerosols, formaldehyde and nitrogen dioxide in the Beijing area: comparison of two profile retrieval approaches, Atmos. Meas. Tech., 2, 941–963, 2015.
https://doi.org/10.5194/amt-8-941-2015

Wang, T., Hendrick, F., Wang, P., Tang, G., Clémer, K., Yu, H., Fayt, C., Hermans, C., Gielen, C., Müller, J.-F., Pinardi, G., Theys, N., Brenot, H., and Van Roozendael, M.: Evaluation of tropospheric SO2 retrieved from MAX-DOAS measurements in Xianghe, China, Atmos. Chem. Phys., 14(20), 11149-11164, 2014.
https://doi.org/10.5194/acp-14-11149-2014

7.3.1. Online quality monitoring

Online quality monitoring plots are continuously generated at DLR and published for O_3, NO_2, BrO, HCHO, SO_2, H2O products as described in Section 7.1.3.

BIRA-IASB provides quality assessment (QA) pages for vertical column amounts of NO_2, HCHO, BrO and SO_2, derived from GOME-2A, GOME-2B and GOME-2C, as well as IASI SO_2. These pages are available under https://cdop.aeronomie.be/quality-assessment/.

System developments:

- As mentioned in the previous reports, the GOME-2 monitoring page now shows time-series for Metop-B and Metop-C. Metop-A was monitored internally by the team until its end-of-life in November 2021.
- As indicated in the previous report, the current monitoring system, based on storage in an SQL database, remains slow in use. A solution for a new system is currently being drafted and is expected to perform much more responsive. This system will be based on gridded data stored in NetCDF file format behind an OpenDAP request mechanism. More on this can be expected in future reports as part of CDOP 4 activities.

Monitoring status:

See example images for NO_2 and SO_2 below.

- GOME-2A: continuing progressive increase of fitting RMS for all monitored species until the end-of-life.
- GOME-2B: No anomalies. Increase in fit residuals can be observed, in line with nominal instrument degradation progressing with age.

- GOME-2C: No anomalies for NO_2, HCHO, and BrO. For SO_2, it is noticed that retrieved columns from GOME-2C are lower than those from GOME-2B. Also, the SO_2 fitting RMS for GOME-2C is larger than for GOME-2B in its early lifetime. The SO_2 product from GOME-2C has seen several improvements in the retrieval setting with respect to the old GOME-2 sensors, but at first sight this is not reflected in the RMS. This needs to be sorted out with DLR.
- IASI SO_2: The offline phase of the IASI SO_2 monitoring, announced in the last report, unfortunately continues to this date. This is related to the system being based on alerts for enhanced SO_2 amounts from the SACS system (sacs.aeronomie.be) that saw an interruption in itsthe generation scheme. We now know that those alerts will not return in their previous form. In CDOP 4, monitoring of SO_2 time-series will be taken over by AUTH.

NO₂ tropospheric column and fitting root-mean-square over India

SO2 total vertical column over Northern China
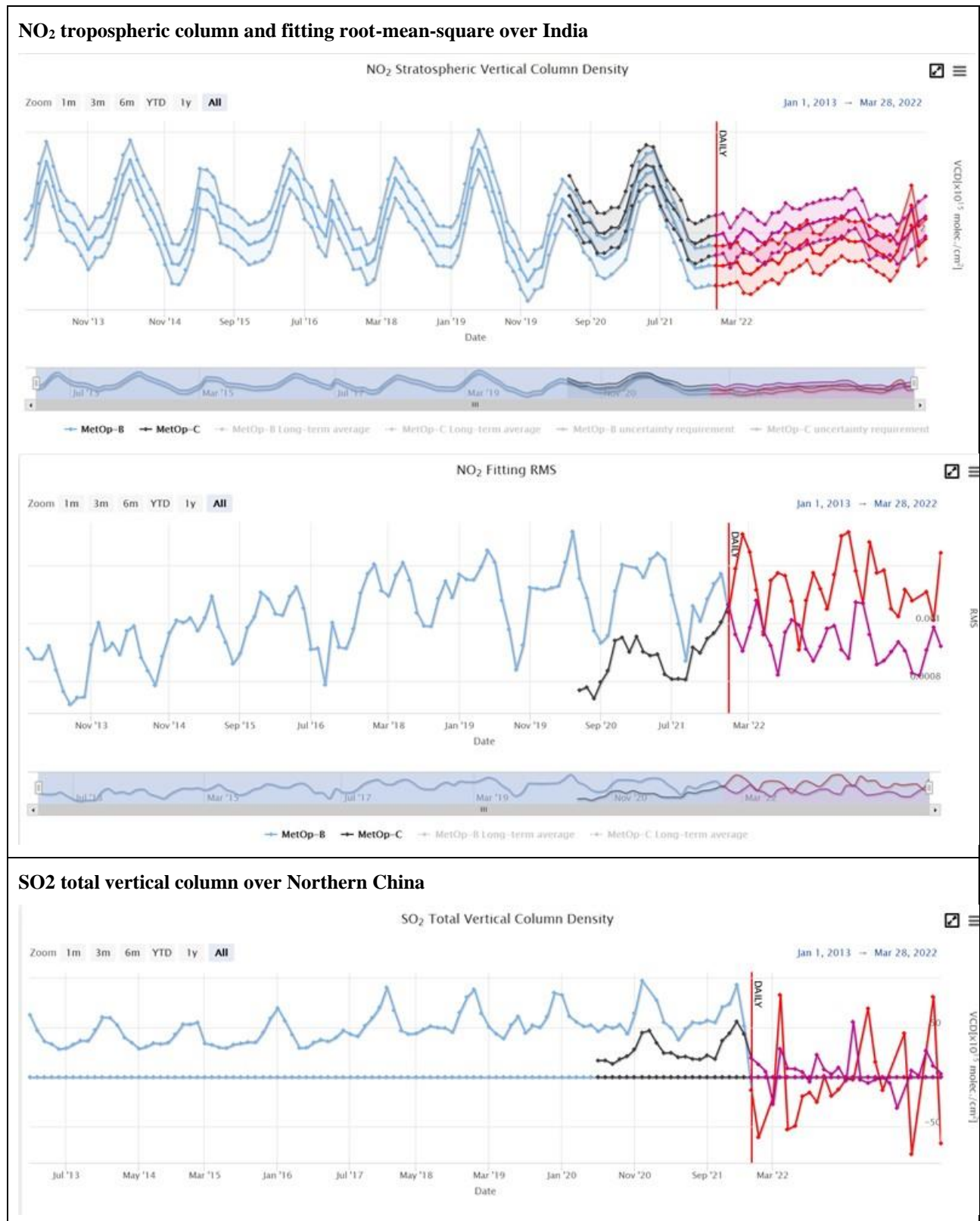
Figure 7.23. Time-series example for NO₂ and SO₂, comparing results from GOME-2B and GOME-2C. For GOME-2B, the blue curve shows monthly averaged values, red shows recent daily averages. The black and magenta curves are for GOME-2C.

7.4. Ozone profile products

Table 7.16. Validation status of ozone profile products

Product Identifier	Product Name	Accuracy	Reference	Validating Institute	Correlative data sources
O3M-38	NRT high-resolution ozone profile	Fulfils threshold accuracy requirements	RD7	KMI DWD	Ozonesonde data from SHADOZ, NDACC, NILU and WOUDC Lidar/microwave data from NDACC
O3M-47			RD8		
O3M-311			RD26		
O3M-39	Offline high-resolution ozone profile	Fulfils threshold accuracy requirements	RD7	KMI DWD	Ozonesonde data from SHADOZ, NDACC, NILU and WOUDC Lidar/microwave data from NDACC
O3M-48			RD8		
O3M-312			RD26		

Validation results can be found in more detail on the at AC SAF validation & quality assessment website.

Validation activities summary:

This summary contains validation results for the GOME-2A, GOME-2B and GOME-2C high-resolution (HR) ozone profile products, retrieved by the Ozone Profile Retrieval Algorithm (OPERA) at KNMI. This validation section focuses on the time period January – December 2021.

The authors of this summary are Dr. Andy Delcloo from KMI and Dr. Peggy Achtert from DWD. More information on how these values are extracted is available in the validation report.

To report the skill scores of GOME-2 ozone profile products in a more condensed way, the statistics for the different output levels of GOME-2 are reduced to two layers: Lower Stratosphere (until an altitude of 30 km) and Upper Stratosphere (up to an altitude of 50 km). Table 7.17 gives an overview on how we define the ranges in height for the different belts for lower stratosphere and upper stratosphere.

The collocation data used for the validation using ozonesonde data are shown in Figure 7.24. The validation for the lower stratosphere is made with ozonesonde data, for the upper stratosphere with lidar and/or microwave data. The stations used in this validation for the lidar/microwave data are the Network for the Detection of Atmospheric Composition Change (NDACC) stations of Bern (microwave), Ny Ålesund (microwave), Payerne (microwave), Hohenpeissenberg (lidar), Table Mountain (lidar), Mauna Loa (microwave/lidar), Eureka (lidar), and Lauder (lidar).
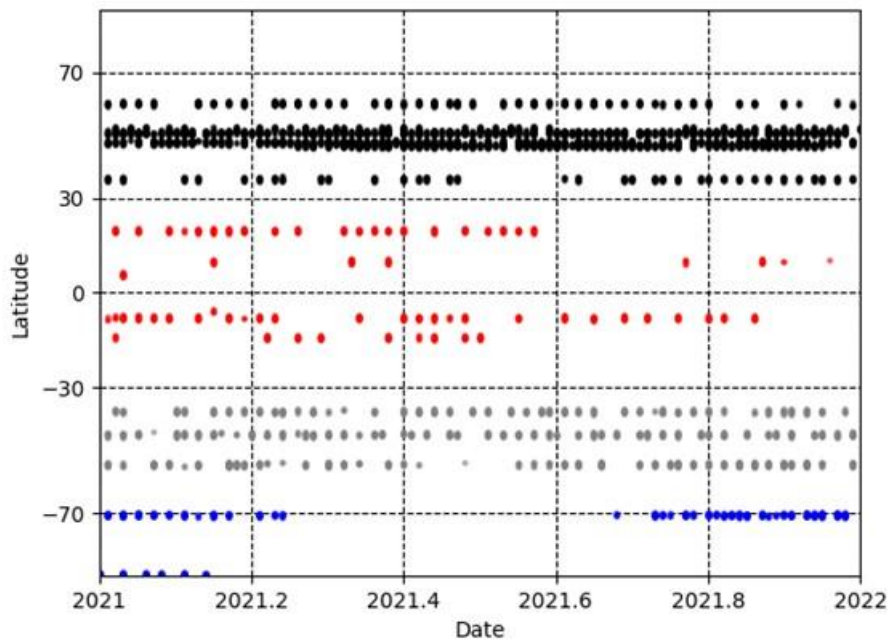
Figure 7.24. Collocation data for the validation with ozonesonde data for the time period January – December 2021.

Table 7.17. Definition of the ranges in km for lower and higher stratosphere for the different latitude belts

	Lower Stratosphere	Upper Stratosphere
Polar Region	12 km – 30 km	30 km – 50 km
Mid-Latitudes	14 km – 30 km	30 km – 50 km
Tropical Region	18 km – 30 km	30 km – 50 km

Relative differences (Eq. 1) are calculated against sounding data, which is convolved with the averaging kernels (Smoothed Sounding):

$$\frac{(GOME\text{-}2 - Smoothed\ Sounding) * 100}{Smoothed\ Sounding} \qquad (1)$$

Table 7.18 shows an overview of the obtained results for the time period January – December 2021 only for the lower and the higher stratosphere, not taking into account the tropospheric ozone column products since a dedicated product is discussed earlier in this report. The statistics for the lower stratosphere are obtained by KMI, the statistics for the higher stratosphere by DWD.

Table 7.18. Absolute Differences (AD), Relative Differences (RD) and standard deviation (STDEV) are shown on the accuracy of GOME-2A/B/C HR ozone profile products for the lower and the higher stratosphere for five different latitude belts for the time period January – December 2021.

	GOME-2A HR					
	Lower Stratosphere			Upper Stratosphere		
	AD	RD	STDEV	AD	RD	STDEV
	(DU)	(%)	(%)	(DU)	(%)	(%)
Northern Polar Region	-	-	-	-3.4	-6.3	10.0
Northern Mid-Latitudes	-14.2	-5.3	15.9	-4.5	-6.2	4.6
Tropical Region	0.2	0.5	6.0	-3.6	-4.6	3.3
Southern Mid-Latitudes	6.7	4.1	12.0	5.3	13.7	30.7
Southern Polar Region	3.2	6.9	26.6	-	-	-
	GOME-2B HR					
	Lower Stratosphere			Upper Stratosphere		
	AD	RD	STDEV	AD	RD	STDEV
	(DU)	(%)	(%)	(DU)	(%)	(%)
Northern Polar Region	-	-	-	-2.5	-4.4	3.5
Northern Mid-Latitudes	1.7	1.1	8.5	-5.0	-8.6	4.6
Tropical Region	5.0	3.9	5.7	-5.0	-7.6	1.8
Southern Mid-Latitudes	8.6	5.0	9.6	-2.7	-6.1	4.9
Southern Polar Region	8.9	14.8	55.0	-	-	-
	GOME-2C HR					
	Lower Stratosphere			Upper Stratosphere		
	AD	RD	STDEV	AD	RD	STDEV
	(DU)	(%)	(%)	(DU)	(%)	(%)
Northern Polar Region	-	-	-	-3.5	-6.7	5.5
Northern Mid-Latitudes	-3.6	-1.0	8.1	-6.8	-9.4	5.2
Tropical Region	0.3	1.0	5.7	-8.7	-10.0	1.8
Southern Mid-Latitudes	8.2	5.3	10.8	-3.5	-5.2	6.6
Southern Polar Region	1.9	10.4	47.5	-	-	-

The target value (15% accuracy) is met in both lower and upper stratosphere for all belts under consideration for Metop-B and Metop-C. The discrepency is highest at high-latitudes, for the mid-latitudes and tropical region, the optimal values are met (10 % accuracy).

More detailed ozone profile validation results can also be found on the AC SAF ozone profile validation website.

7.4.1. Online quality monitoring

Timeline of the vertically integrated Metop-B ozone profile with respect to time is presented in Figure 7.25.

More information and images at the following web addresses
https://www.temis.nl/acsaf/timeseries.php?sat=metopa
https://www.temis.nl/acsaf/timeseries.php?sat=metopb
https://www.temis.nl/acsaf/timeseries.php?sat=metopc

Figure 7.25. Timeline of vertically integrated Metop-B ozone profiles (=total ozone columns) and changes in data processor (vertical lines). The changes in late 2018 / early 2019, including the improved degradation correction, have resulted in much better ozone profiles and have also affected the total ozone columns shown here.

Legend of the coloured vertical lines:

➢ Green: PPF version
➢ Blue: Software version (PGE)
➢ Orange: Algorithm version
➢ Grey: Config version

7.5. Aerosol products

Table 7.19. Validation status of aerosol products

Product Identifier	Product Name	Accuracy	Reference	Validating Institute	Correlative data sources
O3M-61.1	NRT absorbing aerosol height	Fulfils threshold accuracy requirement	RD32	KMI, AUTH	CALIOP, EARLINET
O3M-71.1					
O3M-364					
O3M-62.1	NRT absorbing aerosol index from PMDs	Fulfils threshold accuracy requirement	RD14	KNMI	Comparisons with other satellite instruments: SCIAMACHY, OMI, and intercomparison of GOME-2A with GOME-2B
O3M-72.1					
O3M-362			RD33		Comparisons with the AAI products from GOME-2A and GOME-2B
O3M-14.1	Offline absorbing aerosol height	Fulfils threshold accuracy requirements	RD32	KMI, AUTH	CALIOP, EARLINET
O3M-70.1					
O3M-365					
O3M-63.1	Offline absorbing aerosol index from PMDs	Fulfils threshold accuracy requirements	RD14	KNMI	Comparisons with other satellite instruments: SCIAMACHY, OMI, and intercomparison of GOME-2A with GOME-2B
O3M-73.1					
O3M-363			RD33		Comparisons with the AAI products from GOME-2A and GOME-2B

Validation activities summary:

This summary contains validation results for the GOME-2A, GOME-2B and GOME-2C Absorbing Aerosol Height (AAH) products and is made available by the validation teams of AUTH and KMI. More information on how these values are extracted is available in the validation report validation report.

AAH is a new operational AC SAF product for aerosol layer height detection, developed by KNMI within the AC SAF. It uses the AAI as an indicator to derive the actual height of the absorbing aerosol layer in the O_2-A band using the Fast Retrieval Scheme for Clouds from the Oxygen A band (FRESCO) algorithm (Wang *et al*., 2012; Tilstra *et al*., 2020). The AAH reported by GOME-2 onboard Metop-A, Metop-B and Metop-C, between 2007 and 2019, has been validated by AUTH against ground-based lidar data from the European Aerosol Research Lidar Network (EARLINET) database and by KMI against CALIOP aerosol layer height (De Bock, *et al*. 2020; Michailidis *et al*., 2021).

AUTH results:

At the time of writing this report (rev. 1), there was no updated AAH reference data available. Therefore, all the results are as in AC SAF Operations Report 1/2021.

A wide choice of lidar stations around Europe was made in order to examine the behaviour of the comparisons for different common aerosol loads over the locations (see the first column of Table 7.20). The total number of carefully screened collocations with the EARLINET lidar measurements was 172 for the three GOME-2 instruments. On average, the mean absolute bias (GOME-2 minus lidar height) was found to be -0.18 ± 1.68 km, with a near-Gaussian distribution and minimum and maximum differences of ∼ ±5 km. On a station basis, and with a couple of exceptions, their mean biases fall in the ±1 km range, with an associated standard deviation between 0.5 – 2 km.

Table 7.20. Summary of statistics for the comparisons between GOME-2 AAH and LIDAR ALH for all stations

EARLINET Station	N	Statistical parameters (in km)			
		Mean absolute bias	Std	Min	Max
Athens, Greece	3	-2.00	1.38	-3.6	-1.06
Barcelona, Spain	32	-0.35	1.94	-4.66	2.86
Belsk, Poland	26	0.19	1.52	-3.11	3.24
Bucharest, Romania	10	-0.39	1.26	-0.96	2.96
Évora, Portugal	5	-0.07	1.95	-1.64	3.31
Granada, Spain	32	-0.63	1.79	-3.65	3.9
Lecce, Italy	18	-0.24	1.14	-3.47	2.05
Limassol, Cyprus	11	-0.06	1.64	-2.89	2.80
Minsk, Belarus	5	0.56	0.61	-0.05	1.51
Potenza, Italy	2	-1.40	1.10	-0.64	-0.64
Thessaloniki, Greece	24	-0.05	1.84	-4.71	3.24
Warsaw, Poland	3	1.66	0.53	1.08	2.15
Summary	172	-0.18	1.68	-4.91	3.91

In Figure 7.26, left panel, the histogram of absolute differences between GOME-2 and EARLINET aerosol layer heights, calculated for all collocated cases is shown, with the associated statistics. In the right panel, the scatter plot between GOME-2 AAH and aerosol layer height from EARLINET stations, for the totality of collocated cases is presented. The associated Absorbing Aerosol Index (AAI) value is color-coded.
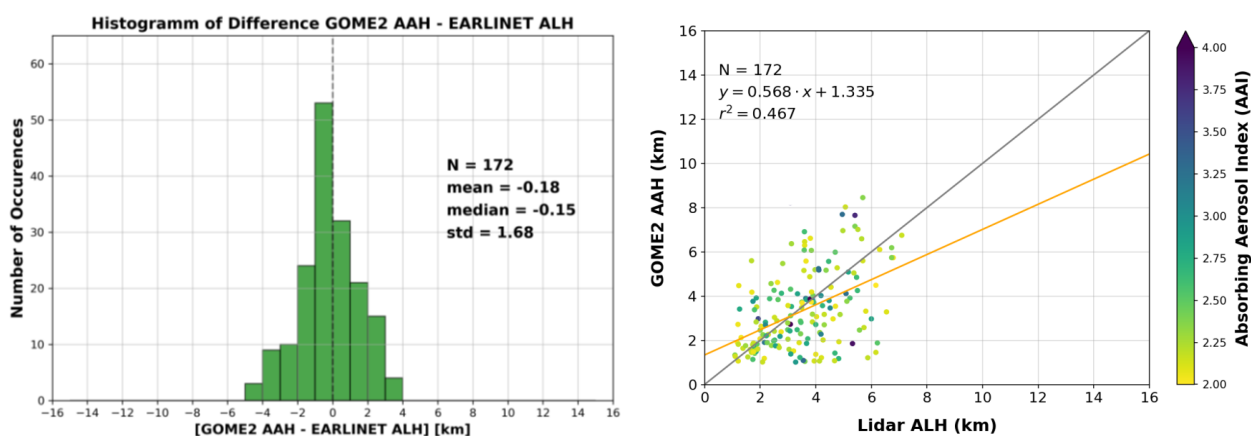
Figure 7.26. Left: Histogram of absolute differences between GOME-2 AAH and aerosol layer height obtained from EARLINET backscatter profiles (using the WCT method), calculated for all collocated cases. Right: Scatter plot between GOME-2 AAH and aerosol layer height from EARLINET stations, for the total of collocated cases. The associated AAI value is color-coded.

Considering the differences, mainly due to the temporal collocation and the difference between the satellite pixel size and the point view of the ground-based observations, these results are quite promising and demonstrate that stable aerosol layers are well captured by the satellite sensors. The official AC SAF requirements for the accuracy of the GOME-2 AAH product state that, for heights <10 km, the threshold accuracy is 3 km, the target accuracy is 2 km, and the optimal accuracy is 1 km. This validation effort shows that for all cases the target accuracy is met, see Table 7.21. For the different regimes, which relate to the degree of cloud cover, please refer to the validation report.

Table 7.21. Percentage of collocated lidar & GOME-2 AAH cases that fulfill the optimal accuracy criteria (first row), the target criteria (second row), the threshold criteria (third row) for Regime A in the first column, Regime B in the second, Regime C in the third and the totality of the collocations in the final column. The regimes are related to the degree of cloud cover.

	Regime A (36 cases)	Regime B (43 cases)	Regime C (3 cases)	Total (82 cases)
Optimal (1 km)	55.8 %	58.3 %	33.3 %	56.1 %
Target (2 km)	81.4 %	66.7 %	33.3 %	73.2 %
Threshold (3 km)	88.4%	75.0 %	66.7 %	81.7 %

KMI results:

At the time of writing this report (rev. 1), there was no updated AAH reference data available. Therefore, all the results are as in AC SAF Operations Report 1/2021.

KMI validated the AAH only for specific case studies related to volcanic eruptions. AAH values are only included in the analysis if the corresponding AAI is higher than 4. CALIOP and GOME data are compared when the distance between both overpasses is maximum 100 km. There is currently no constraint on the time difference between both overpasses.

Compared to the results shown in the validation report, new data has been added to the study (i.e. Fournaise de la Piton 11-12 February 2020, Karymsky 1-2 April 2020, Kavachi 16 March 2020 and Kikai 29-30 April 2020) in this report. The updated results are summarized in Table 7.22.

Overall, just about 50-60 % of the AAH pixels from GOME-2A, GOME-2B and GOME-2C reach the threshold requirements (see Table 7.22 and Figure 7.27). The optimal requirement threshold is reached for GOME-2A, GOME-2B and GOME-2C in 18 %, 25 % and 24 % of the cases, respectively (when comparing the AAH with the minimum CALIOP layer height). If only the

tropospheric aerosol species (as defined by CALIOP) are studied, the results improve. This can also be seen in Table 7.22 (values in brackets).

Table 7.22. Percentage of data for each GOME-2 instrument that reached the threshold, target and optimal accuracy requirements. Values obtained when only considering the tropospheric aerosol species are shown in brackets

GOME-2A		Layer height <10 km	Layer height >10 km	Total
Threshold	**AAH-minC**	56.0 % (69.6 %)	53.1 % (26.4 %)	55.9 % (68.9 %)
	AAH-maxC	56.4 % (69.5 %)	46.8 % (23.6 %)	56.2 % (68.7 %)
Target	**AAH-minC**	39.0 % (48.5 %)	43.5 % (19.1 %)	39.1 % (48.0 %)
	AAH-maxC	38.0 % (46.9 %)	32.4 % (23.6 %)	37.9 % (46.3 %)
Optimal	**AAH-minC**	17.3 % (21.5 %)	29.9 % (10.0 %)	17.6 % (21.3 %)
	AAH-maxC	18.1 % (22.3 %)	15.6 % (10.0 %)	18.1 % (22.1 %)

GOME-2B		Layer height <10 km	Layer height >10 km	Total
Threshold	**AAH-minC**	51.8 % (53.6 %)	22.9 % (11.7 %)	50.9 % (51.6 %)
	AAH-maxC	52.6 % (54.4 %)	20.6 % (10.2 %)	51.6 % (52.2 %)
Target	**AAH-minC**	42.9 % (44.5 %)	20.6 % (5.60 %)	42.2 % (42.6 %)
	AAH-maxC	37.0 % (38.3 %)	17.1 % (7.90 %)	36.4 % (36.8 %)
Optimal	**AAH-minC**	25.1 % (26.0 %)	17.1 % (3.40 %)	24.8 % (24.9 %)
	AAH-maxC	20.5 % (33.1 %)	16.5 % (3.00 %)	20.4 % (31.6 %)

GOME-2C		Layer height <10 km	Layer height >10 km	Total
Threshold	**AAH-minC**	50.8 % (50.8 %)	0.0 % (0.0 %)	46.8 % (46.8 %)
	AAH-maxC	57.1 % (57.1 %)	0.0 % (0.0 %)	52.9 % (52.9 %)
Target	**AAH-minC**	42.2 % (42.2 %)	0.0 % (0.0 %)	38.8 % (38.8 %)
	AAH-maxC	49.1 % (49.1 %)	0.0 % (0.0 %)	45.2 % (45.2 %)
Optimal	**AAH-minC**	26.3 % (26.3 %)	0.0 % (0.0 %)	24.1 % (24.1 %)
	AAH-maxC	34.5 % (34.5 %)	0.0 % (0.0 %)	31.6 % (31.6 %)
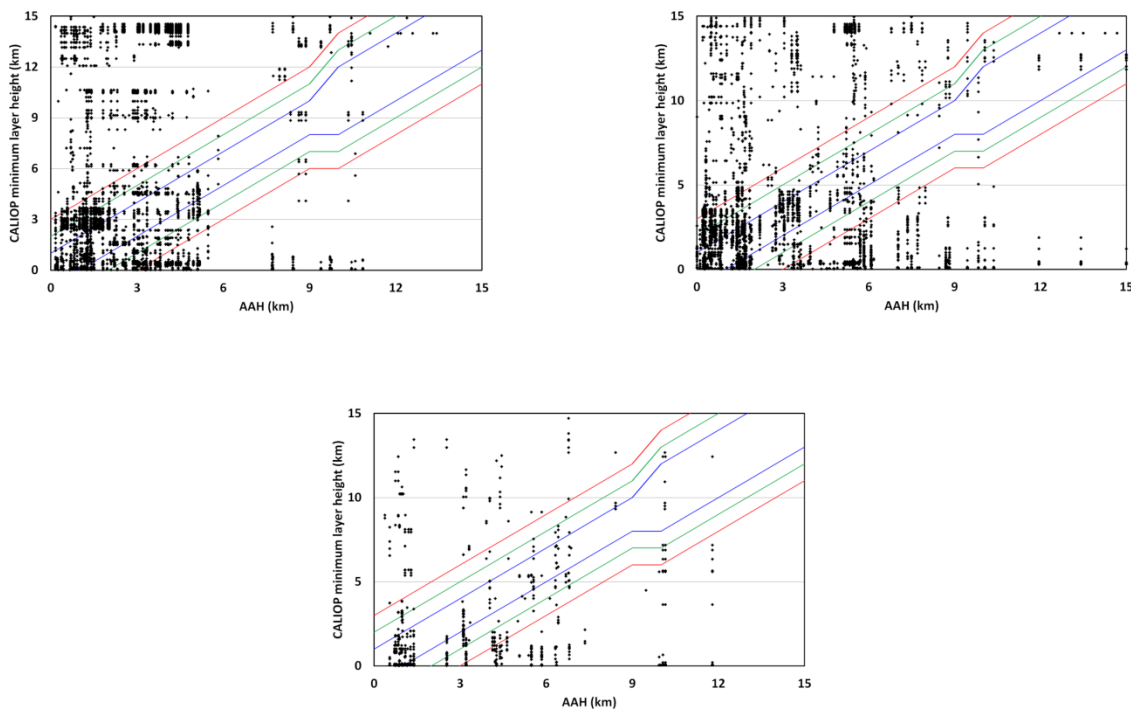
Figure 7.27. Requirement plots for GOME-2A (upper left), GOME-2B (upper right) and GOME-2C (lower middle).The red, green and blue lines represent the threshold, target and optimal requirements. CALIOP pixels are only shown up to a height of 15 km, which is the detection limit of GOME-2.

References:

Michailidis, K., Koukouli, M.-E., Siomos, N., Balis, D., Tuinder, O., Tilstra, L. G., Mona, L., Pappalardo, G. and Bortoli, D.: First validation of GOME-2/MetOp absorbing aerosol height using EARLINET lidar observations, Atmos. Chem. Phys., 21, 3193–3213, 2021. https://doi.org/10.5194/acp-21-3193-2021

Tilstra, L. G., Tuinder, O., Wang, P. and Stammes, P.: ALGORITHM THEORETICAL BASIS DOCUMENT GOME-2 Absorbing Aerosol Height, SAF/AC//KNMI/ATBD/005, 1.4, Royal Netherlands Meteorological Institute, de Bilt, 2019. https://acsaf.org/docs/atbd/Algorithm_Theoretical_Basis_Document_AAH_Apr_2019.pdf, last access: 31 March 2021.

Wang, P., Tuinder, O. N. E., Tilstra, L. G., De Graaf, M. and Stammes, P.: Interpretation of FRESCO cloud retrievals in case of absorbing aerosol events, Atmos. Chem. Phys., 12(19), 9057–9077, 2021. https://doi.org/10.5194/acp-12-9057-2012

De Bock, V., A. Delcloo, K. Michailidis, M. Koukouli and D. Balis, ACSAF Absorbing Aerosol Height products validation report, SAF/AC/AUTH-RMI/VR/001, 1/2020, 3 July 2020. https://acsaf.org/docs/vr/Validation_Report_AAH_Jul_2020.pdf, last access: 31 March 2021.

7.5.1. Online quality monitoring

The online quality monitoring of the AAI in this section show (left duo-plot) the radiance corrections for the PMD-AAI at 340 and 380 nm, and (right duo-plot) the uncorrected residue, and the corrected residue. The rightmost plot is the result of all the corrections and should stay more or less flat when seasonal cycles and differences are removed.

The break in the curves of the latter plot in August 2018 is caused by the introduction of a combination of the 'End-of-Orbit' corrections and a flattening of the AAI across the swath.
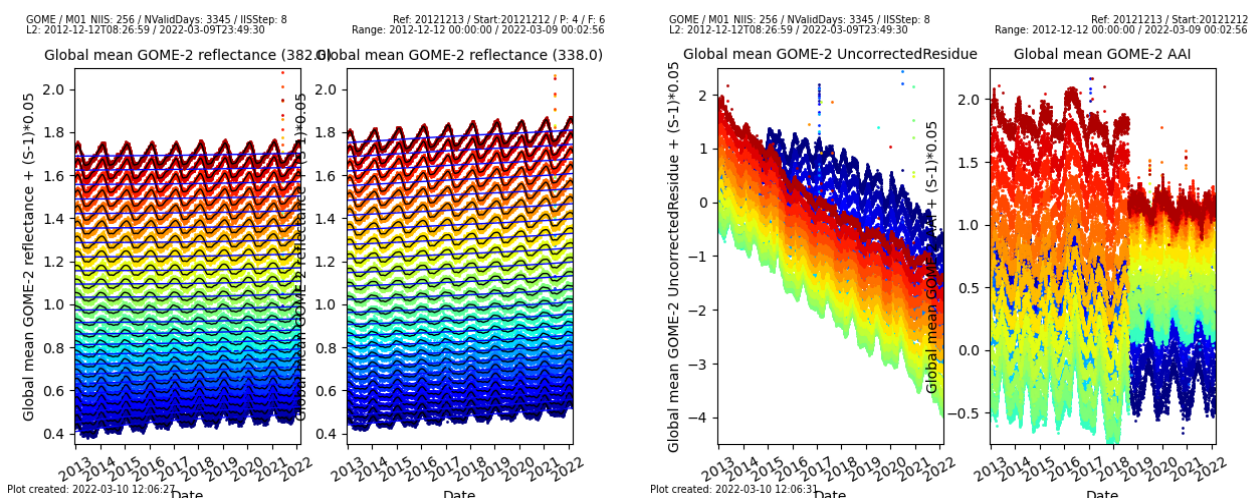
Figure 7.28. Timeline of global mean reflectances at 340 and 380 nm (left) and the uncorrected and corrected AAI from the PMDs of Metop-B.

7.6. UV products

Table 7.23. Validation status of UV products

Product Identifier	Product Name	Accuracy	Reference	Validating Institute	Correlative data sources
O3M-409	NRT UV index, clear-sky	Fulfils threshold accuracy requirements	RD9	DMI	WOUDC, NEUBrew, NSF
O3M-410	NRT UV index, cloud-corrected				
O3M-450 – O3M-464	Offline surface UV	Fulfils target accuracy requirements	RD15	FMI	Brewers and SUV-spectroradiometers from WOUDC, NEUBrew, NSF, NOAA, AUTH and FMI

7.6.1. Online quality monitoring

NUV:

There are two daily updated online quality monitoring entries on the NUV web page. It can be traced that the quality of the NUV products is stable since the last validation.

The first one (http://nuv.dmi.dk/qaqc/nbsp/zonal-mean/) is showing the zonal mean UV index in five longitude zones. The current zonal mean is compared to the two previous years and problems with data quality will show up in these plots. No problems were seen in the reporting period.

The second one (http://nuv.dmi.dk/qaqc/nbsp/measured-uv/) shows a comparison with ground-based measurements for two instruments operated by DMI, one in Copenhagen and one in Greenland. The most recent measurements, preferably only one day old, are shown together with the calculated NUV, details on the comparison can be found on the web page. Problems with the quality of the NUV would show here. Archive page has been included, making it possible to view older data.

OUV:

[Online quality monitoring of offline surface UV](#) has not shown any unexpected, permanent changes in the monitoring value after the latest validation, indicating that the product accuracy has remained within requirements also during the reporting period. The latest OUV validation reports were published in February 2009 covering June 2007 – May 2008 (Metop-A data) and in February 2015 covering June 2012 – May 2013 (Metop-B data).

Figure 7.29 presents the long-term monitoring graph of OUV, which illustrates seasonal variation of **global average of erythemal daily dose** (yellow markers). Any sudden changes would indicate problems with data quality. Additionally, six-month average values (January – June and July – December) are represented by red markers.
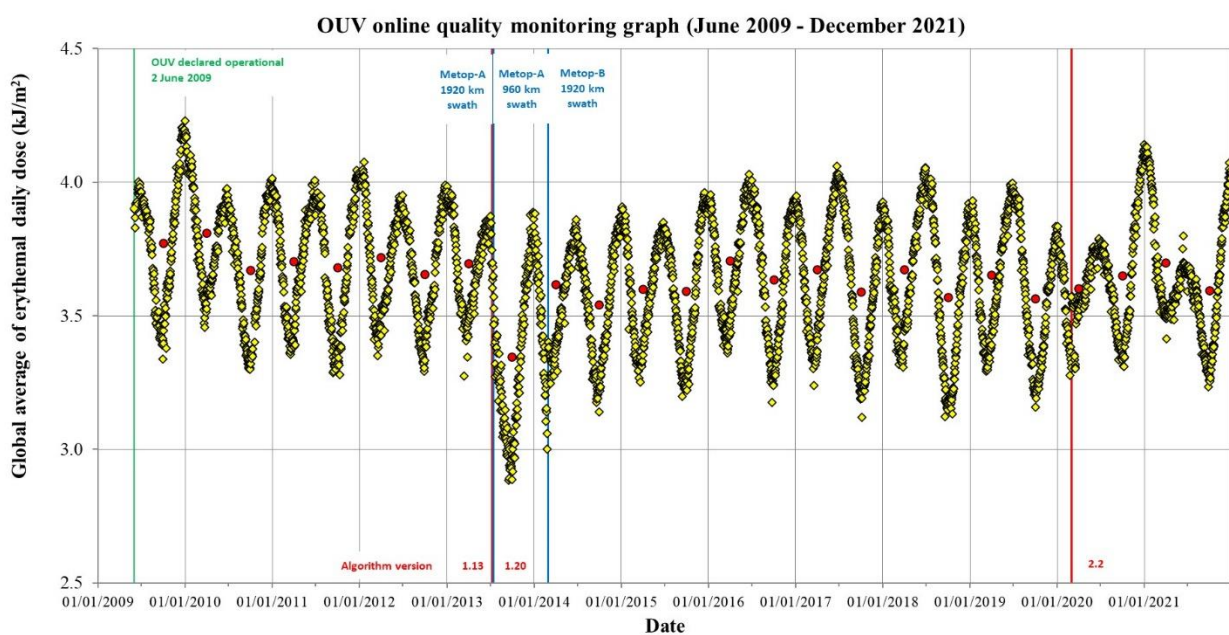
Figure 7.29. OUV long-term monitoring graph.

NOTES:

- GOME-2A was switched from nominal swath width (1920 km) to reduced swath width (960 km) 15 July 2013. The effect to OUV monitoring values can be clearly seen as more wide-spread global average values of erythemal daily dose. This is due to the dominance of lower EDD values in high latitudes when the satellite coverage near the equator is poor due to narrower swath width.

- OUV data processing was switched to use Metop-B data having nominal swath width of 1920 km 1 March 2014

- OUV data processing was switched to use Metop-B+C data 1 March 2020

7.7. IASI NRT products

Table 7.24. Validation status of the IASI CO, SO2, O3 and HNO3 products

Product Identifier	Product Name	Accuracy	Reference	Validating Institute	Correlative data sources
O3M-80	IASI NRT CO	Fulfils threshold accuracy requirement	RD20	LATMOS	FTIR NDACC, MOPITT
O3M-57	IASI NRT SO2	Fulfils threshold accuracy requirement	RD22	AUTH, BIRA-IASB, LATMOS, ULB	MAXDOAS
O3M-44 O3M-49	IASI NRT O3	Fulfils threshold accuracy requirement	*	AUTH, KMI, DWD	GOME-2, balloon sonde, lidar and microwave radiometer, Brewer and Dobson
O3M-81	IASI NRT HNO3	Fulfils threshold accuracy requirement	*	BIRA-IASB	FTIR NDACC (only available in 2021)

* IASI NRT O3 and IASI NRT HNO3 products have been released by EUMETSAT as 'demonstrational', not operational yet. The validation of these products is ongoing.

IASI benchmark validation is performed at ULB and LATMOS.

Dissemination monitoring activities summary:

IASI CO:

The IASI NRT CO product (v6.3) has been declared operational on 2 March 2017. Here we present statistical results when comparing the EUMETSAT product disseminated by EUMETCast in BUFR format (COX) with the native product produced at ULB (FORLI-CO v20191122) for 6 days representative of 6 months: July 15th, August 15th, September 15th, October 15th, for Metop-A, Metop-B and Metop-C, and November 15th and December 15th, 2021, for Metop-B and Metop-C. This allows monitoring if any discrepancy occurs between the two, EUMETSAT and native, products. So far, the discrepancies are found within the numerical errors inherent to the use of different IT infrastructure. Please note that the end of IASI Metop-A mission happened on 15/10/2021, that is why no comparison is shown for November and December. The degradation on the correlation for 15/10/2021 for IASI-A is probably linked to the end of life of the instrument.

CO total column and profiles are investigated. Statistics between COX data and FORLI-CO data (v20191122) are presented in Table 7.25. Profiles correlation ("Correlation") score is computed using the discreet cross correlation integral between two profiles, normalized by the square root of the product of their auto-correlation integral. Score of 1 is expected for perfectly matching profiles, 0 for unrelated ones. Absolute and relative differences are calculated for the total columns. These tables are extracted from the Daily Reports prepared by Daniel Hurtmans at ULB.

Table 7.25. Statistics between COX data and FORLI-CO data for 6 days: July 15th, August 15th, September 15th, October 15th, November 15th and December 15th, 2021.

15/07/2021:

		IASI-a		IASI-b		IASI-c	
		Native	COX	Native	COX	Native	COX
Individual Pixels		561377	560491	559837	558790	557808	556965
Common Pixels		560009 (99.76%)		558349 (99.73%)		556294 (99.73%)	
Correlation	Mean	0.9997±0.0011		0.9995±0.0018		0.9995±0.0014	
	Max	1.0000		1.0000		1.0000	
	Min	0.4873		0.6935		0.8594	
Total Column Differences	Mean (10^{19} mol/cm^2)	0.0047±0.0040		0.0048±0.0050		0.0048±0.0046	
	Max (10^{19} mol/cm^2)	0.3050		1.8811		1.0921	
	Min (10^{19} mol/cm^2)	-1.2289		-0.4039		-1.1705	
Total Column Relative Differences	Mean (%)	2.5818±1.5176		2.6250±1.4145		2.6282±1.3663	
	Max (%)	47.8767		82.3898		72.0969	
	Min (%)	-563.4314		-44.1618		-163.6881	

15/08/2021:

		IASI-c		IASI-a		IASI-b	
		Native	COX	Native	COX	Native	COX
Individual Pixels		536784	536211	534219	533773	538424	539731
Common Pixels		535787 (99.81%)		533326 (99.83%)		535537 (99.22%)	
Correlation	Mean	0.9995±0.0013		0.9997±0.0008		0.9995±0.0015	
	Max	1.0000		1.0000		1.0000	
	Min	0.7650		0.5902		0.7681	
Total Column Differences	Mean (10^{19} mol/cm^2)	0.0056±0.0045		0.0054±0.0040		0.0058±0.0050	
	Max (10^{19} mol/cm^2)	0.4997		0.2126		1.2292	
	Min (10^{19} mol/cm^2)	-0.2458		-0.4703		-0.3056	
Total Column Relative Differences	Mean (%)	2.7374±1.3090		2.6198±1.2591		2.7446±1.3607	
	Max (%)	47.1742		30.3497		72.9498	
	Min (%)	-41.9202		-229.4067		-48.0310	

15/09/2021:

		IASI-a		IASI-b		IASI-c	
		Native	COX	Native	COX	Native	COX
Individual Pixels		350424	351747	518966	518251	518729	518098
Common Pixels		348013 (98.94%)		517835 (99.78%)		517689 (99.80%)	
Correlation	Mean	0.9997±0.0005		0.9995±0.0014		0.9995±0.0016	
	Max	1.0000		1.0000		1.0000	
	Min	0.9388		0.8880		0.3126	
Total Column Differences	Mean (10^{19} mol/cm^2)	0.0055±0.0035		0.0058±0.0041		0.0057±0.0061	
	Max (10^{19} mol/cm^2)	0.2058		0.6557		2.7043	
	Min (10^{19} mol/cm^2)	-0.0894		-0.3586		-1.5717	
Total Column Relative Differences	Mean (%)	2.6730±1.2872		2.8262±1.3642		2.8098±1.3434	
	Max (%)	39.7047		48.3554		90.2745	
	Min (%)	-19.1955		-57.2557		-131.8138	

15/10/2021:

		IASI-b		IASI-a		IASI-c	
		Native	COX	Native	COX	Native	COX
Individual Pixels		548333	547793	232003	229541	539368	542051
Common Pixels		547303 (99.81%)		229172 (98.78%)		534846 (98.67%)	
Correlation	Mean	0.9996±0.0009		0.9997±0.0040		0.9996±0.0008	
	Max	1.0000		1.0000		1.0000	
	Min	0.9141		0.1598		0.8879	
Total Column Differences	Mean (10^{19} mol/cm^2)	0.0060±0.0167		-0.0105±6.2050		0.0058±0.0159	
	Max (10^{19} mol/cm^2)	3.4756		174.6305		4.9256	
	Min (10^{19} mol/cm^2)	-2.6239		-2778.3713		-1.6882	
Total Column Relative Differences	Mean (%)	2.6098±1.3971		0.7076±830.0733		2.6296±1.3469	
	Max (%)	54.5911		99.6799		53.5258	
	Min (%)	-54.7893		-397358.5329		-39.9790	

15/11/2021:

		IASI-c		IASI-b	
		Native	COX	Native	COX
Individual Pixels		505197	504720	501644	503418
Common Pixels		504272 (99.82%)		498377 (99.00%)	
Correlation	Mean	0.9997±0.0012		0.9997±0.0006	
	Max	1.0000		1.0000	
	Min	0.3873		0.9196	
Total Column Differences	Mean (10^{19} mol/cm^2)	0.0051±0.0120		0.0053±0.0124	
	Max (10^{19} mol/cm^2)	2.2699		3.0615	
	Min (10^{19} mol/cm^2)	-2.5496		-1.8751	
Total Column Relative Differences	Mean (%)	2.5892±2.5283		2.6063±1.3654	
	Max (%)	60.1833		56.8165	
	Min (%)	-1450.2134		-59.5805	

15/12/2021:

		IASI-b		IASI-c	
		Native	COX	Native	COX
Individual Pixels		504872	507791	508457	510434
Common Pixels		499848 (98.44%)		504854 (98.91%)	
Correlation	Mean	0.9997±0.0011		0.9997±0.0008	
	Max	1.0000		1.0000	
	Min	0.8281		0.8576	
Total Column Differences	Mean (10^{19} mol/cm^2)	0.0044±0.0033		0.0043±0.0033	
	Max (10^{19} mol/cm^2)	0.1973		0.2623	
	Min (10^{19} mol/cm^2)	-0.2150		-0.0416	
Total Column Relative Differences	Mean (%)	2.4740±1.3635		2.4524±1.3663	
	Max (%)	45.9679		51.2407	
	Min (%)	-28.3797		-16.7928	

Figure 7.30 – Figure 7.35 show the correlation plots for total column between COX data and FORLI-CO for each platform. No critical deviation was found for these dates.
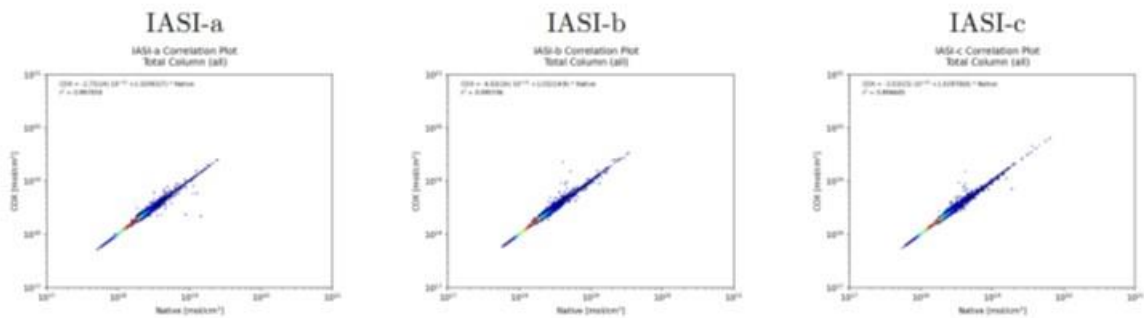
Figure 7.30. Correlation plots for total column between COX data and FORLI-CO for each platform for 15/07/2021. X-axis corresponds to native data (mol/cm^2) and Y-axis corresponds to COX data (mol/cm^2).
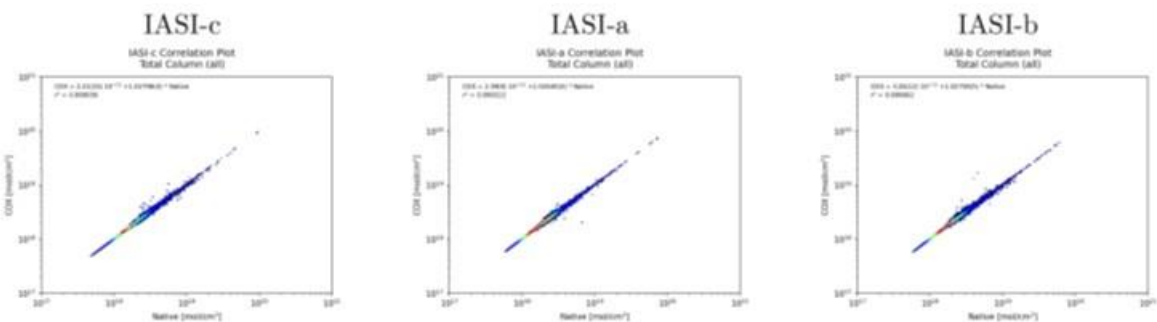
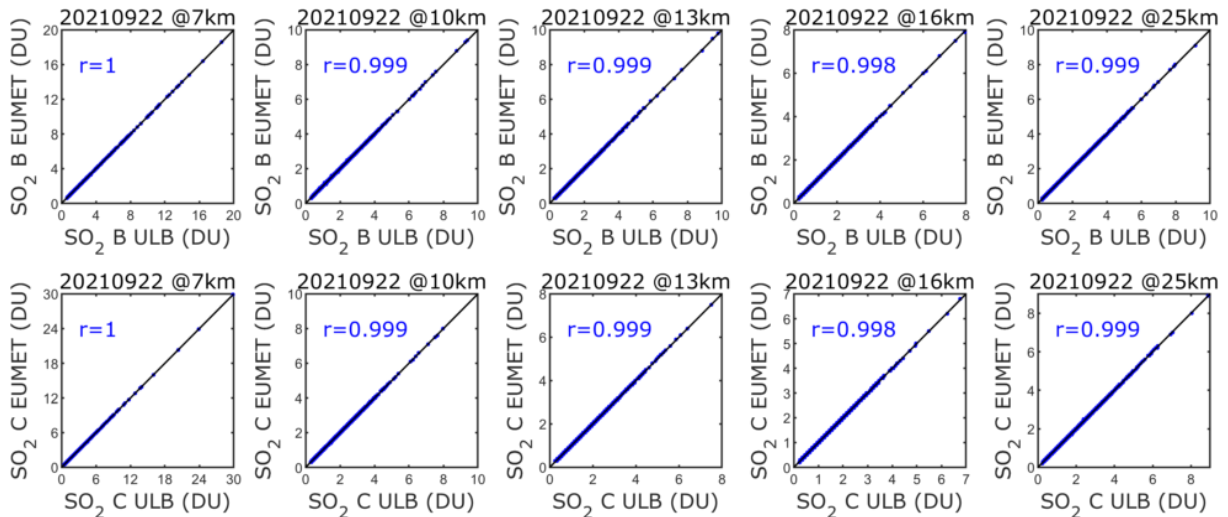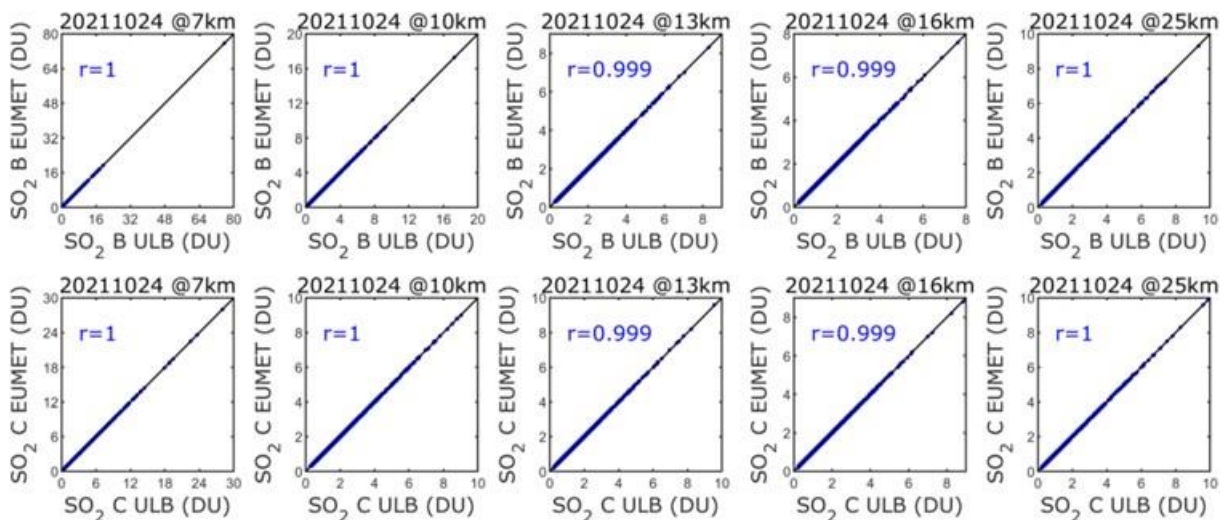**Figure 7.31. Same as Figure 7.30 but for 15/08/2021.**
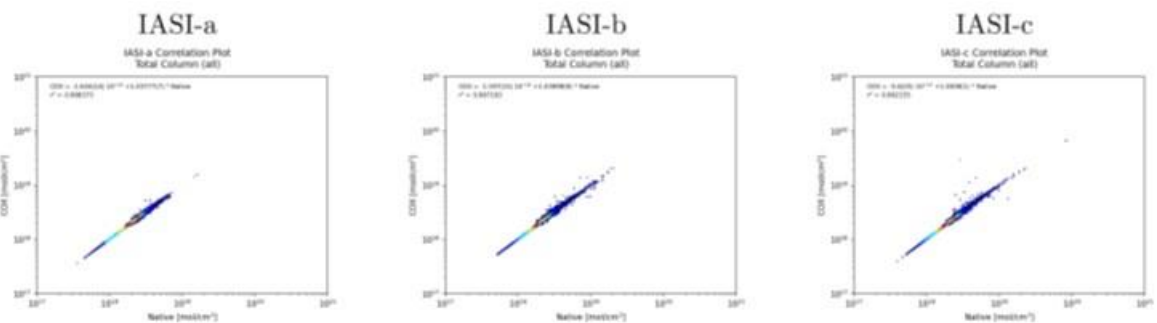
Figure 7.32. Same as Figure 7.30 but for 15/09/2021.
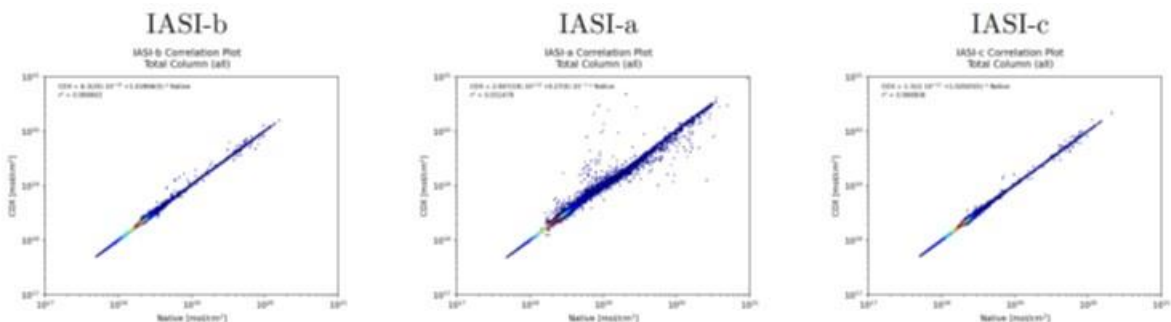
Figure 7.33. Same as Figure 7.30 but for 15/10/2021.
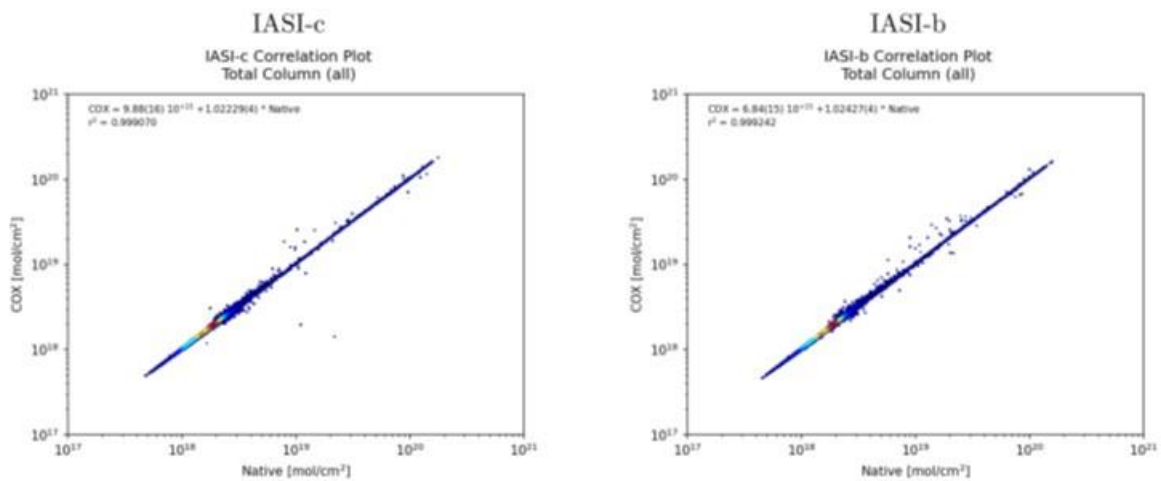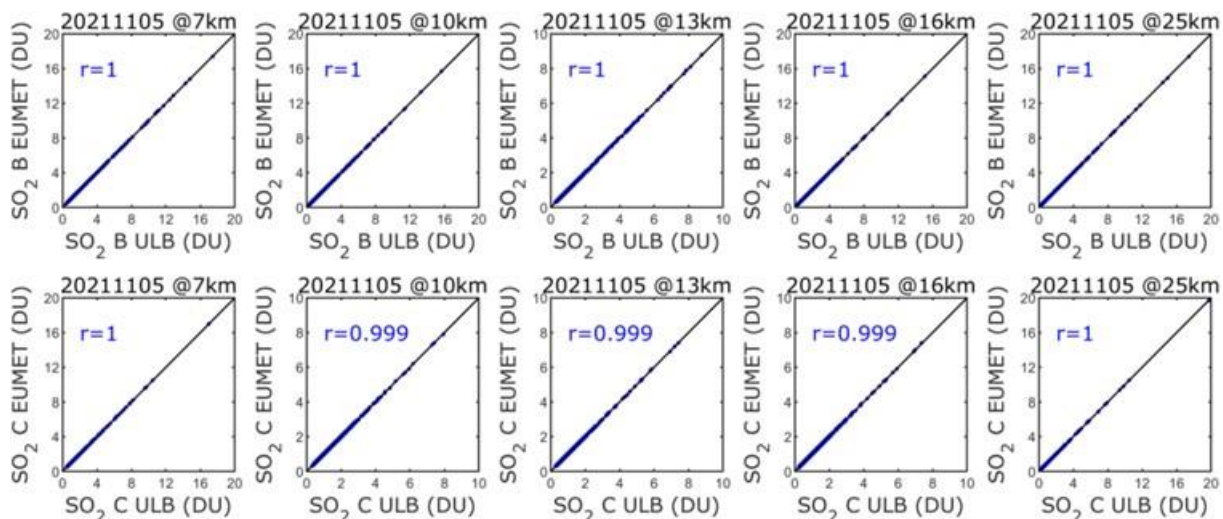
Figure 7.34. Same as Figure 7.30 but for 15/11/2021.
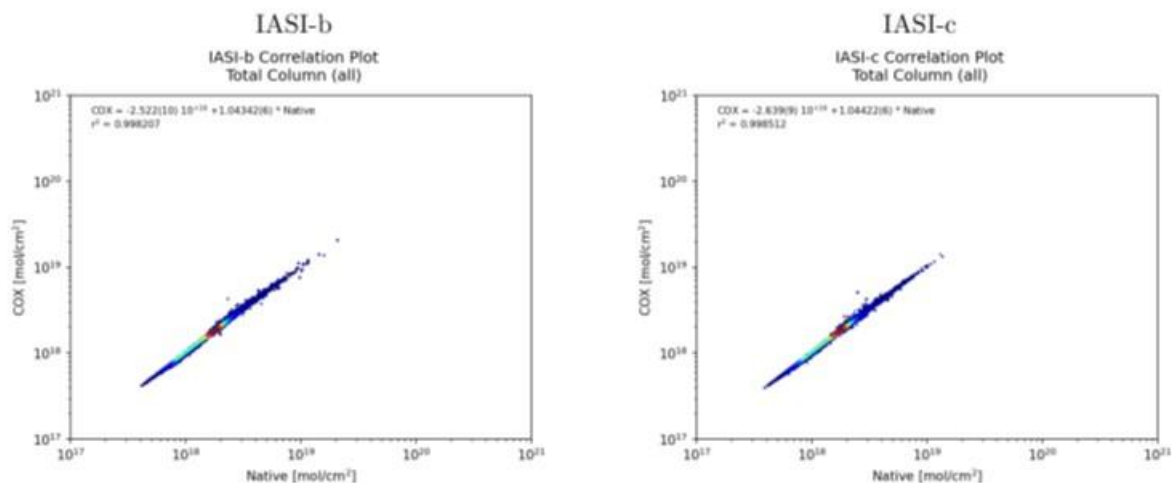
Figure 7.35. Same as Figure 7.30 but for 15/12/2021.

Note that a frequency distribution of the correlation coefficients (separated for each platform) will be provided when EUMETSAT will update the IASI CO retrieval algorithm at the EUMETSAT facilities. (In response to Action 3 (OR-9)).

IASI SO2:

The IASI BRESCIA SO2 retrieval algorithm has been implemented in the PPF v6.3 at EUMETSAT (operational release on 18/04/2018). Here we compare the EUMETSAT product disseminated by EUMETCast in BUFR format (SO2 EUMET) with the native product produced at ULB (SO2 ULB) for 7 days between July and December 2021, for Metop-A (only 2 days before the end of Metop-A), B and C. We choose to study 21/07/2021, 14/08/2021, 21/09/2021, 22/09/2021, 24/10/2021, 28/10/2021 and 05/11/2021.

For each of the seven days, scatterplots for the different estimated altitudes (7, 10, 13, 16 and 25 km) are presented (Figure 7.36 – Figure 7.41). The data have been filtered following the recommendations of the Product User Manual (Section 5.2.2, i.e. we kept the pixels in the neighbourhood (± 10 degrees) of SO2_BT_DIFFERENCE > 1K pixels, and did not use the pixels with a SO2_BT_DIFFERENCE < 0.4K.

We recall here that when the IASI L2 pressure and temperature profiles are not available, ECMWF forecasts (3h, interpolated in time and space) data are used in the EUMETSAT API. These pixels are flagged with SO2_QFLAG = 11, and are not part of the comparison.

Correlation coefficients (in blue) are ~1.

So far, the discrepancies are found within the numerical errors inherent to the use of different IT infrastructure.
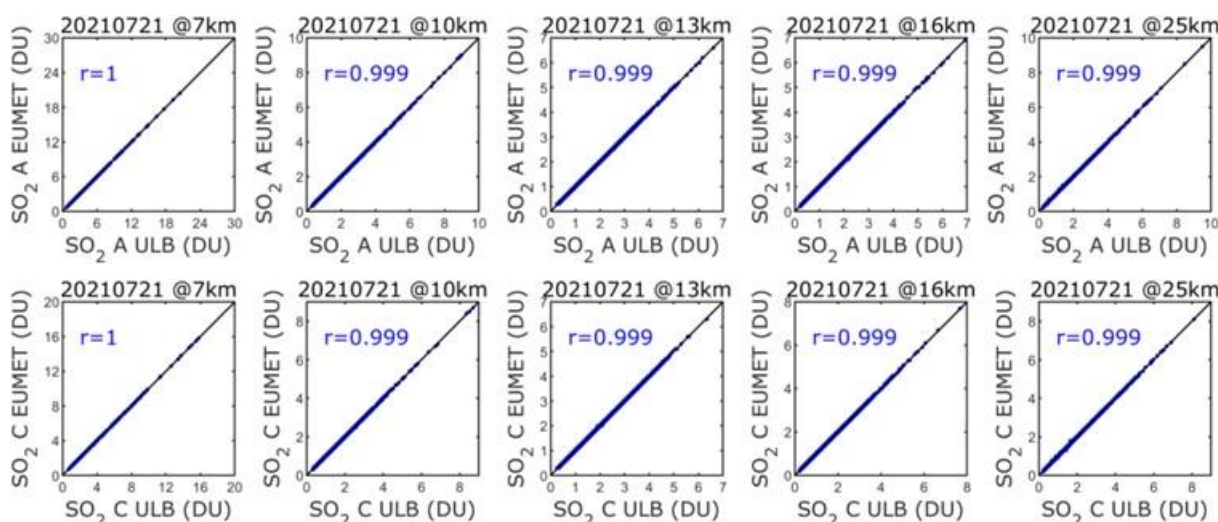
Figure 7.36. Scatterplots for Metop-A (top) and Metop-C (bottom): SO2 EUMET versus SO2 ULB for 21/07/2021, for the 5 estimated altitudes (7, 10, 13, 16 and 25 km). There is no Metop-B data for this day.
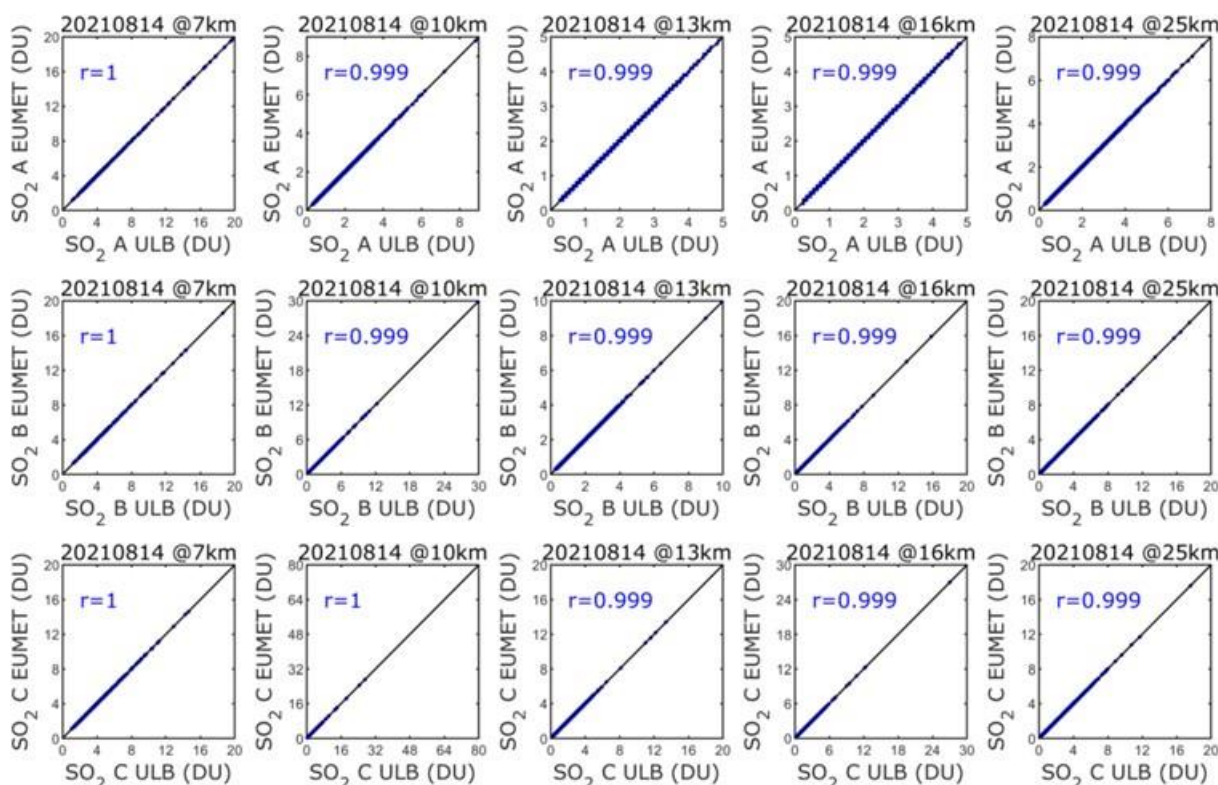
Figure 7.37. Scatterplots for Metop-A (top), Metop-B (middle) and Metop-C (bottom): SO2 EUMET versus SO2 ULB for 14/08/2021, for the 5 estimated altitudes (7, 10, 13, 16 and 25 km).
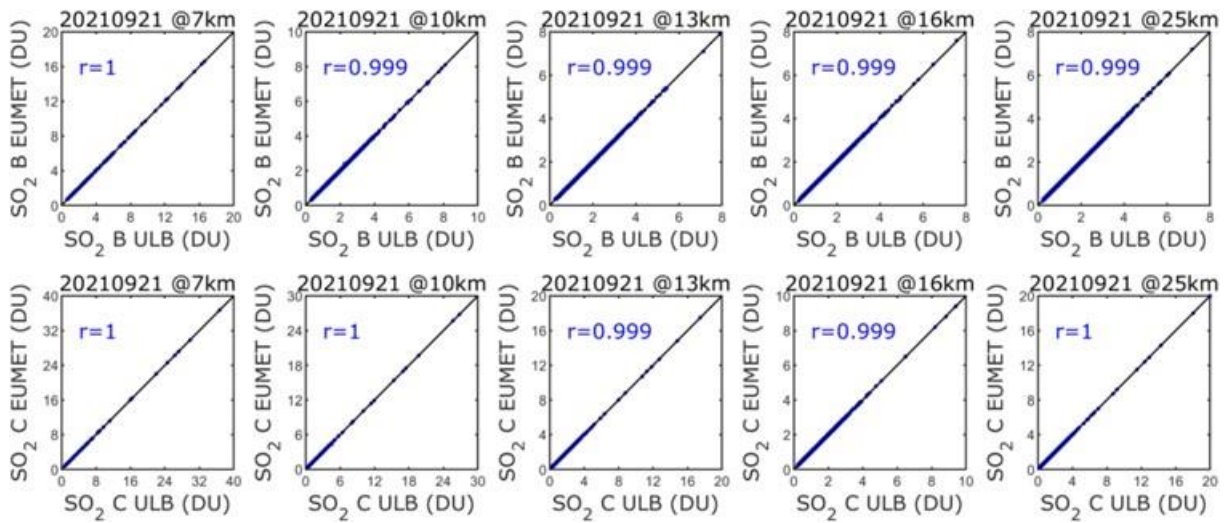
Figure 7.38. Scatterplots for Metop-B (top) and Metop-C (bottom): SO2 EUMET versus SO2 ULB for 21/09/2021, for the 5 estimated altitudes (7, 10, 13, 16 and 25 km).

Figure 7.39. Same as Figure 7.36 but for 22/09/2021.

Figure 7.40. Same as Figure 7.36 but for 24/10/2021.
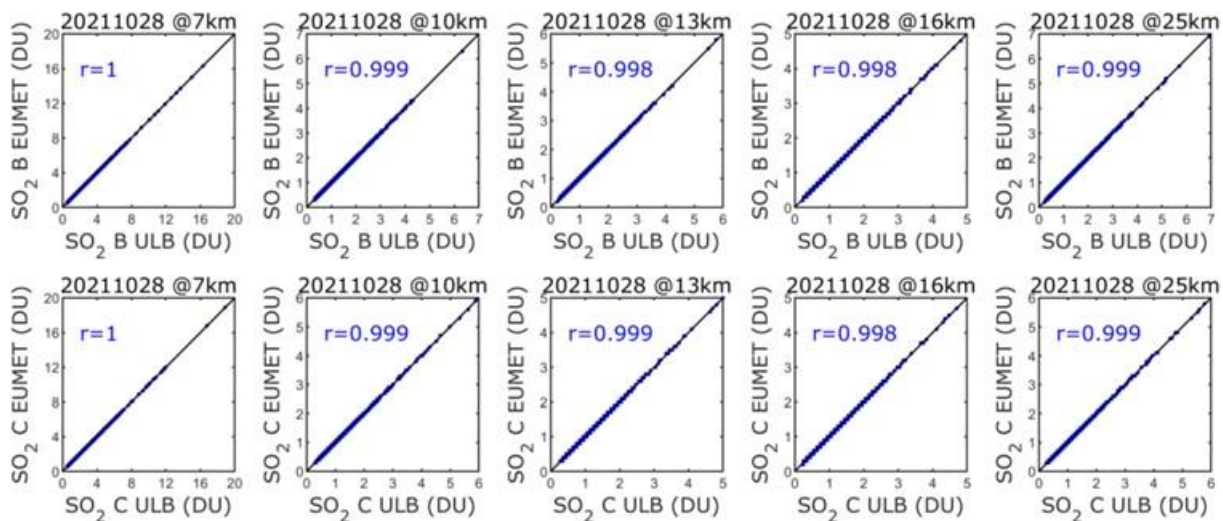
Figure 7.41. Same as Figure 7.36 but for 28/10/2021.

Figure 7.42. Same as Figure 7.36 but for 05/11/2021.

IASI O3:

The IASI NRT O3 product (v6.5) has been released on 4 December 2019 as demonstration product. Here we present statistical results when comparing the EUMETSAT product disseminated by EUMETCast in BUFR format (OZO) with the native product produced at ULB (FORLI-O3 v20191122) for 6 days representative of 6 months: July 15th, August 15th, September 15th, October 15th, November 15th and December 15th, 2021, for Metop-A, Metop-B and Metop-C. This allows monitoring if any discrepancy occurs between the two, EUMETSAT and native, products. The data have been filtered following the recommendations of the Product User Manual. Furthermore, data associated with DOFS>2 have also been filtered out. Note that no comparison is shown for IASI/Metop-A for November and December 2021, because of IASI/Metop-A end of life.

O3 total and 0 – 6 km column are investigated. Detailed statistics for total column between OZO data and FORLI-O3 data (v20191122) for each of the 6 days are presented in Table 7.26. No critical deviation was found for these dates.

Table 7.26. Statistics for total column between OZO data and FORLI-O3 data for 6 days: July 15th, August 15th, September 15th, October 15th, November 15th and December 15th, 2021. The smaller amount of data for IASI/Metop-A for October is due to the degradation of the instrument involving oversampled measurements.

15 July 2021	IASI-C		IASI-B		IASI-A	
	Native	BUFR	Native	BUFR	Native	BUFR
Individual Pixels	381155	100033	376033	98429	382229	100860
Common Pixels	87541 (22.97%)		86281 (22.95%)		88397 (23.13%)	
Correlation	0.9987		0.9988		0.9987	
Mean Total Column Differences (DU)	1.9030±1.4724		1.9111±1.4272		1.7778±1.5110	
Mean Total Column Relative Differences (%)	0.6530±0.4997		0.6565±0.4860		0.6135±0.5122	

15 August 2021	IASI-C		IASI-B		IASI-A	
	Native	BUFR	Native	BUFR	Native	BUFR
Individual Pixels	379708	102273	382332	102979	376131	102475
Common Pixels	89505 (23.57%)		89406 (23.38%)		89442 (23.78%)	
Correlation	0.9990		0.9990		0.9989	
Mean Total Column Differences (DU)	2.0444±1.4162		2.0478±1.3625		1.8804±1.4532	
Mean Total Column Relative Differences (%)	0.7054±0.4906		0.7065±0.4733		0.6494±0.5010	

15 September 2021	IASI-C		IASI-B		IASI-A	
	Native	BUFR	Native	BUFR	Native	BUFR
Individual Pixels	377963	99888	374382	99646	248329	68009
Common Pixels	88710 (23.47%)		88391 (23.61%)		59976 (24.15%)	
Correlation	0.9996		0.9997		0.9996	
Mean Total Column Differences (DU)	2.2286±1.1075		2.2318±1.0397		2.0495±1.1541	
Mean Total Column Relative Differences (%)	0.7804±0.3935		0.7824±0.3697		0.7237±0.4115	

15 October 2021	IASI-C		IASI-B		IASI-A	
	Native	BUFR	Native	BUFR	Native	BUFR
Individual Pixels	378007	97876	382724	96346	130909	30223
Common Pixels	86465 (22.87%)		85753 (22.41%)		27033 (20.65%)	
Correlation	0.9996		0.9996		0.9998	
Mean Total Column Differences (DU)	2.2030±1.3940		2.2336±1.3853		2.0269±1.5751	
Mean Total Column Relative Differences (%)	0.8014±0.5833		0.8227±0.6404		0.6637±0.5105	

15 November 2021	IASI-C		IASI-B		IASI-A	
	Native	BUFR	Native	BUFR	Native	BUFR
Individual Pixels	363541	96011	366717	97445	IASI/Metop-A end of life	
Common Pixels	85213 (23.44%)		85846 (23.41%)			
Correlation	0.9996		0.9996			
Mean Total Column Differences (DU)	2.2278±1.4409		0.8234±0.5793			
Mean Total Column Relative Differences (%)	2.2837±1.3724		0.8473±0.5834			

15 December 2021	IASI-C		IASI-B		IASI-A	
	Native	BUFR	Native	BUFR	Native	BUFR
Individual Pixels	378742	99693	375664	99205	IASI/Metop-A end of life	
Common Pixels	87460 (23.09%)		87092 (23.18%)			
Correlation	0.9994		0.9994			
Mean Total Column Differences (DU)	2.3098±1.5606		0.8291±0.5576			
Mean Total Column Relative Differences (%)	0.8291±0.5576		0.8187±0.5633			

Figure 7.43 and Figure 7.44 show the correlation plots for total and 0 – 6 km columns, respectively, between OZO data and FORLI-O3 for each platform. Correlation coefficients (in blue) are ~1.

So far, the discrepancies are found within the numerical errors inherent to the use of different IT infrastructure.
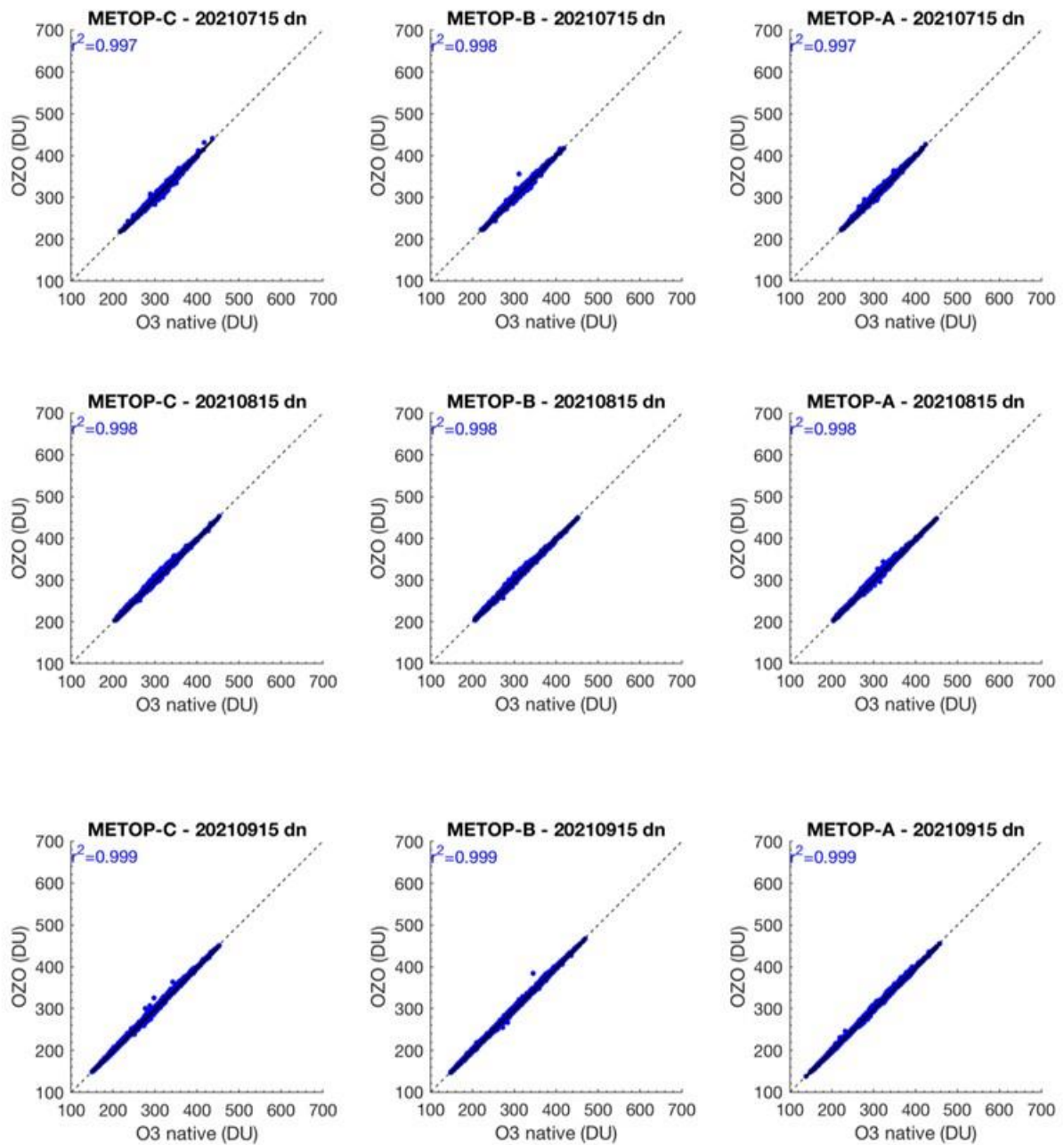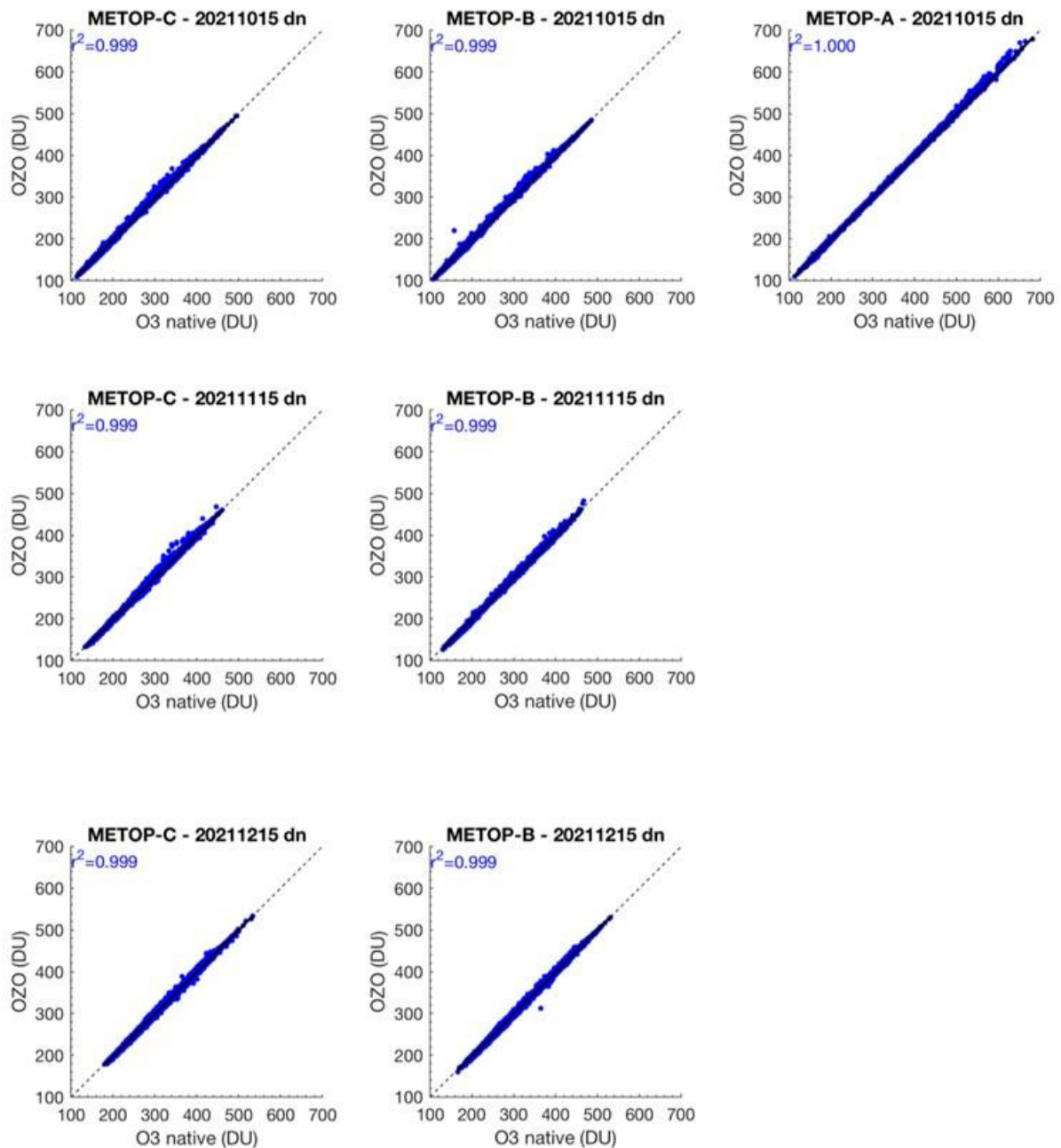
Figure 7.43. Correlation plots for total column between OZO and FORLI-O3 data for each platform for 6 days: July 15th, August 15th, September 15th, October 15th, November 15th and December 15th, 2021. X-axis corresponds to Native data (DU) and Y-axis corresponds to OZO data (DU). No comparison is shown for IASI/Metop-A for November and December 2021 because of its end of life.
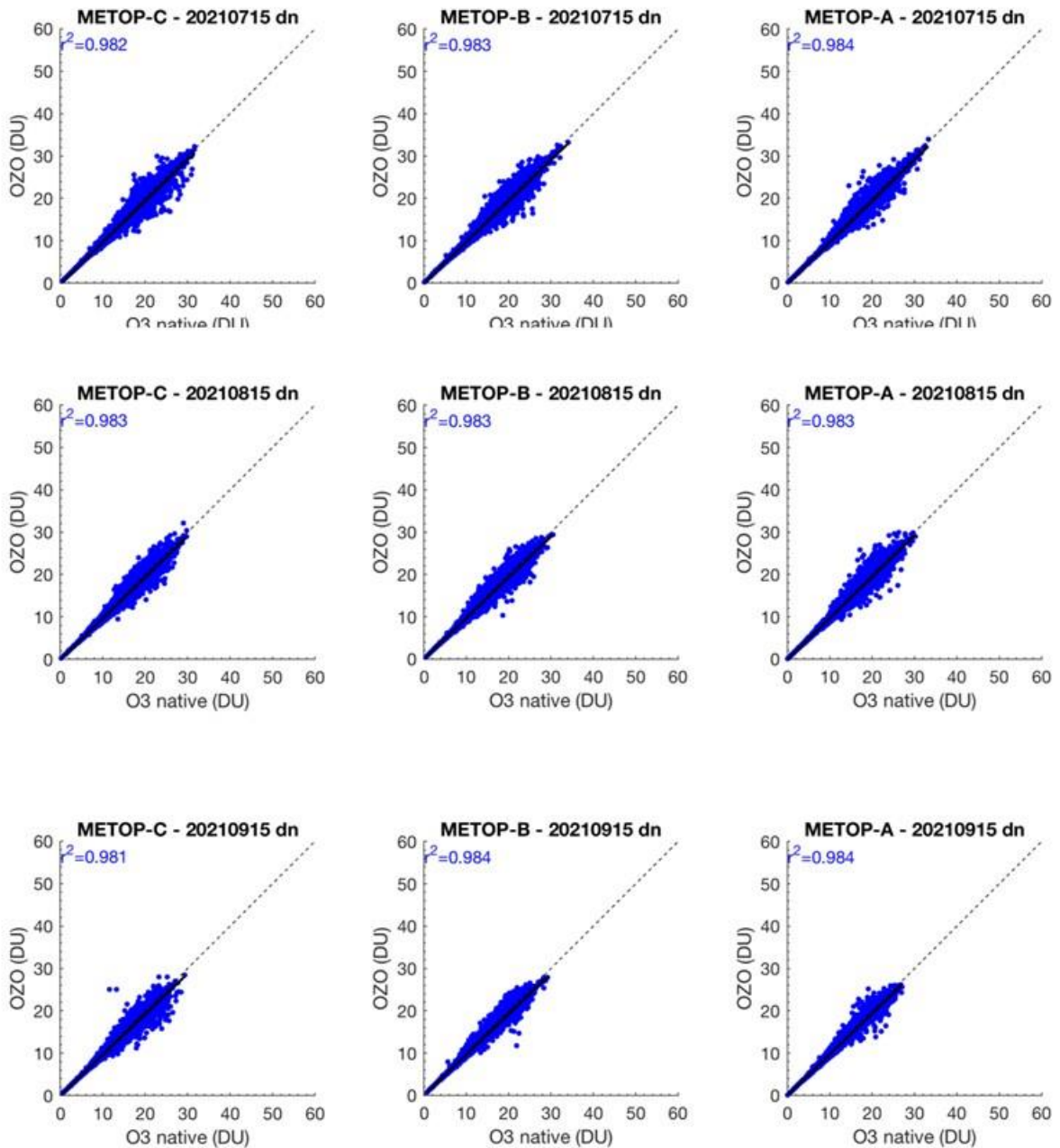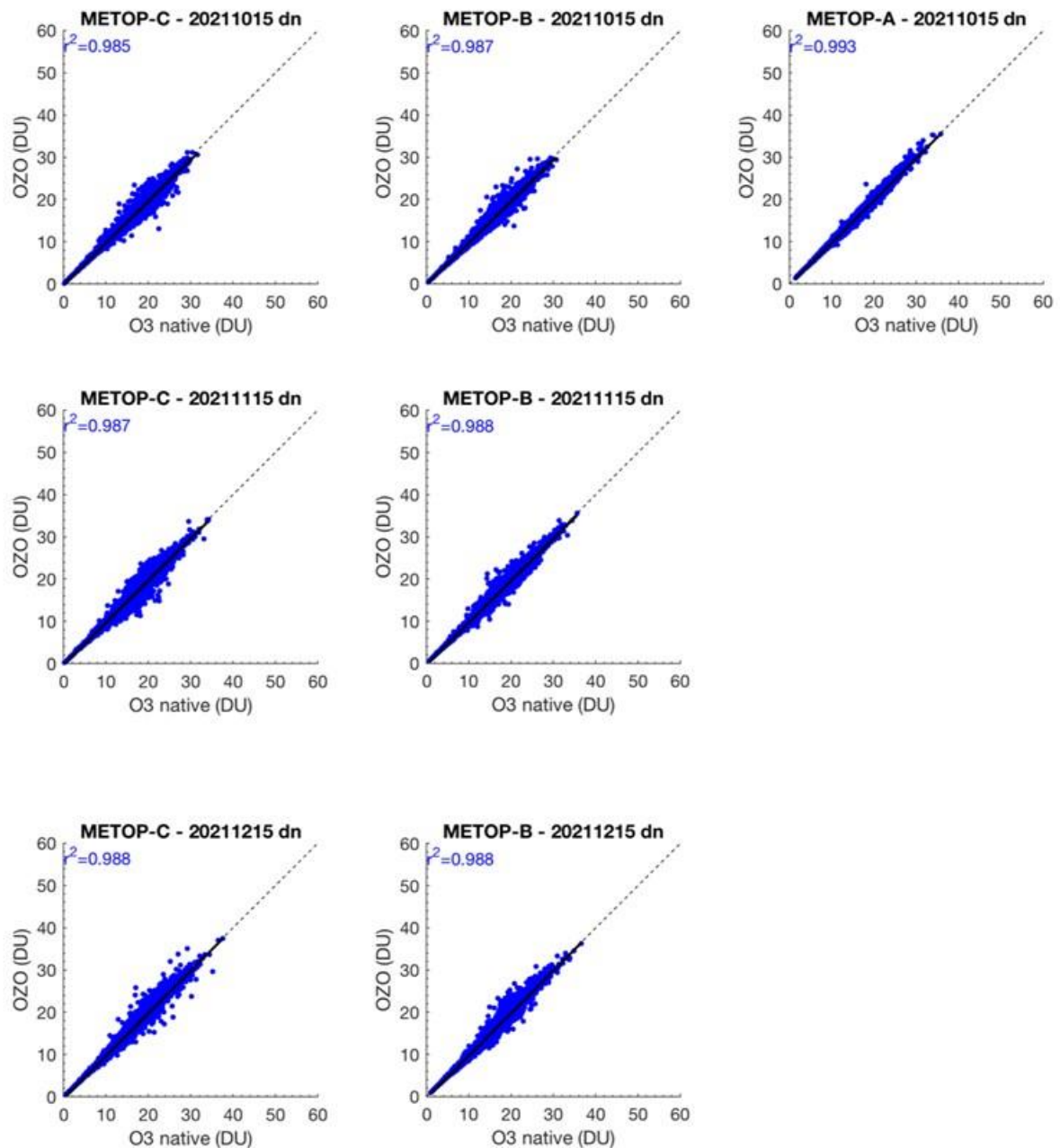
Figure 7.44. Correlation plots for 0-6km column between OZO and FORLI-O3 data for each platform for 6 days: July 15th, August 15th, September 15th, October 15th, November 15th and December 15th, 2021. X-axis corresponds to Native data (DU) and Y-axis corresponds to OZO data (DU). No comparison is shown for IASI/Metop-A for November and December 2021 because of its end of life.

IASI HNO3:

The IASI NRT HNO3 product (v6.5) has been released on 4 December 2019 as demonstration product. Here we present statistical results when comparing the EUMETSAT product disseminated by EUMETCast in BUFR format (NAC) with the native product produced at ULB (FORLI-HNO3 v20191122) for 6 days representative of 6 months: July 15th, August 15th, September 15th, October 15th, November 15th and December 15th, 2021, for Metop-A, Metop-B and Metop-C. This allows

monitoring if any discrepancy occurs between the two, EUMETSAT and native, products. The data have been filtered following the recommendations of the Product User Manual. Note that no comparison is shown for IASI/Metop-A for November and December 2021, because of IASI/Metop-A end of life.

HNO_3 total column is investigated. Detailed statistics for total column between NAC data and FORLI-HNO3 data (v20191122) for each of the six days are presented in Table 7.27. No critical deviation was found for these dates.

Table 7.27. Statistics for total column between NAC data and FORLI-HNO3 data for 6 days: July 15th, August 15th, September 15th, October 15th, November 15th and December 15th, 2021. The smaller amount of data for IASI/Metop-A for October is due to the degradation of the instrument involving oversampled measurements.

15 July 2021	IASI-C		IASI-B		IASI-A	
	Native	BUFR	Native	BUFR	Native	BUFR
Individual Pixels	305139	75491	298808	73767		
Common Pixels	67730 (22.20%)		66286 (22.18%)		68961 (22.11%)	
Correlation	0.9993		0.9993		0.9997	
Mean Total Column Differences (DU)	0.0067±0.0314		0.0069±0.0958		0.0085±0.0205	
Mean Total Column Relative Differences (%)	0.5971±1.3932		0.6012±5.7199		0.6972±1.3113	

| 15 August 2021	IASI-C		IASI-B		IASI-A	
	Native	BUFR	Native	BUFR	Native	BUFR
Individual Pixels	287335	75840	287614	75172	298886	77838
Common Pixels	67425 (23.47%)		66699 (23.19%)		69171 (23.14%)	
Correlation	0.9879		0.9996		0.9997	
Mean Total Column Differences (DU)	0.0068±0.1257		0.0077±0.0272		0.0082±0.0232	
Mean Total Column Relative Differences (%)	0.6376±8.7568		0.6781±1.4324		0.7155±1.3267	

15 September 2021	IASI-C		IASI-B		IASI-A	
	Native	BUFR	Native	BUFR	Native	BUFR
Individual Pixels	274446	74178	266828	266828	189510	189510
Common Pixels	64297 (23.43)		63842 (23.93%)		44609 (23.54%)	
Correlation	0.9952		0.9998		0.9997	
Mean Total Column Differences (DU)	0.0065±0.0717		0.0070±0.0167		0.0063±0.0176	
Mean Total Column Relative Differences (%)	0.6296±4.6963		0.6535±1.2606		0.5966±1.2241	

15 October 2021	IASI-C		IASI-B		IASI-A	
	Native	BUFR	Native	BUFR	Native	BUFR
Individual Pixels	278983	72263	277796	71943	116630	23498
Common Pixels	62314 (22.34%)		61770 (22.24%)		19586 (16.79%)	
Correlation	0.9998		0.9998		0.9999	
Mean Total Column Differences (DU)	0.0062±0.0154		0.0066±0.0153		0.6516±1.2027	
Mean Total Column Relative Differences (%)	0.0062±0.0154		0.6516±1.2027		0.9079±1.2686	

15 November 2021	IASI-C		IASI-B		IASI-A	
	Native	BUFR	Native	BUFR	Native	BUFR
Individual Pixels	284702	68717	284718	68722	IASI/Metop-A end of life	
Common Pixels	59535 (20.91%)		59516 (20.90%)			
Correlation	0.9146		0.9998			
Mean Total Column Differences (DU)	0.0033±0.3794		0.0053±0.0177			
Mean Total Column Relative Differences (%)	0.4192±43.6310		0.6342±1.2758			

15 December 2021	IASI-C		IASI-B		IASI-A	
	Native	BUFR	Native	BUFR	Native	BUFR
Individual Pixels	280865	67865	279573	66514	IASI/Metop-A end of life	
Common Pixels	59876 (21.32%)		58370 (20.88%)			
Correlation	0.9998		0.9998			
Mean Total Column Differences (DU)	0.0054±0.0182		0.0051±0.0184			
Mean Total Column Relative Differences (%)	0.6703±1.3286		0.6428±1.2844			

Figure 7.45 shows the correlation plots for total column, respectively, between NAC data and FORLI-HNO3 for each platform. Correlation coefficients (in blue) are ~1.

So far, the discrepancies are found within the numerical errors inherent to the use of different IT infrastructure.
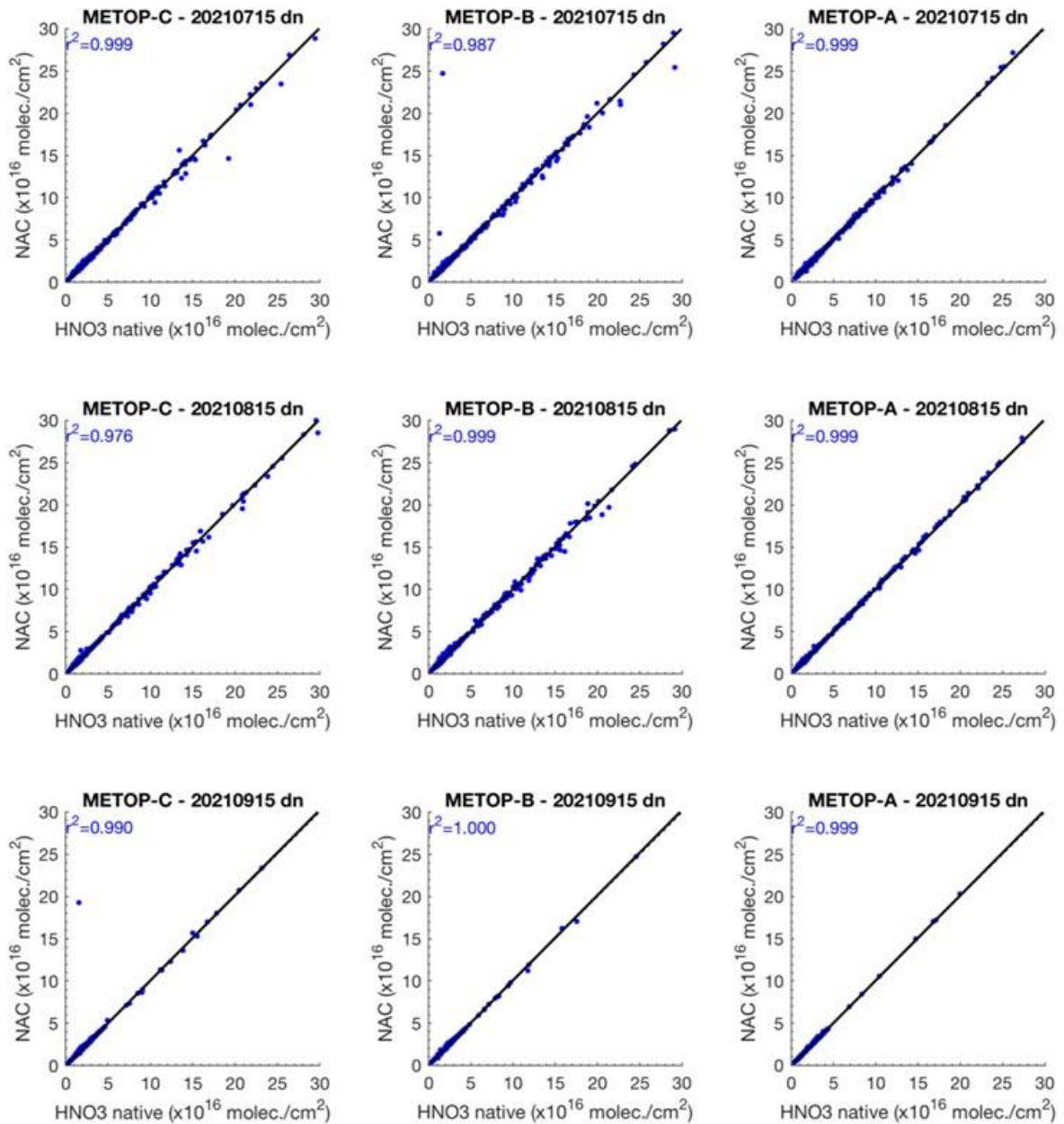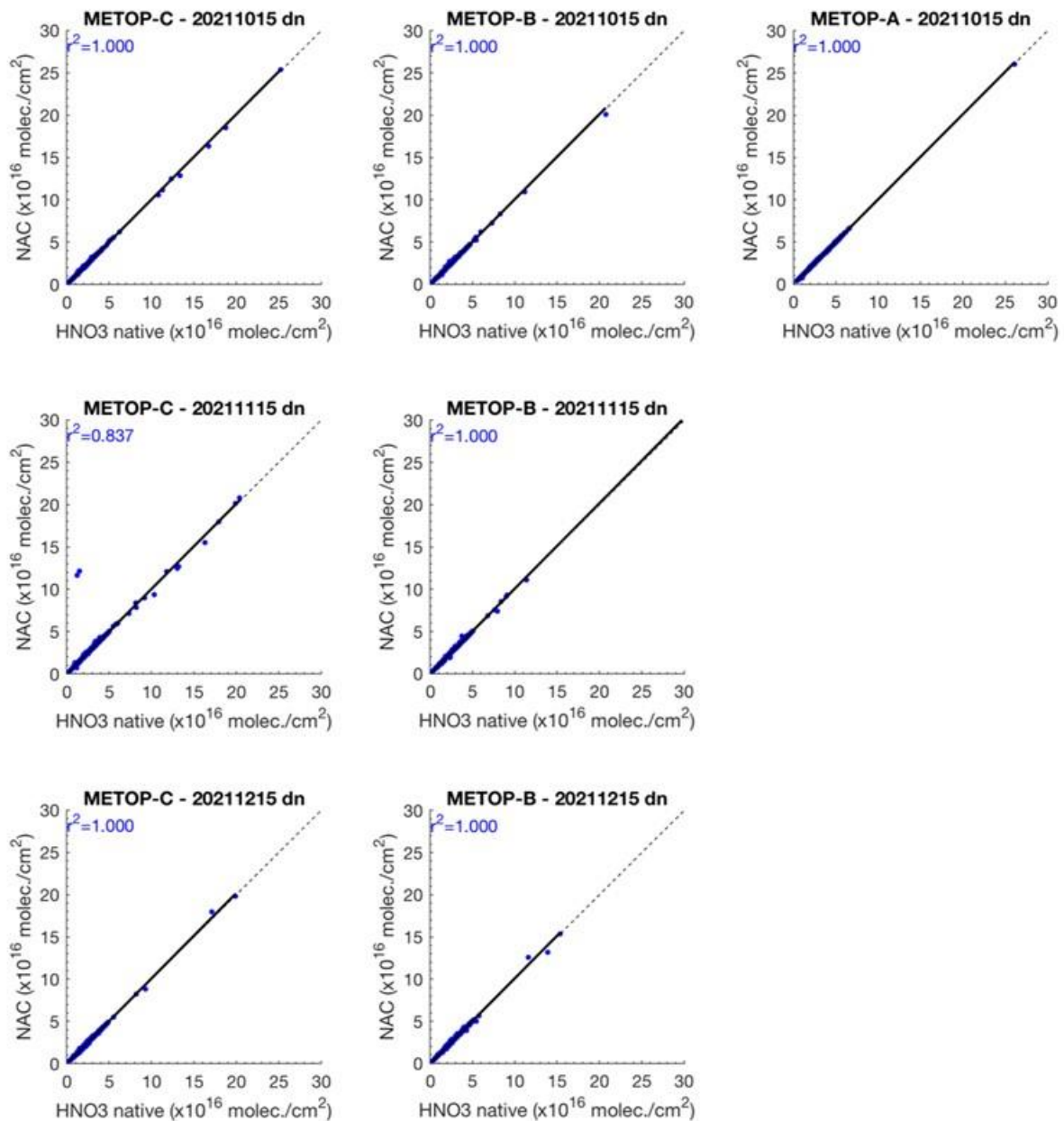
Figure 7.45. Correlation plots for total column between NAC and FORLI-HNO3 data for each platform for 6 days: July 15th, August 15th, September 15th, October 15th, November 15th and December 15th, 2021. X-axis corresponds to Native data (molec/cm^2) and Y-axis corresponds to NAC data (molec/cm^2). No comparison is shown for IASI/Metop-A for November and December 2021 because of its end of life.

Validation with CO FTIR ground-based data

This section presents the work of Bavo Langerock (BIRA-IASB) that compared the Metop-A/B/C IASI CO data against FTIR measurement data available from the NDACC (Network for the Detection of Atmospheric Composition Change). The Copernicus Atmosphere Monitoring Service (CAMS) projects supports selected NDACC instruments and Pis for rapid delivery of quality

measurements to the NDACC data host ([contract CAMS27](#)). Recent FTIR measurement data is now available for many more sites (in this study data from 22 sites is used).

These ground-based, remote-sensing instruments are sensitive to the CO abundance in the troposphere and lower stratosphere, i.e. between the surface and up to 20 km altitude. CO total columns are validated (from surface to 100 km). A description of the FTIR instruments and retrieval methodology can be found at https://nors.aeronomie.be. The typical uncertainty on the FTIR CO column is approximately 3 %, which is also used in the color scale in Figure 7.47. Due to the absence of solar light during local winter, the number of measurements at Arrival Heights in Antarctica (latitude = -77.8°) is limited. The Harestua data has only recently joined the CAMS27 project and therefore also has a limited number of co-locations.

In this comparison each FTIR measurement is co-located to all IASI measurements within a time difference of 3 hours and within a distance of 50 km to the effective location of the FTIR measurement (this effective location is calculated along the line of sight of the FTIR measurement). The IASI *a priori* is substituted in the FTIR retrieval and subsequently the FTIR retrieved profile with the IASI *a priori* is smoothed using the IASI averaging kernel, as described in Rodgers *et al.*, 2003. In the plots the relative differences are calculated using the latter FTIR columns (smoothed with the IASI averaging kernels). This validation methodology is described in more detail in Ronsmans *et al.*, 2016. All figures for the individual stations can be browsed on https://cdop.aeronomie.be.

Table 7.28. Statistics between IASI-B/C and FTIR CO smoothed total columns for the entire time period January 2017 – November 2021 (the column "std" is the standard deviation of the local FTIR columns relative to the standard deviation of the IASI columns)

	Metop-B					Metop-C				
	# meas.	Std.	R	rel. Diff.	Std. Rel. Diff.	# meas.	Std.	R	rel. Diff.	Std. Rel. Diff.
Eureka	990	0.7	0.87	12.07	14.03					
Ny Ålesund	97	1.2	0.90	14.45	8.58	47	1.0	0.94	18.53	7.71
Thule	4544	0.8	0.87	2.03	9.78	1742	0.8	0.88	4.82	8.68
Kiruna	839	1.1	0.80	-4.43	7.51	376	1.2	0.77	-3.99	7.37
Harestua	242	1.0	0.87	6.77	5.88					
St. Petersburg	1079	0.9	0.85	4.16	6.70	238	0.9	0.76	5.65	6.97
Bremen	394	0.8	0.87	5.95	7.26	114	1.0	0.88	6.01	6.15
Garmisch	2431	0.9	0.90	-1.20	6.91	827	0.9	0.93	-1.55	6.01
Zugspitze	2273	1.0	0.90	-0.40	5.49	756	0.9	0.89	-1.45	5.34
Jungraujoch	639	1.0	0.94	-0.86	4.31	339	1.0	0.95	-2.01	4.34
Toronto	948	0.8	0.81	17.08	12.73	521	0.7	0.88	18.84	11.37
Rikubetsu	51	0.8	0.74	5.03	9.69	19	0.8	0.89	2.41	5.43
Boulder	1799	0.8	0.89	-2.84	9.06	1689	0.9	0.90	-3.28	8.16
Izana	644	1.1	0.94	-4.59	3.65	176	1.2	0.97	-5.48	3.38
Mauna Loa	907	1.1	0.94	-2.56	5.45	195	1.1	0.94	-5.02	4.46
Altzomoni	702	1.3	0.92	5.60	5.90	170	1.1	0.96	1.01	4.70
Paramaribo	97	0.9	0.89	9.52	7.24	25	1.2	0.80	5.93	5.09
Porto Velho	263	0.8	0.97	7.60	8.50					
La Reunion Maido	1790	1.0	0.98	0.69	3.86	351	1.1	0.98	1.72	3.90
Wollongong	1520	0.9	0.90	2.65	8.31	722	0.8	0.91	3.63	10.21
Lauder	1978	0.9	0.92	5.66	7.08	993	0.9	0.97	5.58	5.17

Arrival Heights	311	0.8	0.80	11.77	12.64	183	1.0	0.96	10.43	5.55
Average for all sites		0.94	0.88	4.28	7.75		0.98	0.90	3.25	6.32

The correlation coefficients of the Taylor diagrams (Figure 7.46 and Table 7.28) are generally ranging from ~0.8 to nearly 1, showing a very good agreement between the IASI and FTIR data, for Metop-A/B/C. However, some sites are special:

1. Rikubetsu, Ny Ålesund, Kiruna and Harestua have only few co-located measurements and are statistically less relevant
2. Toronto has a low correlation although the site has many co-locations. This may be due to some co-locations where the IASI concentration is much higher than observed by the FTIR and probably related to false co-locations during fire events. The FTIR time-series seems to suffer from outliers being too low.

3. At Thule and Eureka the satellite underestimates the CO columns by up to 50 % during the early spring weeks and is related to a reduced sensitivity of the IASI CO product during local spring. At Kiruna the underestimation is not so strong, up to 30 %.

The Taylor diagrams in Figure 7.46 and statistics in Table 7.28 also show that the standard deviations of the FTIR columns values are smaller compared the satellite standard deviation probably due to higher noise on the satellite time-series (almost all site points are shifted left of the satellite reference, typically with a factor of 0.8 to 1 of the standard deviation of the satellite CO columns).

Figure 7.47 shows the time-series of bi-weekly mean relative differences for the time period January 2017 – November 2021. Red indicates a positive bias (IASI > NDACC) while blue indicates an underestimation of the satellite retrievals. The chosen color scale is based on the FTIR typical uncertainty. The IASI retrieval uncertainty should be added (typically around 4 %), so only biases above 5 % are to be considered significant. In the Northern Hemisphere a seasonal changing bias is observed: overestimation during summer and underestimation during winter months. A similar seasonal dependence but less pronounced is observed in the Southern Hemisphere. A longer time period is required to study this seasonal dependence in more detail.

We can conclude that for most of the 22 stations included in the comparison, mean relative differences, or biases, are less than 10 % (see the individual station plots at https://cdop.aeronomie.be/ under Validation Results). For the Eureka, Ny Ålesund and Arrival Heights stations, located at high latitudes, biases are larger. A similar bias is found by Buchholz *et al.* (2017) when comparing with MOPITT data. When looking at the stations between -60° and 60°, the Toronto station shows the largest biases (mean bias = 13.6 %) which seems to be due to outliers.

The IASI data are generally overestimated with the overall bias being below 5 % (Table 7.28) hence not significant compared to the combined total uncertainty.
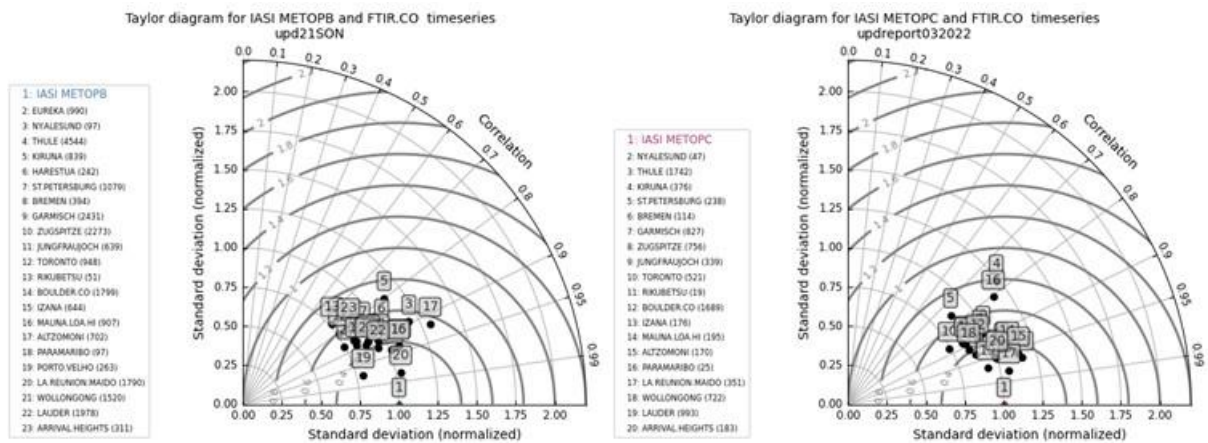
Figure 7.46. Correlation plots for IASI-B (left) and IASI-C (right) CO total columns against 22 NDACC FTIR sites. The stations are slightly shifted to the left, indicating that the satellite time-series has a higher standard deviation (more noisy).
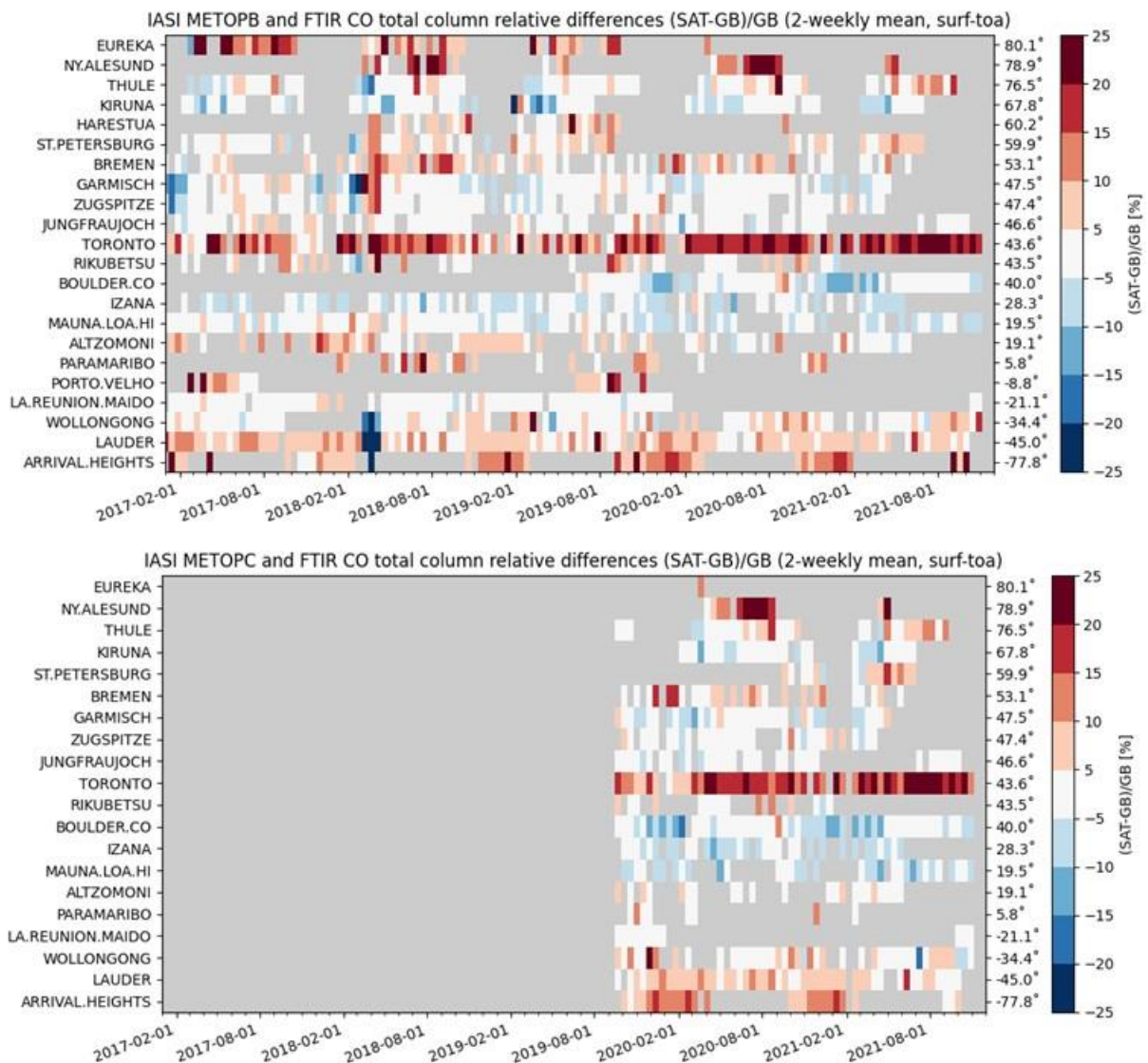

Figure 7.47. Time-series of bi-weekly relative difference for IASI-B (top) and IASI-C (bottom). Not all stations have co-locations with the Metop-C satellite. Although the Metop-C time-series is too short to

deduce robust statistics, the time-series of the bias seems to correspond closely to the Metop-B time-series.

References:

Buchholz, R. R., Deeter, M. N., Worden, H. M., Gille, J., Edwards, D. P., Hannigan, J. W., Jones, N. B., Paton-Walsh, C., Griffith, D. W. T., Smale, D., Robinson, J., Strong, K., Conway, S., Sussmann, R., Hase, F., Blumenstock, T., Mahieu, E., and Langerock, B.: Validation of MOPITT carbon monoxide using ground-based Fourier transform infrared spectrometer data from NDACC, Atmos. Meas. Tech., 10, 1927-1956, 2017.
https://doi.org/10.5194/amt-10-1927-2017

Ronsmans, G., Langerock, B., Wespes, C., Hannigan, J. W., Hase, F., Kerzenmacher, T., Mahieu, E., Schneider, M., Smale, D., Hurtmans, D., De Mazière, M., Clerbaux, C., and Coheur, P.-F.: First characterization and validation of FORLI-HNO$_3$ vertical profiles retrieved from IASI/Metop, Atmos. Meas. Tech., 9, 4783-4801,2016.
https://doi.org/10.5194/amt-9-4783-2016

8. List of AC SAF users

The institutes of registered users of AC SAF products are listed below.

8.1. FMI archive

Europe:

Armenia:
- ICHD

Austria:
- Central Institute for Meteorology and Geodynamics
- Private individual
- Sistema GmbH
- University of Veterinary Medicine
- University of Vienna (2 users)

Belarus:
- National Academy of Sciences
- State University

Belgium:
- BIRA-IASB
- Ghent University (6 users)
- KMI
- KU Leuven
- ULB (3 users)

Bulgaria:
- Bulgarian Academy of Science
- Space Research and Technology Institute (2 users)

Croatia:
- J. J. Strossmayer University of Osijek

Czech Republic:
- Czech Hydrometeorological Institute (4 users)
- Global Change Research Institute

Denmark:
- Aarhus University (2 users)
- DMI (2 users)

Estonia:
- Estonian Environment Agency
- Intertrust

Finland:
- FMI (10 users)
- Häme University of Applied Sciences
- University of Helsinki (3 users)

France:
- AERIS/ICARE
- Aix-Marseille University
- CNRS (3 users)
- Laboratory of Atmospheric Optics
- Lasem
- LATMOS
- LISA (2 users)
- LISA-CNRS
- LPC2E-CNRS
- LSCE-IPSL-CNRS
- Météo France (4 users)
- Mines Paristech
- Private Individual
- University of La Reunion
- University of Lille
- University of Paris Est Creteil

Germany:
- ask – Innovative Visualisierungslösungen GmbH
- Datiaperti
- DLR (2 users)
- DWD (4 users)
- EUMETSAT (19 users)
- Federal Office for Radiation Protection
- Forschungszentrum Jülich GmbH (3 users)
- Fraunhofer Institute
- Gymnasium Olching
- Oldenburg University
- Private individual
- Max Planck Institute for Chemistry (6 users)
- Sabrina Szeto Consulting
- Technical University of Munich
- University of Bremen (3 users)
- University of Cologne
- University of Konstanz
- University of Münster
- University of Potsdam
- University of Rostock

Greece:
- AUTH (4 users)
- Hellenic Centre for Marine Research
- National Technical University of Athens
- Private Individual
- University of Athens
- University of the Aegean

- University of Crete (2 users)

Hungary:
- Eötvös Loránd University (2 users)
- Hungarian Academy of Sciences
- Hungarian Meteorological Service (2 users)
- Individual
- University of Szeged

Ireland:
- National University of Ireland Galway
- Trinity College Dublin

Italy:
- ARPA Valle d'Aosta
- B-Open Solutions S.r.l. (2 users)
- CNR-ISAC
- European Space Agency
- fabbricadigitale
- IFAC-CNR (2 users)
- LaMMA Consortium (2 users)
- MEEO / Julia Wagemann Consulting
- National Institute for Astrophysics
- Parthenope University of Naples
- Private Individual
- Regional Environmental Protection Agency Calabria
- University of Bologna
- University of Florence
- University of Milan
- University of Modena and Reggio Emilia
- University of Venice

Lithuania:
- Lithuanian National Meteorological Service
- Vilnius University (2 users)

Malta:
- University of Malta

Moldova:
- Academy of Sciences

The Netherlands:
- BESSR
- KNMI (5 users)
- S[&]T Corporation
- Wageningen University & Research (2 users)

Norway:
- Norwegian Institute for Air Research (2 users)
- UiT The Arctic University of Norway

Poland:
- CloudFerro
- Institute of Environmental Protection (2 users)
- Institute of Geodesy and Cartography
- Military University of Technology
- University of Warsaw

Portugal:
- Instituto Dom Luiz
- Instituto Português do Mar e da Atmosfera (4 users)
- University of Aveiro
- University of Lisbon
- University of Trás-os-Montes and Alto Douro (2 users)

Republic of North Macedonia:
- Hydrometeorological Service

Romania:
- Babes-Bolyai University (3 users)
- Global Top Systems
- INCAS
- INOE (3 users)
- National Meteorological Administration (3 users)
- University of Galați (3 users)
- Politehnica University of Bucharest

Russia:
- Altai State University
- Daghestan Scientific Centre of Russian Academy of Sciences
- Federal Research Center Krasnoyarsk Scientific Center of the Siberian Branch of the RAS (2 users)
- Fedorov Institute of Applied Geophysics
- Institute of Atmospheric Physics
- Institute of Computational Modeling of the Siberian Branch of the RAS
- Institute of Global Climate and Ecology
- Irkutsk State Transport University
- Moscow State University
- Planeta (2 users)
- Research Center of Ecological Safety
- Roscosmos
- St. Petersburg State University
- Tomsk State University of Control Systems and Radioelectronics

Serbia:
- Geographical institute "Jovan Cvijic", SASA

Slovakia:
- Private Individual

Slovenia:
- Bide-san, s.p.

Spain:
- Autonomous University of Barcelona
- Barcelona Supercomputing Center
- Basque Meteorology Agency
- CREAF-CSIC-UAB
- I.E.S. Punta del Verde
- Modeliza
- Pablo de Olavide University
- Polytechnic University of Catalonia (2 users)
- State Meteorological Agency
- University of Alicante
- University of Extremadura
- University of Granada
- University of Málaga
- University of Valencia (2 users)
- University of Valladolid (2 users)

Sweden:
- NBI/Handelsakademin
- SMHI (5 users)
- The Swedish Defence Research Agency

Switzerland:
- Swiss Federal Laboratories for Materials & Technology

Turkey:
- Hacettepe University
- Istanbul University
- Middle East Technical University
- Turkish State Meteorological Service (2 users)

Ukraine:
- Taras Shevchenko National University of Kyiv
- UHMC
- Ukrainian Hydrometeorological Institute (2 users)

United Kingdom:
- Airbus S.A.S.
- ECMWF (2 users)
- ESA
- IDEMS International
- London School of Hygiene and Tropical Medicine
- Private individual
- Rutherford Appleton Lab
- Satavia Ltd. (2 users)
- Satellite Applications Catapult
- Science and Technology Facilities Council (2 users)
- siHealth Ltd.
- University College London

- University of Birmingham
- University of Edinburgh
- University of Leeds (3 users)
- University of Leicester
- University of Oxford
- University of York

Asia:

Bangladesh:
- Institute of Forestry and Environmental Sciences
- Stamford University
- University of Dhaka

China:
- Anhui Institute of Optics and Fine Mechanics
- Anhui Institute of Meteorological Sciences
- Beijing Municipal Environmental Monitoring Center
- Beijing Normal University (2 users)
- China Academy of Sciences (5 users)
- China Meteorological Administration
- China University of Mining and Technology (3 users)
- Chinese Academy of Meteorological Sciences (2 users)
- Fudan University
- HTHJ
- Institute of Earthquake Forecasting
- Institute of Remote Sensing and Digital Earth (3 users)
- Jiangsu Meteorological Observatory
- Jiangsu Normal University (2 users)
- Lanzhou University (2 users)
- Lanzhou Jiaotong University
- Nanjing University
- Nanjing University of Information Science & Technology (6 users)
- National Satellite Meteorological Center
- National University of Defense Technology
- Northeast Normal University
- Peking University (2 users)
- School
- Shandong University
- Shanghai University
- State Environmental Protection Key Lab of Satellite Remote Sensing
- Sun Yat-Sen University
- The Chinese University of Hong Kong (2 users)
- The Institute of Atmospheric Physics (3 users)
- Tsinghua University (2 users)
- (unknown) (2 users)
- University of Science and Technology
- Xiamen University

- Zhejiang University (2 users)

India:
- Anna University
- Aryabhatta Research Institute of Observational Sciences
- Banaras Hindu University
- Birla Institute of Technology
- Bose Institute
- Council of Scientific and Industrial Research
- CSIR-NIO
- CSIR-NPL
- Dibrugarh University
- "Education"
- IIT KGP
- Indian Institute of Remote Sensing
- Indian Institute of Science Education and Research
- Indian Institute of Technology Kharagpur (4 users)
- Indian Institute of Technology Roorkee (2 users)
- Indian Institute of Tropical Meteorology (3 users)
- Indian Space Research Organization (2 users)
- Jawaharlal Nehru Technological University, Kakinada
- Jawaharlal Nehru University
- Malaviya National Institute of Technology Jaipur
- Mangalore University
- MSRIT
- National Atmospheric Research Laboratory (3 users)
- National Centre for Medium Range Weather Forecasting
- National Remote Sensing Centre
- Savitribai Phule Pune University (2 users)
- School of Planning and Architecture, Bhobal
- SIG
- University of Calcutta
- University of Hyderabad
- University of Kalyani
- Vikram Sarabhai Space Centre (2 users)
- Vindhyan Ecology and Natural History Foundation

Indonesia:
- Meteorology, Climatology, and Geophysical Agency (2 users)
- National Institute for Aeronautics and Space
- Sumatera Institute of Technology

Japan:
- Chiba University
- Japan Meteorological Agency
- Kyushu University
- National Institute for Environmental Studies
- Waseda University

Malaysia:
- Science University of Malaysia
- Malaysian Space Agency
- National University of Malaysia (5 users)
- University Malaysia Sabah

Myanmar:
- Yangon Technological University

Nepal:
- International Centre for Integrated Mountain Development (2 users)
- Institute for Advanced Sustainability Studies
- Institute of Tibetan Plateau Research
- Institute of Engineering

Pakistan:
- University of the Punjab
- National University of Sciences & Technology

Philippines:
- Manila Observatory

Singapore:
- National University of Singapore (2 users)

South Korea:
- Chungnam National University (2 users)
- Gangneung–Wonju National University
- Gwangju Institute of Science and Technology (2 users)
- Korea Polar Research Institute
- National Institute of Environmental Research (2 users)
- National Meteorological Satellite Center
- Yonsei University (3 users)
- Kongju National University
- Seoul National University

Sri Lanka:
- Central Environmental Authority

Taiwan:
- Academia Sinica
- National Central University (2 users)
- Research Center for Environmental Changes

Thailand:
- Asian Institute of Technology
- King Mongkut's Institute of Technology Ladkrabang

Vietnam:
- University of Science (2 users)

Middle East:

Iran:
- Islamic Azad University
- University
- Atmospheric Science & Meteorological Research Center

Iraq:
- Al Iraqia University

Israel:
- Israel Institute for Biological Research
- University of Tel Aviv (2 users)

Oman:
- Sultan Qaboos University

Saudi Arabia:
- King Abdullah University of Science and Technology
- Private individual

United Arab Emirates:
- Khalifa University
- Masdar Institute
- Uruk Engineering & Contracting

North America:

Canada:
- Dalhousie University

United States of America:
- Caltech
- Colorado State University
- Florida State University
- Hampton University
- Harvard-Smithsonian Center for Astrophysics
- Joint Center for Satellite Data Assimilation
- Massachusetts Institute of Technology
- Michigan Technological University (4 users)
- NASA (2 users)
- Naval Research Laboratory
- NOAA
- Princeton University
- Private Individual
- SpaceKnow Inc.
- The Aerospace Corporation
- Trinity Consultants Inc.
- University of Alabama in Huntsville
- University of Alaska (2 users)
- University of California (2 users)
- University of Central Florida

- University of Colorado Boulder
- University of Washington
- Unknown
- USGS
- U.S. Environmental Protection Agency

South America:

Argentina:
- Universidad Nacional de Córdoba
- Universidad Nacional de Rosario

Brazil:
- APAC
- Federal University of Western Pará
- LAPIS
- Universidade Federal de Alagoas

Colombia:
- Universidad EAFIT

Ecuador:
- Universidad San Francisco de Quito (2 users)

Guatemala:
- Ambente
- INSIVUMEH

Mexico:
- Instituto Politecnico Nacional

Paraguay:
- Universidad San Carlos

Uruguay:
- Universidad de la República

Australia / New Zealand:

- Australian National University
- Bureau of Meteorology
- University of Canterbury
- University of Melbourne (2 users)
- University of Southern Queensland (2 users)
- University of Sydney

Africa:

Algeria:
- Meteo Algeria

Cameroon:
- African Institute for Mathematical Sciences

Egypt:
- Egyptian Meteorological Authority (2 users)

- National Research Institute of Astronomy and Geophysics

Eritrea:
- Department of Environment

Ethiopia:
- Addis Ababa University

Ghana:
- Ghana Meteorological Agency
- University of Energy and Natural Resources

Morocco:
- Abdelmalek Essaadi University
- EM5D
- Maroc Météo
- University of Hassan II Casablanca

Nigeria:
- Abdou Moumouni University
- Federal University Lafia

South Africa:
- South African Weather Service
- Stellenbosch University
- University of KwaZulu-Natal
- University of Pretoria
- University of the Witwatersrand

Registered users: **530**

8.2. DLR archive

Europe:

Austria:
- University of Innsbruck
- University of Veterinary Medicine
- University of Vienna

Belarus:
- National Academy of Sciences

Belgium:
- BIRA-IASB (6 users)
- Ghent University (3 users)
- KMI
- ULB (2 users)

Bulgaria:
- Space Research and Technology Institute (2 users)

Czech Republic:
- Charles University
- Czech Hydrometeorological Institute (5 users)
- Global Change Research Institute

Denmark:
- Aarhus University (2 users)

Estonia:
- Estonian Environment Agency
- Intertrust

Finland:
- FMI (7 users)
- Häme University of Applied Sciences
- University of Helsinki (2 users)

France:
- AERIS/ICARE
- Aix-Marseille University
- CNRS (3 users)
- Institute of Environmental Geosciences
- Laboratory of Atmospheric Optics
- Lasem
- LATMOS (3 users)
- LISA
- LISA-CNRS
- LSCE-IPSL-CNRS
- LPC2E-CNRS
- Météo France (3 users)
- Mines Paristech
- University of La Reunion

Germany:
- ask – Innovative Visualisierungslösungen GmbH
- Datiaperti
- DLR (4 users)
- DWD (2 users)
- EUMETSAT (18 users)
- Forschungszentrum Jülich GmbH (2 users)
- Fraunhofer Institute
- Gymnasium Olching
- Heidelberg University
- Max Planck Institute for Chemistry (5 users)
- Private individual
- Sabrina Szeto Consulting
- Technical University of Munich
- University of Bremen (6 users)
- University of Cologne (2 users)

- University of Hannover
- University of Münster

Greece:
- AUTH (4 users)
- Hellenic Centre for Marine Research
- National Technical University of Athens
- Private Individual
- University of Athens
- University of Crete (2 users)

Hungary:
- Hungarian Meteorological Service (2 users)
- Individual
- University of Szeged

Iceland:
- Private individual

Ireland:
- National University of Ireland Galway
- Trinity College Dublin

Italy:
- B-open Solutions S.r.l. (2 users)
- CNR-ISAC
- fabbricadigitale
- IFAC-CNR
- LaMMA Consortium
- MEEO / Julia Wagemann Consulting
- National Institute of Geophysics and Volcanology
- Private Individual
- Regional Environmental Protection Agency Calabria
- University of Florence
- University of Modena and Reggio Emilia
- University of Venice

Lithuania:
- Lithuanian National Meteorological Service

Malta:
- University of Malta

The Netherlands:
- BESSR
- KNMI (6 users)
- S[&]T Corporation
- Wageningen University & Research (2 users)

Norway:
- UiT The Arctic University of Norway

Poland:
- CloudFerro
- Institute of Environmental Protection (2 users)
- Institute of Geodesy and Cartography
- Institute of Meteorology and Water Management-NRI
- Military University of Technology
- University of Warsaw

Portugal:
- Instituto Dom Luiz (2 users)
- Instituto Português do Mar e da Atmosfera (3 users)
- University of Tras-os-Montes and Alto Douro

Romania:
- Babes-Bolyai University (3 users)
- Global Top Systems
- INOE (4 users)
- National Meteorological Administration (2 users)
- University of Galați (3 users)
- Politehnica University of Bucharest

Russia:
- Altai State University
- Institute of Computational Modeling of the Siberian Branch of the RAS
- Institute of Global Climate and Ecology
- Irkutsk State Transport University
- Planeta

Serbia:
- Geographical institute "Jovan Cvijic", SASA

Slovakia:
- Private Individual

Slovenia:
- Bide-san, s.p.

Spain:
- Autonomous University of Barcelona
- CREAF-CSIC
- Modeliza
- Pablo de Olavide University
- Polytechnic University of Catalonia (2 users)
- State Meteorological Agency
- Universitat Politècnica de València
- University of Alicante
- University of Granada (2 users)
- University of Extremadura (2 users)
- University of Oviedo
- University of Valencia (2 users)
- University of Valladolid

Sweden:
- SMHI (4 users)
- The Swedish Defence Research Agency (3 users)

Switzerland:
- Swiss Federal Laboratories for Materials & Technology
- WMO

Turkey:
- Hacettepe University
- Kastamony University
- Middle East Technical University
- Turkish State Meteorological Service (2 users)

Ukraine:
- UHMC
- Ukrainian Hydrometeorological Institute

UK:
- Airbus S.A.S.
- ECMWF (4 users)
- ESA
- IDEMS International
- Hibarcus
- London School of Hygiene and Tropical Medicine
- Private individual
- Satavia Ltd. (2 users)
- Satellite Applications Catapult
- Science and Technology Facilities Council (2 users)
- siHealth Ltd.
- University of Birmingham
- University of Leeds (2 users)
- University of Leicester (2 users)
- University of York

Asia:

Bangladesh:
- Institute of Forestry and Environmental Sciences
- University of Dhaka

China:
- Anhui Institute of Meteorological Sciences University of Dhaka
- Anhui Institute of Optics and Fine Mechanics (2 users)
- Anhui University
- Beijing Municipal Environmental Monitoring Center
- Beijing Normal University
- Chinese Academy of Meteorological Sciences
- China Academy of Sciences (6 users)
- China University of Mining and Technology (3 users)
- HTHJ

- Institute of Geographic Sciences and Natural Resources Research, China Academy of Sciences
- Institute of Remote Sensing and Digital Earth
- Jiangsu Meteorological Observatory
- Jiangsu Normal University (2 users)
- Jinan University
- Lanzhou University
- Nanjing University
- Nanjing University of Information Science & Technology (3 users)
- National Satellite Meteorological Center
- Northeast Normal University
- Peking University
- School
- Shandong University
- Shanghai University
- State Environmental Protection Key Lab of Satellite Remote Sensing
- The Chinese University of Hong Kong (2 users)
- The Institute of Atmospheric Physics (2 users)
- University of Calcutta
- (unknown) (3 users)
- Wuhan University of Technology
- Zhejiang Academy of Agricultural Sciences
- Zhejiang University

India:
- Anna University
- Aryabhatta Research Institute of Observational Sciences
- Banaras Hindu University
- Birla Institute of Technology
- Bose Institute
- Central University of Hyderabad
- CSIR-NIO
- Dibrugarh University (2 users)
- "Education"
- IIT KGP
- Indian Institute of Remote Sensing
- Indian Institute of Science Education and Research
- Indian Institute of Technology Kharagpur (2 users)
- Indian Institute of Technology Roorkee (2 users)
- Indian Institute of Tropical Meteorology (3 users)
- Indian Space Research Organization (2 users)
- Jawaharlal Nehru University
- Malaviya National Institute of Technology Jaipur
- MSRIT
- National Atmospheric Research Laboratory
- National Centre for Medium Range Weather Forecasting
- Savitribai Phule Pune University (2 users)
- School of Planning and Architecture, Bhobal

- SIG
- University of Hyderabad
- University of Kalyani
- Vikram Sarabhai Space Centre

Indonesia:
- Meteorology, Climatology, and Geophysical Agency (2 users)
- National Institute for Aeronautics and Space
- Sumatera Institute of Technology

Japan:
- Chiba University
- Japan Meteorological Agency
- Kyushu University (4 users)
- National Institute for Environmental Studies
- Remote Sensing Technology Center of Japan
- Waseda University

Malaysia:
- Malaysian Space Agency
- National University of Malaysia (4 users)
- University Malaysia Sabah

Myanmar:
- Yangon Technological University

Nepal:
- Institute for Advanced Sustainability Studies
- Institute of Engineering
- International Centre for Integrated Mountain Development (2 users)

Pakistan:
- National University of Sciences and Technology
- University of the Punjab

Singapore:
- National University of Singapore (2 users)

South Korea:
- Chungnam National University (2 users)
- Gwangju Institute of Science and Technology (2 users)
- Korea Polar Research Institute
- National Institute of Environmental Research (2 users)
- National Meteorological Satellite Center
- Seoul National University (4 users)
- Ulsan National Institute of Science and Technology
- Yonsei University (5 users)

Sri Lanka:
- Central Environmental Authority

Taiwan:
- National Central University

Thailand:
- King Mongkut's Institute of Technology Ladkrabang

Vietnam:
- University of Science (2 users)

Middle East:

Iran:
- Khavaran Institute of Higher Education
- University
- University of Tehran

Iraq:

- Al Iraqia University

Israel:

- Ben-Gurion University

Saudi Arabia:
- Private individual

United Arab Emirates:
- Khalifa University
- Masdar Institute
- Uruk Engineering & Contracting

North America:

Canada:
- Environment and Climate Change Canada (3 users)

USA:
- Arizona State University
- Caltech
- Colorado State University
- Florida State University
- Johns Hopkins University
- Hampton University
- Harvard University (3 users)
- Joint Center for Satellite Data Assimilation
- Massachusetts Institute of Technology
- Michigan Technological University (2 users)
- NASA (7 users)
- NOAA (3 users)
- Princeton University
- Private Individual
- Smithsonian Astrophysical Observatory
- SpaceKnow Inc.

- Trinity Consultants Inc.
- University of Alabama in Huntsville
- University of Alaska (2 users)
- University of California (2 users)
- University of Central Florida
- University of Colorado Boulder
- University of Houston
- University of Illinois
- University of Maryland (3 users)
- University of North Carolina at Chapel Hill
- University of Washington (2 users)
- University of Wisconsin-Madison
- Unknown
- USGS
- U.S. Environmental Protection Agency
- Utah State University

South America:

Argentina:
- Argentine Air Force
- Universidad Nacional de Rosario

Brazil:
- APAC
- LAPIS
- Universidade Federal de Alagoas
- University of São Paulo

Colombia:
- Universidad EAFIT

Ecuador:
- Universidad San Francisco de Quito

Guatemala:
- Ambente
- INSIVUMEH

Mexico:
- Instituto Politecnico Nacional

Paraguay:
- Universidad San Carlos

Uruguay:
- Universidad de la República

Australia / New Zealand:

- Environmental Systems & Services
- University of Canterbury
- University of Melbourne (2 users)

- University of Southern Queensland
- University of Wollongong

Africa:

Algeria:
- Meteo Algeria

Cameroon:
- African Institute for Mathematical Sciences

Egypt:
- Egyptian Meteorological Authority (2 users)
- National Research Institute of Astronomy and Geophysics

Eritrea:
- Department of Environment

Ghana:
- Ghana Meteorological Agency

Morocco:
- Abdelmalek Essaadi University
- EM5D
- Maroc Météo
- National Center for Meteorological Research
- University of Hassan II Casablanca

Nigeria:
- Federal University Lafia

South Africa:
- South African Weather Service
- Stellenbosch University
- University of Pretoria
- University of the Witwatersrand
- Ware Jacob Enterprises

Registered users: **470**

8.3. DMI (NUV product via FTP)

- Meteorological Institute of Romania
  $\Rightarrow$ Several commercial companies obtain the data from MIR
- Danish Meteorological Institute, Denmark
- TrygFonden, Denmark
- Department for Health, Greenland Homerule
- The Danish Cancer Society, Denmark
- Libraries of Hjørring Community
- RayMio
- Richard McKenzie, New Zealand
- Elian Wolfram, Laser Research Center and Applications, Argentina
- KMI, Belgium

Registered users: **10**

8.4. KNMI (unofficial NRT AAI via FTP)

- FMI, Finland
- William B. Hanson Center for Space Science, USA
- University of Leicester, UK

Registered users: **3**

8.5. Known international projects that use EUMETCast or WMO/GTS

- MACC project
- SACS service
- Temis WWW service
- ESA GlobVapour
- ESA CCI Ozone project

8.6. EUMETCast

Country	Count	Country	Count	Country	Count
Albania	4	Iceland	1	Portugal	5
Algeria	4	India	1	Qatar	3
Angola	1	Iran, Islamic Republic of	32	Reunion	1
Armenia	1	Iraq	2	Romania	10
Austria	19	Ireland	7	Russian Federation	7
Azerbaijan	3	Israel	4	Rwanda	2
Belgium	10	Italy	281	San Marino	1
Benin	1	Jordan	1	Saudi Arabia	3
Bosnia and Herzegovina	1	Kazakhstan	6	Senegal	5
Botswana	4	Kenya	6	Serbia	2
Brazil	3	Kuwait	2	Seychelles	1
Bulgaria	6	Kyrgyzstan	1	Slovakia	6
Burkina Faso	1	Latvia	1	Slovenia	1
Cameroon	2	Lebanon	4	South Africa	5
Canada	1	Lesotho	2	South Sudan	1
China	4	Liberia	1	Spain	43
Congo	1	Libya	1	Sudan	1
Congo, Democratic Republic of	1	Lithuania	2	Sweden	5
Croatia	1	Luxembourg	1	Switzerland	15
Cyprus	1	Madagascar	3	Syrian Arab Republic	1
Czech Republic	20	Malawi	2	Tajikistan	1
Denmark	5	Mali	1	Tanzania, United Republic of	3
Egypt	3	Malta	2	Togo	1
Estonia	3	Mauritania	3	Tunisia	3
Eswatini	2	Mauritius	2	Turkey	7
Ethiopia	5	Moldova, Republic of	1	Turkmenistan	1
Finland	5	Morocco	5	Uganda	2
France	56	Mozambique	2	Ukraine	3
Gabon	1	Namibia	1	United Arab Emirates	3
Georgia	1	The Netherlands	21	United Kingdom	112
Germany	104	Niger	2	United States	1
Ghana	5	Nigeria	6	Uzbekistan	1
Greece	18	Norway	4	Vietnam	1
Guinea-Bissau	2	Oman	2	Yemen	1
Hong Kong	1	Pakistan	1	Zambia	3
Hungary	10	Poland	12	Zimbabwe	2
TOTAL (January 2022)	**999**				

9. Updates during the reporting period

Listed below are the major configuration updates concerning operational data processing and archiving. If new versions of relevant AC SAF documents are released during the reporting period, they should be listed here also.

9.1. Software updates

Nothing to report.

9.2. Hardware updates

Nothing to report.

9.3. Documentation updates

20 September   FMI: AC SAF Operations Report (issue 1/2021 rev. 1)

29 October   FMI: AC SAF Product Requirements Document (issue 1.8)

8 November: ULB/LATMOS: Product User Manual for IASI-C NRT CO

1 December: FMI: AC SAF Product Requirements Table

7 December: FMI: AC SAF Master Schedule (version 8)

9 December: FMI: AC SAF Operations Report (issue 2/2020 rev. 2)

9 December: FMI: AC SAF Operations Report (issue 1/2021 rev. 2)

14 December: FMI: AC SAF Service Specification (issue 1.5)

14 December: FMI: AC SAF Product Requirements Document (issue 1.9)

21 December: FMI: AC SAF Product Requirements Document (issue 1.8.1)

10. Changes and usage statistics of the web portal

Listed below are the major changes in the appearance and content on the AC SAF main web pages. Additionally some web page usage statistics gathered by Google Analytics are listed.

10.1. Changes in appearance and content

Table 10.1. Changes in appearance and content of the main AC SAF web pages during the reporting period

Date	Description
19 November	*ozone_qa/index.html* and *cgi-bin/monthly_comparison.pl*: Metop-A replaced by Metop-C

In addition to updates above, following routine updates are conducted whenever necessary:

- The links to public AC SAF user documents are updated whenever new documents or new versions of existing documents become available
- The "top story" on the front page is updated
- News list on the front page is updated

10.2. Web page statistics

Google Analytics tracking service continuously monitors AC SAF web portal usage. Following diagrams and tables present some statistics gathered during the reporting period.
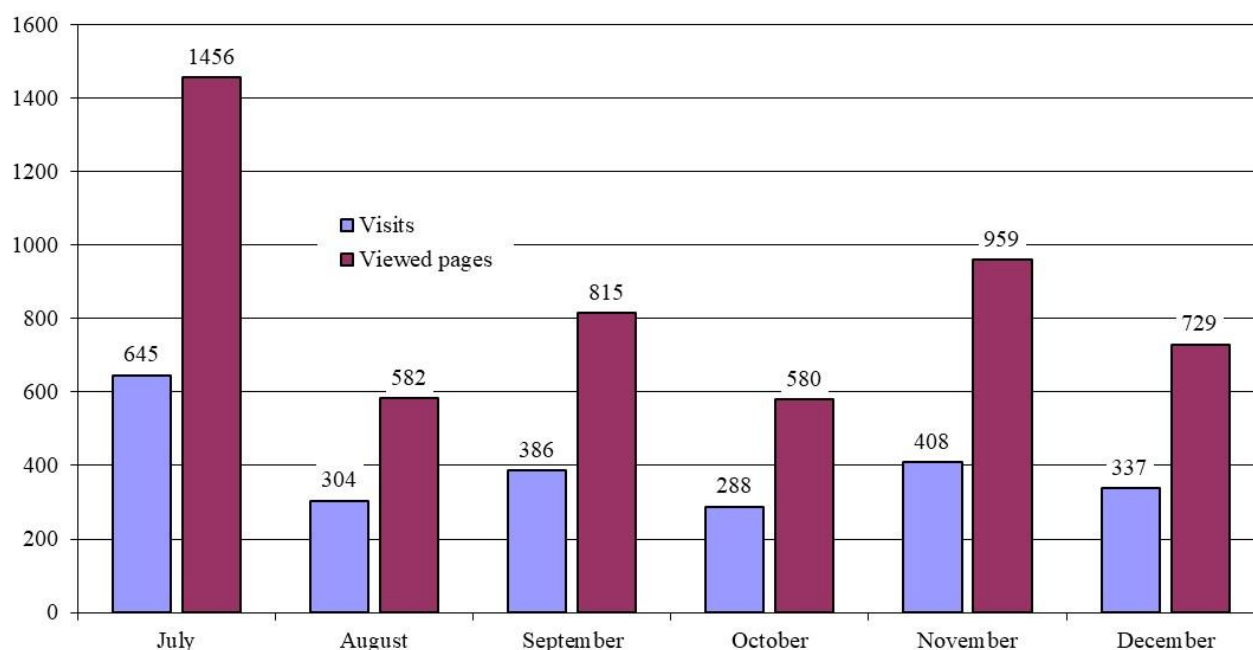

Figure 10.1. Individual visits to the web portal and number of viewed pages

Table 10.2. TOP 5 visiting countries (number of visits in brackets)

July	USA (56)	China (42)	Germany (35)	Belgium (34)	India (28)
August	Belgium (39)	China (38)	USA (23)	Germany (21)	Finland (11)
September	China (43)	Germany (34)	USA (27)	Belgium (25)	Spain (25)
October	China (43)	Belgium (24)	USA (21)	Germany (15)	UK (11)
November	USA (46)	China (40)	Germany (27)	Belgium (16)	Finland (16)
December	China (33)	USA (29)	UK (18)	Belgium (17)	Germany (15)
Σ	China (231)	USA (202)	Belgium (148)	Germany (123)	UK (77)

Table 10.3. TOP 5 pages (number of views in brackets)

| July	index (1187)	offline_access (43)	datarecord_access (28)	nrt_access (22)	product_list (16)
August	index (233)	offline_access (59)	datarecord_access (34)	nrt_access (28)	products/not_so2 (18)
September	index (343)	offline_access (49)	datarecord_access (48)	nrt_access (33)	products/not_so2 (28)
October	index (243)	offline_access (42)	datarecord_access (31)	atbds (16)	products/not_so2 (16)
November	index (330)	offline_access (66)	nrt_access (45)	datarecord_access (44)	cgi-bin/monthly_ comparison (30)
December	index (292)	offline_access (93)	datarecord_access (38)	registration_form (31)	nrt_access (29)
Σ	index (2628)	offline_access (352)	datarecord_access (223)	nrt_access (171)	registration_form (101)
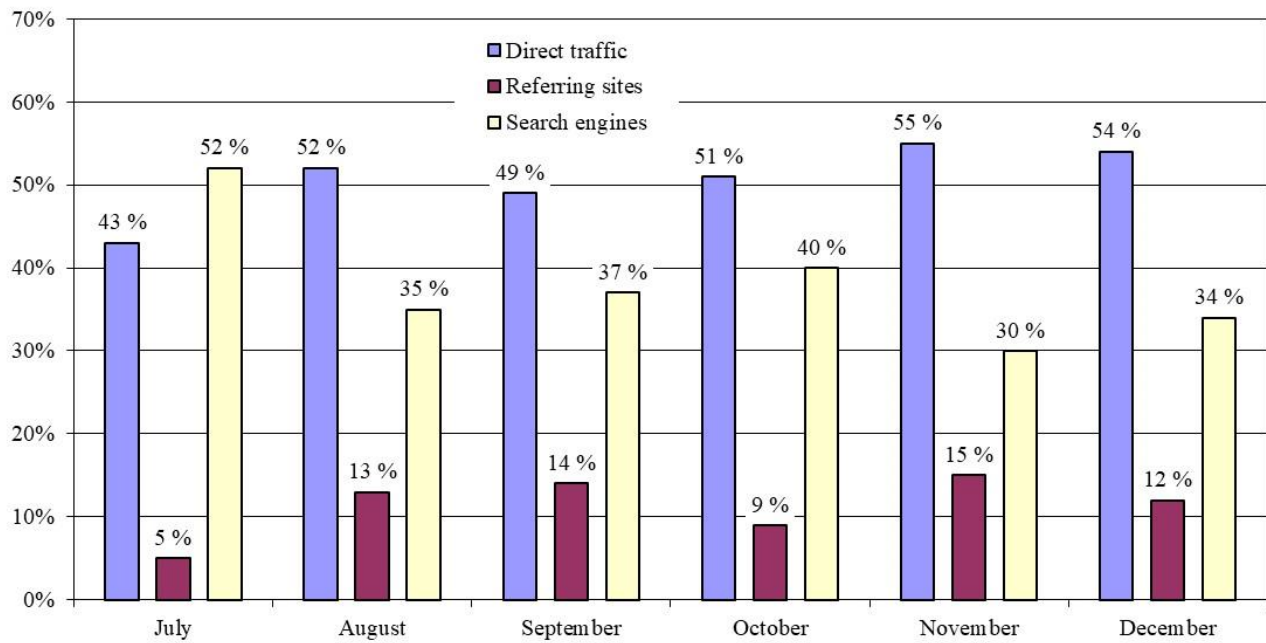
Figure 10.2. Traffic sources by type

APPENDIX 1

Table A.1 presents the overall summary of orders from AC SAF archive at FMI, sorted by product types, during the reporting period

Table A.2 presents a detailed summary of product orders from AC SAF archive at FMI during the reporting period.

Table A.1. Overall summary of product orders, by product type, during the reporting period

Product type	Number of orders	Number of users	Number of products	Total size
OOP-A	1	1	4198	206 GB
OOP-B	0	-	-	-
OHP-A	11	8	2243	554 GB
OHP-B	8	5	2200	542 GB
OHP-C	3	2	447	111 GB
ARS-A	21	1	6318	6.38 GB
ARS-B	23	2	6347	6.40 GB
ARS-C	22	3	6577	6.64 GB
ARP-A	2	2	29	199 MB
ARP-B	16	2	496	3.41 GB
ARP-C	16	3	669	4.60 GB
OUV-A	5	4	8454	57.0 MB
OUV-B	77	8	70291	128 MB
OUV-AB	65	5	15735	78.0 MB
OUV-BC	77	8	39185	17.2 MB
LER-MSC-AB	0	-	-	-
LER-PMD-AB	0	-	-	-

Table A.2. More detailed summary of product orders during the reporting period

JULY			
Product type	Number of products	Order size	Institute / company
ARS-C	865	874 MB	CSIR-NIO, India
ARS-A ARS-B ARS-C	113 114 114	341 MB	AUTH, Greece
ARS-A ARS-B ARS-C	184 182 183	565 MB	AUTH, Greece
ARP-B ARP-C	14 14	193 MB	FMI, Finland
ARS-A ARS-B ARS-C	439 440 440	1.32 GB	AUTH, Greece

Product type	Number of products	Order size	Institute / company
ARS-A ARS-B ARS-C	439 439 439	1.33 GB	AUTH, Greece
ARS-A ARS-B ARS-C	423 423 425	1.28 GB	AUTH, Greece
ARS-A ARS-B ARS-C	395 397 386	1.18 GB	AUTH, Greece
ARS-A ARS-B ARS-C	440 439 435	1.32 GB	AUTH, Greece
ARP-B ARP-C	14 13	186 MB	FMI, Finland
ARS-A ARS-B ARS-C	424 423 238	1.09 GB	AUTH, Greece
ARS-A ARS-B ARS-C	423 423 425	1.28 GB	AUTH, Greece
ARS-A ARS-B ARS-C	424 426 421	1.27 GB	AUTH, Greece
ARS-A ARS-B ARS-C	438 438 440	1.32 GB	AUTH, Greece
ARS-A ARS-B	426 425	850 MB	AUTH, Greece
ARP-B ARP-C	57 57	783 MB	FMI, Finland
ARP-B ARP-C	57 57	783 MB	FMI, Finland
ARP-B ARP-C	71 71	974 MB	FMI, Finland
ARP-B ARP-C	14 14	192 MB	FMI, Finland
ARP-B ARP-C	14 13	185 MB	FMI, Finland
OHP-A	15	3.51 GB	Universidad San Francisco de Quito, Ecuador
OUV-B	7 Selected subset: DNADD, PLADD, UVADD, UVBDD, DNADR, PLADR, UVADR, UVBDR, UVI Region: global (98.3 MB in total)		Xiamen University, China
AUGUST			
Product type	**Number of products**	**Order size**	**Institute / company**
ARP-B ARP-C	14 13	185 MB	FMI, Finland

ARP-B ARP-C	43 43	591 MB	FMI, Finland
ARP-B ARP-C	14 14	192 MB	FMI, Finland
ARS-A ARS-B ARS-C	439 439 440	1.36 GB	AUTH, Greece
ARS-A ARS-B ARS-C	423 423 425	1.28 GB	AUTH, Greece
OHP-A	14	3.92 GB	Altai State University, Russia
ARS-A ARS-B ARS-C	100 100 99	308 MB	AUTH, Greece
ARP-B ARP-C	13 13	178 MB	FMI, Finland
ARS-A ARS-B ARS-C	28 28 29	87.7 GB	AUTH, Greece
ARP-B ARP-C	71 71	975 MB	FMI, Finland
ARS-A ARS-B ARS-C	108 108 107	331 MB	AUTH, Greece
OUV-AB OUV-B OUV-BC	Time series for 1687 days Selected subset: UVADD, UVBDD, UVI Location: 1.00E 45.00N (139 kB in total)		Private Individual, France
OUV-B OUV-BC	Time series for 1322 days Selected subset: UVI Location: 4.49W 48.39N (79.9 kB in total)		Private Individual, France
OUV-B OUV-BC	Time series for 1309 days Selected subset: UVI Location: 4.49W 48.39N (79.1 kB in total)		Private Individual, France
OUV-AB OUV-B OUV-BC	Time series for 1687 days Selected subset: UVADD, UVBDD, UVI Location: 48.00E 1.50N (250 kB in total)		Private Individual, France
OUV-B OUV-BC	Time series for 1309 days Selected subset: UVI Location: 7.26E 43.70N (79.1 kB in total)		Private Individual, France
ARP-B ARP-C	57 56	775 MB	FMI, Finland

OUV-AB OUV-B OUV-BC	Time series for 1693 days Selected subset: UVI Location: 7.26E 48.39N (102 kB in total)	Private Individual, France
OUV-AB OUV-B OUV-BC	Time series for 1693 days Selected subset: UVI Location: 7.26E 48.39N (102 kB in total)	Private Individual, France
OUV-AB OUV-B OUV-BC	Time series for 1693 days Selected subset: UVI Location: 1.33W 47.12N (102 kB in total)	Private Individual, France
OUV-AB OUV-B OUV-BC	Time series for 1693 days Selected subset: UVI Location: 1.33W 47.12N (102 kB in total)	Private Individual, France
OUV-AB OUV-B OUV-BC	Time series for 1693 days Selected subset: UVI Location: 1.33W 47.12N (102 kB in total)	Private Individual, France
OUV-AB OUV-B OUV-BC	Time series for 1693 days Selected subset: UVI Location: 1.33W 47.12N (102 kB in total)	Private Individual, France
OUV-AB OUV-B OUV-BC	Time series for 1693 days Selected subset: UVI Location: 1.33W 47.12N (102 kB in total)	Private Individual, France
OUV-AB OUV-B OUV-BC	Time series for 1693 days Selected subset: UVI Location: 1.33W 47.12N (102 kB in total)	Private Individual, France
OUV-AB OUV-B OUV-BC	Time series for 1693 days Selected subset: UVI Location: 1.33W 47.12N (102 kB in total)	Private Individual, France
OUV-AB OUV-B OUV-BC	Time series for 1693 days Selected subset: UVI Location: 1.33W 47.12N (102 kB in total)	Private Individual, France
OUV-AB OUV-B OUV-BC	Time series for 1693 days Selected subset: UVI Location: 1.27E 43.37N (102 kB in total)	Private Individual, France

OUV-AB OUV-B OUV-BC	Time series for 1693 days Selected subset: UVI Location: 1.15E 45.40N (102 kB in total)	Private Individual, France
OUV-AB OUV-B OUV-BC	Time series for 1693 days Selected subset: UVI Location: 2.20E 48.50N (102 kB in total)	Private Individual, France
OUV-AB OUV-B OUV-BC	Time series for 1693 days Selected subset: UVI Location: 1.33W 47.12N (102 kB in total)	Private Individual, France
OUV-AB OUV-B OUV-BC	Time series for 1693 days Selected subset: UVI Location: 1.15E 45.50N (102 kB in total)	Private Individual, France
OUV-AB OUV-B OUV-BC	Time series for 1693 days Selected subset: UVI Location: 4.32W 48.24N (102 kB in total)	Private Individual, France
OUV-AB OUV-B OUV-BC	Time series for 1693 days Selected subset: UVI Location: 2.26E 44.55N (102 kB in total)	Private Individual, France
OUV-AB OUV-B OUV-BC	Time series for 1693 days Selected subset: UVI Location: 2.26E 44.55N (102 kB in total)	Private Individual, France
OUV-AB OUV-B OUV-BC	Time series for 1693 days Selected subset: UVI Location: 1.33W 47.12N (102 kB in total)	Private Individual, France
OUV-AB OUV-B OUV-BC	Time series for 1693 days Selected subset: UVI Location: 4.31W 48.24N (102 kB in total)	Private Individual, France
OUV-AB OUV-B OUV-BC	Time series for 1693 days Selected subset: UVI Location: 1.27E 43.37N (102 kB in total)	Private Individual, France
OUV-AB OUV-B OUV-BC	Time series for 1693 days Selected subset: UVI Location: 0.36W 44.50N (102 kB in total)	Private Individual, France

OUV-AB OUV-B OUV-BC	Time series for 1693 days Selected subset: UVI Location: 1.40W 49.39N (102 kB in total)		Private Individual, France
OUV-AB OUV-B OUV-BC	Time series for 1693 days Selected subset: UVI Location: 5.23E 43.18N (102 kB in total)		Private Individual, France
OUV-AB OUV-B OUV-BC	Time series for 1693 days Selected subset: UVI Location: 1.33W 43.29N (102 kB in total)		Private Individual, France
OUV-AB OUV-B OUV-BC	Time series for 1693 days Selected subset: UVI Location: 3.52E 43.37N (102 kB in total)		Private Individual, France
OUV-AB OUV-B OUV-BC	Time series for 1693 days Selected subset: UVI Location: 3.00E 43.11N (102 kB in total)		Private Individual, France
OUV-AB OUV-B OUV-BC	Time series for 1693 days Selected subset: UVI Location: 1.28W 43.30N (102 kB in total)		Private Individual, France
OUV-AB OUV-B OUV-BC	Time series for 1693 days Selected subset: UVI Location: 4.50E 45.45N (102 kB in total)		Private Individual, France
OUV-AB OUV-B OUV-BC	Time series for 1693 days Selected subset: UVI Location: 2.20E 48.50N (102 kB in total)		Private Individual, France
OUV-AB OUV-B OUV-BC	Time series for 1693 days Selected subset: UVI Location: 3.03E 50.38N (102 kB in total)		Private Individual, France
OUV-AB OUV-B OUV-BC	Time series for 1693 days Selected subset: UVI Location: 5.03E 47.20N (102 kB in total)		Private Individual, France
OHP-A OHP-B	850 850	421 GB	Max Planck Institute for Chemistry, Germany

EUMETSAT Satellite Application Facility on Atmospheric Composition Monitoring

OPERATIONS REPORT 2/2021 rev. 1

SEPTEMBER			
Product type	**Number of products**	**Order size**	**Institute / company**
OUV-B OUV-BC		Time series for 731 days Selected subset: ERYDD, UVADD, UVBDD, UVADR, UVBDR, UVI Location: 54.73W 2.41S (84.8 kB in total)	Federal University of Western Pará, Brazil
OUV-B OUV-BC		Time series for 731 days Selected subset: ERYDD, DNADD, PLADD, VITDD, UVADD, UVBDD, ERYDR, DNADR, PLADR, VITDR, UVADR, UVBDR, JO1D, JNO2, UVI Location: 54.73W 2.41S (400 kB in total)	Federal University of Western Pará, Brazil
OUV-A OUV-AB OUV-B OUV-BC		Time series for 4963 days Selected subset: ERYDD, UVADD, UVBDD, ERYDR, UVADR, UVBDR, UVI Location: 54.73W 2.41S (626 kB in total)	Federal University of Western Pará, Brazil
OUV-AB OUV-B OUV-BC		Time series for 1693 days Selected subset: UVI Location: 1.28W 43.30N (102 kB in total)	Private Individual, France
OUV-AB OUV-B OUV-BC		Time series for 1693 days Selected subset: UVI Location: 1.15E 45.50N (102 kB in total)	Private Individual, France
OUV-AB OUV-B OUV-BC		Time series for 1693 days Selected subset: UVI Location: 2.26E 44.55N (102 kB in total)	Private Individual, France
OUV-AB OUV-B OUV-BC		Time series for 1693 days Selected subset: UVI Location: 1.27E 43.37N (102 kB in total)	Private Individual, France
OUV-AB OUV-B OUV-BC		Time series for 1693 days Selected subset: UVI Location: 2.20E 48.50N (102 kB in total)	Private Individual, France

OUV-AB OUV-B OUV-BC	Time series for 1693 days Selected subset: UVI Location: 4.31S 48.24N (102 kB in total)	Private Individual, France
OUV-AB OUV-B OUV-BC	Time series for 1693 days Selected subset: UVI Location: 1.33S 47.12N (102 kB in total)	Private Individual, France
OUV-AB OUV-B OUV-BC	Time series for 1693 days Selected subset: UVI Location: 4.50E 45.45N (102 kB in total)	Private Individual, France
OUV-AB OUV-B OUV-BC	Time series for 1693 days Selected subset: UVI Location: 3.52E 43.37N (102 kB in total)	Private Individual, France
OUV-AB OUV-B OUV-BC	Time series for 1693 days Selected subset: UVI Location: 3.03E 50.38N (102 kB in total)	Private Individual, France
OUV-AB OUV-B OUV-BC	Time series for 1693 days Selected subset: UVI Location: 1.33W 43.29N (102 kB in total)	Private Individual, France
OUV-AB OUV-B OUV-BC	Time series for 1693 days Selected subset: UVI Location: 5.23E 43.18N (102 kB in total)	Private Individual, France
OUV-AB OUV-B OUV-BC	Time series for 1693 days Selected subset: UVI Location: 5.03E 47.20N (102 kB in total)	Private Individual, France
OUV-AB OUV-B OUV-BC	Time series for 1693 days Selected subset: UVI Location: 0.36W 44.50N (102 kB in total)	Private Individual, France
OUV-AB OUV-B OUV-BC	Time series for 1693 days Selected subset: UVI Location: 3.00E 43.11N (102 kB in total)	Private Individual, France
OUV-AB OUV-B OUV-BC	Time series for 1693 days Selected subset: UVI Location: 1.40W 49.39N (102 kB in total)	Private Individual, France

OUV-BC	Time series for 6 days Selected subset: UVI Location: 4.49W 48.39N (935 B in total)	Private Individual, France
OUV-AB OUV-B OUV-BC	Time series for 1693 days Selected subset: UVI Location: 1.33W 47.12N (102 kB in total)	Private Individual, France
OUV-AB OUV-B OUV-BC	Time series for 1693 days Selected subset: UVI Location: 1.33W 47.12N (102 kB in total)	Private Individual, France
OUV-AB OUV-B OUV-BC	Time series for 1693 days Selected subset: UVI Location: 1.33W 47.12N (102 kB in total)	Private Individual, France
OUV-AB OUV-B OUV-BC	Time series for 1693 days Selected subset: UVI Location: 1.33W 47.12N (102 kB in total)	Private Individual, France
OUV-AB OUV-B OUV-BC	Time series for 1693 days Selected subset: UVI Location: 1.33W 47.12N (102 kB in total)	Private Individual, France
OUV-AB OUV-B OUV-BC	Time series for 1704 days Selected subset: UVI Location: 8.40E 41.55N (103 kB in total)	Private Individual, France
OUV-AB OUV-B OUV-BC	Time series for 1704 days Selected subset: UVI Location: 1.33W 47.12N (103 kB in total)	Private Individual, France
OUV-AB OUV-B OUV-BC	Time series for 1704 days Selected subset: UVI Location: 9.30E 42.40N (103 kB in total)	Private Individual, France
OUV-AB OUV-B OUV-BC	Time series for 1704 days Selected subset: UVI Location: 1.33W 47.12N (103 kB in total)	Private Individual, France
OUV-AB OUV-B OUV-BC	Time series for 1704 days Selected subset: UVI Location: 8.40E 41.55N (103 kB in total)	Private Individual, France

Product type	Number of products	Order size	Institute / company
OUV-AB OUV-B OUV-BC	Time series for 1704 days Selected subset: UVI Location: 9.10E 41.24N (103 kB in total)		Private Individual, France
ARS-A ARS-B ARS-C	14 14 14	42.1 MB	AUTH, Greece
ARP-A	14	94.2 MB	AEMET, Spain
OUV-B OUV-BC	Time series for 1572 days Selected subset: UVI Location: 56.62W 64.20S (94.9 kB in total)		FMI, Finland
OUV-A OUV-AB OUV-B OUV-BC	Time series for 5227 days Selected subset: ERYDR Location: 56.62W 64.20S (314 kB in total)		FMI, Finland
OCTOBER			
Product type	**Number of products**	**Order size**	**Institute / company**
OUV-B OUV-BC	Time series for 1094 days Selected subset: ERYDD, DNADD, PLADD, VITDD, UVADD, UVBDD Location: 5.50W 56.50N (127 kB in total)		LaMMA Consortium, Italy
OUV-B	Time series for 1 day Selected subset: ERYDD, DNADD, PLADD, VITDD, UVADD, UVBDD Location: 5.50W 56.50N (823 B in total)		LaMMA Consortium, Italy
OOP-A	4198	206 GB	EUMETSAT, Germany
ARP-C	171	1.18 GB	KMI, Belgium
ARS-A ARS-B ARS-C	142 142 142	438 MB	AUTH, Greece
ARS-A ARS-B ARS-C	57 57 56	175 MB	AUTH, Greece
OUV-B OUV-BC	Time series for 418 days Selected subset: ERYDD Location: 24.96E 60.20N (25.7 kB in total)		FMI, Finland
OHP-A OHP-B OHP-C	6 6 7	4.69 GB	IFAC-CNR, Italy

Product type	Number of products	Order size	Institute / company
OHP-A OHP-B OHP-C	14 14 15	10.5 GB	IFAC-CNR, Italy
NOVEMBER			
Product type	**Number of products**	**Order size**	**Institute / company**
ARS-A ARS-B ARS-C	439 439 440	1.36 GB	AUTH, Greece
OUV-A OUV-AB OUV-B OUV-BC	5267 Selected subset: ERYDD, UVI Region: 18.5-23.5E, 41.5-46.5N (125 MB in total)		Geographical institute "Jovan Cvijic", Serbia
OHP-A OHP-B	454 454	160 GB	University of Science and Technology, China
OHP-A OHP-B	425 425	210 GB	University of Science and Technology, China
ARP-B ARP-C	14 14	191 MB	FMI, Finland
ARS-B ARS-C	14 14	28.6 MB	FMI, Finland
ARS-B	14	14.3 MB	FMI, Finland
ARP-B	15	104 MB	FMI, Finland
OUV-BC	Time series for 320 days Selected subset: UVBDD, UVBDR Location: 50.86E 4.68N (23.3 kB in total)		KU Leuven, Belgium
OUV-B OUV-BC	Time series for 366 days Selected subset: UVBDD, UVBDR Location: 4.68E 50.8N (26.6 kB in total)		KU Leuven, Belgium
OUV-B OUV-BC	Time series for 366 days Selected subset: PLADD, PLADR Location: 4.68E 50.8N (26.6 kB in total)		KU Leuven, Belgium
OUV-A	Time series for 366 days Selected subset: UVBDD, UVBDR Location: 4.68E 50.8N (26.6 kB in total)		KU Leuven, Belgium
ARP-C	35	244 MB	FMI, Finland
OUV-A OUV-AB OUV-B OUV-BC	4963 Selected subset: ERYDD, UVI Region: 18.0-23.5E, 41.5-46.5N (117 MB in total)		Geographical institute "Jovan Cvijic", Serbia

	DECEMBER		
Product type	**Number of products**	**Order size**	**Institute / company**
ARP-A ARP-B	15 14	202 MB	FMI, Finland
OHP-A	14	3.51 GB	Universidad San Francisco de Quito, Ecuador
OHP-B OHP-C	423 425	210 GB	University of Crete, Greece
OHP-A	423	103 GB	University of Crete, Greece
OHP-A OHP-B	14 14	6.84 GB	University of Galati, Romania
OHP-A OHP-B	14 14	6.84 GB	University of Galati, Romania

APPENDIX 2

Table A.3 presents a detailed summary of failed product orders from AC SAF archive at FMI during the reporting period. The middle column indicates whether the failure was related to problems with AC SAF archive and/or ordering system or was the problem on the user's side.

Table A.3. Summary of failed product orders during the reporting period

Date	Error type	Failure description and details
		Order ID: User institute: Order contents: Ordering log error message: ' ' Failure description: Corrective action: Final outcome: